FILE COPY

SECURITY CLASSIFICATION OF THIS PAGE

REPORT DOCUMENTATION PAGE

Form Approved OMB No. 0704-0188

1a. REPORT SECURITY CLASSIFICATION
UNCLASSIFIED

1b. RESTRICTIVE MARKINGS
NONE

AD-A217 889

3. DISTRIBUTION/AVAILABILITY OF REPORT
APPROVED FOR PUBLIC RELEASE; DISTRIBUTION UNLIMITED.

5. MONITORING ORGANIZATION REPORT NUMBER(S)
AFIT/CI/CIA-89-149

6a. NAME OF PERFORMING ORGANIZATION
AFIT STUDENT AT UNIV OF COLORADO

6b. OFFICE SYMBOL (If applicable)

7a. NAME OF MONITORING ORGANIZATION
AFIT/CIA

6c. ADDRESS (City, State, and ZIP Code)

7b. ADDRESS (City, State, and ZIP Code)
Wright-Patterson AFB OH 45433-6583

8a. NAME OF FUNDING/SPONSORING ORGANIZATION

8b. OFFICE SYMBOL (If applicable)

9. PROCUREMENT INSTRUMENT IDENTIFICATION NUMBER

8c. ADDRESS (City, State, and ZIP Code)

10. SOURCE OF FUNDING NUMBERS

PROGRAM ELEMENT NO.	PROJECT NO.	TASK NO.	WORK UNIT ACCESSION NO.

11. TITLE (Include Security Classification) (UNCLASSIFIED)
EXPERIMENTAL INVESTIGATION OF THE MECHANISMS UNDERLYING VORTEX KINEMATICS IN UNSTEADY SEPARATED FLOWS

12. PERSONAL AUTHOR(S)
SCOTT JEFFREY SCHRECK

13a. TYPE OF REPORT
THESIS/~~DISSERTATION~~

13b. TIME COVERED
FROM _____ TO _____

14. DATE OF REPORT (Year, Month, Day)
1989

15. PAGE COUNT
145

16. SUPPLEMENTARY NOTATION
APPROVED FOR PUBLIC RELEASE IAW AFR 190-1
ERNEST A. HAYGOOD, 1st Lt, USAF
Executive Officer, Civilian Institution Programs

17. COSATI CODES

FIELD	GROUP	SUB-GROUP

18. SUBJECT TERMS (Continue on reverse if necessary and identify by block number)

19. ABSTRACT (Continue on reverse if necessary and identify by block number)

DTIC
ELECTE
FEB 12 1990
S D
D

20. DISTRIBUTION/AVAILABILITY OF ABSTRACT
☒ UNCLASSIFIED/UNLIMITED ☐ SAME AS RPT. ☐ DTIC USERS

21. ABSTRACT SECURITY CLASSIFICATION
UNCLASSIFIED

22a. NAME OF RESPONSIBLE INDIVIDUAL
ERNEST A. HAYGOOD, 1st Lt, USAF

22b. TELEPHONE (Include Area Code)
(513) 255-2259

22c. OFFICE SYMBOL
AFIT/CI

DD Form 1473, JUN 86 Previous editions are obsolete. SECURITY CLASSIFICATION OF THIS PAGE

AFIT/CI "OVERPRINT"

EXPERIMENTAL INVESTIGATION OF THE MECHANISMS UNDERLYING VORTEX KINEMATICS IN UNSTEADY SEPARATED FLOWS

by

SCOTT JEFFREY SCHRECK

B.S., United States Air Force Academy, 1981

M.S., Air Force Institute of Technology, 1983

Accesion For
NTIS CRA&I ☒
DTIC TAB ☐
Unannounced ☐
Justification
By
Distribution/
Availability Codes
Dist | Avail and/or Special
A-1

A thesis submitted to the

Faculty of the Graduate School of the

University of Colorado in partial fulfillment

of the requirements for the degree of

Doctor of Philosophy

Department of Aerospace Engineering Sciences

1989

DTIC COPY INSPECTED 5

90 02 12 034

This thesis for the Doctor of Philosophy degree by

Scott Jeffrey Schreck

has been approved for the

Department of

Aerospace Engineering Sciences

by

_____

Marvin W. Luttges

_____

Donald A. Kennedy

Date_____

ACKNOWLEDGMENTS

I would like to thank Dr. Marvin Luttges, whose patient teaching and friendly guidance have enabled me to attain this goal. I also wish to express my gratitude to Dr. Donald Kennedy, Dr. C.-Y. Chow, Dr. Franklin Essenburg and Dr. Peter Freymuth, my committee members, whose collective diversity has considerably broadened my education here at the University.

Wolfgang Bank and Russell Meinzer have provided me with invaluable technical assistance. These gentlemen are talented craftsmen whose expertise and dedication to their work have been essential to the successful completion of my experimental research. I am also deeply grateful to my colleagues, who are also my friends, for their assistance and comradery during my three years here at Boulder.

Finally, my family has given me their constant encouragement and loyal support throughout my life. To them I dedicate this thesis.

CONTENTS

CHAPTER

I. INTRODUCTION 1

II. HISTORICAL REVIEW 4

Physical Foundations of Unsteady Separated Flows 5

Early Work in Unsteady Separation 6

Sinusoidal Pitching 8

Constant Rate Pitching 11

Focus of Current Experiments 17

III. VORTEX STRUCTURE 19

Introduction 19

Experimental Methods 20

Results 24

Spanwise Visualization of the Leading Edge Vortex 24

Anemometric Corroboration of Visualization 37

IV. VORTEX KINEMATICS 45

Introduction 45

Experimental Methods 46

Results 49

Qualitative Descriptions of Structures 50

Quantitative Characterizations of Structures 60

V. SURFACE FLOWS 81

Introduction 81

Experimental Methods 83

Results 86

Hotwire Anemometry Data 86

Correlations Between Vortex Kinematics and Surface Anemometry 101

VI. DISCUSSION 117

Vortex Structure 117

Vortex Kinematics 120

Surface Flows 128

VII. CONCLUSIONS 134

Vortex Structure 135

Initiation 135

Convection 136

Growth 137

Kinematics of Other Structures 139

VIII. BIBLIOGRAPHY 141

FIGURES

Figure

3-1. Leading edge vortex development for K = 1.0, MPA = 10 degrees, with splitter plate 25

3-2. Leading edge vortex development for K = 2.0, MPA = 10 degrees, with splitter plate 26

3-3. Leading edge vortex development for K = 1.0, MPA = 10 degrees, without splitter plate 27

3-4. Leading edge vortex development for K = 2.0, MPA = 10 degrees, without splitter plate 28

3-5. Leading edge vortex position histories for K = 1.0 and 2.0, MPA = 10 degrees, with and without splitter plate 34

3-6. Leading edge vortex area histories for K = 1.0 and 2.0, MPA = 10 degrees, with and without splitter plate 35

3-7. Visualization and velocity profiles for leading edge vortex at 0.20 chord 39

3-8. Visualization and velocity profiles for leading edge vortex at 0.40 chord 40

3-9. Visualization and velocity profiles for leading edge vortex at 0.60 chord 41

3-10. Visualization and velocity profiles for leading edge vortex at 0.80 chord 42

4-1. Time series visualization of leading edge vortex initiation 51

4-2. Representative leading edge vortex position history 54

4-3. Representative leading edge vortex area history 55

4-4. Visualization of representative ancillary structures 59

4-5. Time during cycle of leading edge vortex initiation 62

4-6. Leading edge vortex position histories for MPA = 0, 5 and 10 degree 63

4-7. Leading edge vortex position histories for MPA = 20, 30 and 40 degrees 64

4-8. Average leading edge vortex convection rate vs. K 66

4-9. Leading edge vortex area histories for MPA = 0, 5 and 10 degrees 67

4-10. Leading edge vortex area histories for MPA = 20, 30 and 40 degrees 68

4-11. Average leading edge vortex area growth rate vs. K 69

4-12. Time during cycle of leading and trailing edge vortex initiation 71

4-13. Trailing edge vortex area histories for MPA = 20, 30, 40 degrees 73

4-14. Average trailing edge vortex area growth rate vs. K 74

4-15. Ancillary structure wavelength vs. K 76

4-16. Average leading edge vortex convection rate vs. K, before and after maximum upward pitch angle 79

4-17. Average leading edge vortex area growth rate vs. K, before and after maximum upward pitch angle 80

5-1. Surface flow velocity histories for K = 2.0, MPA = 20 degrees, upper surface 91

5-2. Visualization of leading edge vortex initiation 94

5-3. Surface flow velocity histories for K = 2.0, MPA = 5 degrees, lower surface 95

5-4. Upper surface flow reversal histories 98

5-5. Lower surface flow reversal histories 99

5-6. Correlation of surface flow velocity and leading edge vortex convection velocity 103

5-7. Correlation of surface flow velocity and leading edge vortex growth rate 104

5-8. Correlation of leading edge vortex development parameters with vortex area for K = 0.5 and 2.0, MPA = 0 degrees..... 106

5-9. Correlation of leading edge vortex development parameters with vortex area for K = 0.5 and 2.0, MPA = 20 degrees..... 107

5-10. Correlation of surface flow velocity and leading edge vortex convection velocity..... 110

5-11. Correlation of surface flow velocity and leading edge vortex convection velocity for plate pitching up..... 111

5-12. Correlation of surface flow velocity and leading edge vortex convection velocity for plate pitching down..... 112

5-13. Correlation of surface flow velocity and leading edge vortex growth rate for plate pitching up..... 114

5-14. Correlation of surface flow velocity and leading edge vortex growth rate for plate pitching down..... 115

5-15. Time-averaged surface flow velocity vs. reduced frequency..... 116

Schreck, Scott J. (Ph.D., Aerospace Engineering Sciences)

Experimental Investigation of the Mechanisms Underlying Vortex Kinematics in Unsteady Separated Flows

Thesis directed by Professor Marvin W. Luttges

Current research in the area of unsteady separated flows has been strongly motivated by potential enhancements to air vehicle performance. Dynamic motions of lifting surfaces give rise to the emergence and fleeting presence of energetic, large-scale vortical structures characteristic of unsteady separated flow fields. While present over the lifting surface, these vortices substantially augment lift and moment coefficients and exact only modest penalties in terms of elevated drag coefficients. However, the feasibility of utilizing unsteady separation relies upon thorough comprehension of the fluid dynamic mechanisms responsible for vortex presence and behavior. To date, these mechanisms remain relatively obscure.

Unsteady separated flow fields in the vicinity of a flat plate oscillating sinusoidally in pitch about the quarterchord were investigated for a broad range of pitching parameters. Phase locked photography of smoke flow visualization was employed in conjunction with hotwire anemometry to quantify vortex development as well as some of the primary boundary layer interactions contributing to the observed vortex kinematics. Leading edge vortex development was strongly influenced by both the freestream and boundary layer flows. These and other observations facilitated formulation of an conceptual model which accounts for many of these observations. Quantitative refinement of such a model is one methodology through which unsteady separation may

eventually be understood, predicted and controlled for employment in future air vehicles. (EMK) Key words: Vortices
Vortex kinematics
Unsteady separated flow
Aerodynamics
(EMK)

CHAPTER I

INTRODUCTION

The science of fluid dynamics is replete with circumstances affirming the strong and pervasive influence exercised by vortex dominated unsteady separated flows. Through random variation and natural selection, nature has succeeded magnificently in exploiting unsteady separation. Over hundreds of millions of years, numerous living creatures have come to utilize unsteady separation to enhance locomotion. This group of animals is exemplified by birds and insects, as well as fish and marine reptiles and mammals (Lighthill, 1975).

In stark contrast to nature, the fluid dynamic machines created by man have historically been handicapped by unsteady separated flows. Unsteady separation can cause flutter, buffeting and vibrations in fixed wing aircraft and missiles, and imposes severe mechanical loads on helicopter rotor blades and marine propellers. Unsteady separation is also encountered in turbomachinery, where it can generate stall, surge, blade flutter, inlet distortions and noise (McCroskey, 1982).

Early in this century, with the science of aerodynamics still in its infancy, simplicity demanded that researchers content themselves with investigations in the steady state regime. Airfoils were assumed to maintain static orientation with respect to a constant velocity freestream. Provided angle

of attack did not exceed stall angle, the surrounding flow remained attached, and airfoil performance could be quantified in terms of lift, drag and moment.

These early trends in aerodynamics and aircraft engineering endured well into this century, with the preponderance of research and aircraft design limited to the attached flow, steady state regime. In this regime, airfoil pressure distributions, and therefore force coefficients, were well understood to be primarily determined by airfoil thickness distribution, camber, angle of attack, Reynolds number and Mach number.

Since that time, experimental investigations have shown that the energetic, vortex dominated flow fields typical of unsteady separation are capable of amplifying lift coefficients four to five fold compared to the corresponding static angle of attack circumstance (Carr et al., 1977). Unfortunately, the physics underlying these enhanced dynamic force coefficients is not as thoroughly understood as are the corresponding static angle of attack mechanisms. This understanding has been hampered by the temporally varying, spatially disparate and generally nonlinear nature of the unsteady separated flowfield.

In spite of this imperfect understanding, utilization of unsteady separation has, for quite some time, been proposed as a means for enhancing flight vehicle performance. Herbst (1981) has completed extensive analyses in support of a concept termed "supermaneuverability". This concept blends post-stall and side-slipping maneuvers with direct thrust control to achieve rapid aircraft attitude changes likely to yield unsteady separation. In contrast, Jumper (1988) has suggested that unsteady separation can be used to enhance flight vehicle attributes other than maneuverability. Instead, when maneuverability

and range are competing aircraft design parameters, unsteady separation may be employed to fulfill maneuverability requirements. This allows air vehicle configuration to be modified in such a way as to gain a substantial range increment.

Clearly, unsteady separation has significant application potential, but comprehension of the phenomenon is incomplete. To optimally harness these unsteady separated flow fields, the underlying physics must be understood in sufficient detail to predict behaviors for a variety of complex body shapes undergoing diverse kinematics. The leading edge vortex appears to play a central and pivotal role in the evolution of unsteady separated flow fields on airfoils. As such, studying the development of this structure in the vicinity of a relatively simple body experiencing well behaved motion should provide added foundation for understanding and predicting the overall behavior of unsteady separated flows in a more general context.

CHAPTER II

HISTORICAL REVIEW

All of the diverse manifestations of unsteady separated flow share a single distinguishing characteristic. That is, the fleeting presence of energetic vortical structures. These vortices initiate when the boundary layer separates from the surface of a solid body and subsequently grow and are shed from the body. The energetic nature of these vortices radically alters the flow about the body, prompting drastic variations in the attendant fluid dynamic forces. Thus, strong motivation exists for understanding the physics responsible for these structures. Unfortunately, the time-dependent, viscous nature of the flow field renders comprehension of the physics quite convoluted.

Unsteady separation has been extensively investigated experimentally, theoretically and, more recently, computationally. The parameter space encompassed by these investigations is vast and a variety of experimental, theoretical and computational techniques have been employed. This review focuses primarily upon those experimental efforts which have characterized either the kinematics of large-scale vortices or the influence of these vortices upon adjacent solid bodies, and then attempted to unravel the physics responsible for the observed kinematics or influences. For a history of analytical and computational progress in the field of unsteady separation, the reader is referred to the extensive reviews compiled by McCroskey (1977, 1982)

and Telionis (1975).

Physical Foundations of Unsteady Separated Flows

Flow fields exhibiting prominent observable entities such as vortices, separated flow and wakes, of which unsteady separated flows are a subset, have been the subject of intense analysis for an extended period of time. According to Rosenhead (1963), the Navier-Stokes equations were derived independently by Navier (1823), Poisson (1831), Saint-Venant (1843) and Stokes (1845). Although solution of the unsimplified Navier-Stokes equations was impossible at the time, the generality and physical rigor intrinsic to these equations permitted Stokes to draw out specific implications regarding vorticity conservation. However, Prandtl and Tietjens (1934) point out that the theoretical treatment of discrete vortex kinematics commenced only after Helmholtz (1858) had enunciated his classical theorems regarding circulation conservation. Shortly thereafter, Kelvin (1869) confirmed the work of Helmholtz and provided some simplified supporting mathematical proof (Lamb, 1932).

The Navier-Stokes equations also encompassed the physics responsible for flow separation and wakes in the vicinity of bodies immersed in viscous flows. As in the case of vortex kinematics, though, lack of a rigorous solution precluded application of these equations to the problem of viscous fluid motion (Schlichting, 1955). The penetrating physical insight of Prandtl (1904) gave rise to the formulation of a viscous flow model which confined the effects of viscosity to a shallow region adjacent to the solid surface over which the fluid flowed. In articulating this model, Prandtl had, in a large part, laid the foundations for the science of fluid dynamics.

Early Work in Unsteady Separation

During the founding years of fluid dynamics, considerations of simplicity restricted research to the steady state regime. Experimental and analytical tools available to early aerodynamicists did not facilitate thorough investigation of unsteady separated flows. Even if the means for exploring unsteady separation had existed, contemporary control system technology would have tended to hamper exploitation of this knowledge. Thus, the prospect of comprehending or exploiting unsteady separation was considered unfeasible. Aerodynamicists concentrated instead upon the steady state regime, where understanding and utilization had proven realizable.

These early trends in aerodynamics and aircraft engineering endured well into this century, with the preponderance of research concentrated in the attached flow, steady state regime. However, certain efforts did transcend these bounds, many of them pertaining to the field of aeroelasticity. In Germany, during the early part of this century, the relationship between the aerodynamics and the mechanical vibrations of aircraft structural components was meticulously investigated. Bublitz (1988) has compiled a comprehensive history of the development of aeroelasticity in Germany during this period.

Although theoretical in nature, an investigation by Birnbaum (1923) does merit reference in this review. Birnbaum considered the problem of an infinitesimally thin flat plate undergoing harmonic flapping in two-dimensional, inviscid flow. The calculations performed in conjunction with this study revealed, among other results, the significance of a parameter which he termed reduced frequency. Since then, reduced frequency has experienced wide use in

experimental, theoretical and computational work dealing with unsteady separation.

Pertinent experimental work concerning unsteady separation was also accomplished in the early decades of this century. Kramer (1932) studied the effect of an individual gust on the lift of an airfoil. This was accomplished by statically mounting an airfoil in the test facility, and then temporally varying the angle of attack by changing the direction of the freestream using a system of louvers. Maximum lift coefficient was seen to increase linearly with the rate at which the freestream direction varied.

Using smoke flow visualization, Lippisch (1935) succeeded in making a movie film of an unsteady separated flow circumstance somewhat different from that studied by Kramer. Instead of rotating the freestream flow past a static airfoil, Lippisch pitched an airfoil in a constant freestream. The visualization results were of high quality and revealed a delay in flow separation from the airfoil upper surface as static stall angle was exceeded. However, a large vortex which initiated and subsequently developed over the airfoil upper surface escaped parametric evaluation. This apparent oversight may have been attributable to a lack of vortex cohesiveness or to a deficiency of visualizing medium within the vortex interior. In either case, the vortical nature of unsteady separation continued to elude researchers.

Experimental research in unsteady separation was also being pursued at this time in the United States. In contrast to German studies, American work tended more toward aircraft applications. Silverstein and colleagues (1938) studied the change in maximum lift coefficient due to aircraft pitching at constant rate. This effort was carried out using the same full scale aircraft,

first in a wind tunnel and then in free flight. Tests were conducted in the incompressible flight regime, at nondimensional pitch parameter values on the order of 0.01. Satisfactory agreement was noted between wind tunnel and free flight values of maximum lift coefficient. Most importantly, appreciable transient increments to maximum lift coefficient were observed relative to static pitch angle tests.

Harper and Flanigan (1948) extended the work of Silverstein, et al. to the compressible flight regime using nondimensional pitch parameter values comparable to those used in the earlier effort. Maximum lift coefficient data gathered in free flight tests of a full scale aircraft were once again corroborated by wind tunnel data, this time using a 1/20 scale model. Harper and Flanigan obtained good agreement between free flight and wind tunnel data. In addition, they noted that the transitory increase in maximum lift coefficient with nondimensional pitch rate varied with Mach number and, within the experimental range, a limit in this increase appeared to have been reached.

Studies such as those done by Silverstein et al. and Harper and Flanigan pointed convincingly toward the application potential of unsteady separation. However, appreciation for physics underlying the experimental results seems to have been lacking. Even the realization that large-scale, energetic vortical structures were responsible for the separation delay and augmented lift coefficients appears to have escaped the attention of researchers.

Sinusoidal Pitching

In the sixties, research in unsteady separation continued to be oriented toward aircraft application. However, emphasis shifted away from enhancement

of fixed wing aircraft flying qualities. Instead, researchers began to explore the transient loading which took place on helicopter rotor blades (Ham and Garelick, 1968; Liiva and Davenport, 1969). As such, many studies examined airfoils pitching sinusoidally at rates and amplitudes to designed emulate unsteady separation occurring on helicopter blades. One of the key issues these studies sought to resolve was the disagreement between predicted and observed unsteady load temporal variation. Investigations such as these led to initial characterization of the unsteady separated flow field kinematics and contributed substantially to comprehending the physics responsible for these kinematics. The initial studies conducted by Carta (1960), Ham and Garelick (1968) and McCroskey and Fisher (1972) linked the transient loading associated with unsteady separation to large scale vortices.

Later experiments by Carr et al. (1977) and McAlister and Carr (1978) expanded the parameter range of the earlier studies, thus yielding a more complete understanding of the influences of mean pitch angle, pitching frequency and airfoil geometry as well as Reynolds and Mach number effects. These later studies used a multiplicity of measuring techniques, including smoke flow visualization, hotwire anemometry and surface pressure transducers. Analysis and correlation of the resulting data clarified the relationship between the transient loading due to the dynamic stall vortex and events transpiring within the boundary layer.

Subsequent studies using sinusoidal pitching continued to be oriented toward flight vehicle application, although perhaps not as strongly as in earlier work. Nonetheless, sinusoidal pitching continued to be a viable means for investigating the physics of unsteady separation due to the well-behaved nature

of the elicited flow fields (Robinson and Luttges, 1984).

Research concerning the control of unsteady separated flow structures on a sinusoidally oscillating airfoil was carried out and examined the response of leading edge vortex behavior to changes in airfoil pitching parameters. In addition to effects due to alterations in pitching parameters, two novel mechanisms were employed which were intended to influence leading edge vortex kinematics. The first mechanism consisted of a periodically deployable vortex generator (Luttges et al., 1985), and the second took the form of airpulse injection from the oscillating airfoil upper surface (Luttges et al., 1985; Robinson and Luttges, 1986).

Drastic alterations to leading edge vortex behavior occurred in response to changes in airfoil pitching parameters, and as a result of employing either the vortex generator or air pulse injection. Thus, it was concluded that these approaches, as well as others not yet examined, held considerable promise for flow control. In addition, this search for control methodologies provided significant insight into the physics responsible for the observed leading edge vortex behavior.

Still other efforts employing sinusoidal pitching have characterized the wake structure downstream of the airfoil. Robinson et al. (1986b) studied the wake behind a NACA 0015 airfoil oscillating sinusoidally in pitch for a broad range of pitching parameter values. Flow visualization revealed tandem vortical structures forming in the wake of the oscillating airfoil. Impingement of these structures on a pressure instrumented airfoil downstream of the oscillating airfoil elicited unsteady pressure distributions and corresponding transient loading of appreciable magnitude. It was concluded that the interaction of such

a wake with a trailing body could produce serious adverse effects.

Using flow visualization, Freymuth (1988a) has also investigated the structure of the wake downstream of an airfoil oscillating sinusoidally in pitch. The objective of this work was to definitely identify propulsive wake signatures as well as the processes which gave rise to the observed wake. At a reduced frequency of 2.9, a vortex street was observed wherein vortices tended to be driven downstream by the influence of vortices of opposing sign on the opposite side of the wake. As such, the reactive force experienced by the airfoil was directed upstream. Separation regions situated on the airfoil surface were seen to be swept off and subsequently incorporated into the vortices, contributing to the strength of these structures.

Constant Rate Pitching

Like sinusoidal pitching, constant rate pitching first experienced substantial use in studies concerning unsteady separation on helicopter rotor blades. Ham and Garelick (1968) sought to investigate the physics responsible for the "dynamic stall" which imposed extreme transient mechanical loads upon these blades during a certain interval of the blade cycle. Since, during this interval, blade angle of attack experienced approximately linear increase, constant rate pitching was chosen to simulate the circumstance.

Ham and Garelick pitched a pressure instrumented NACA 0012 airfoil from 0 to 30 degrees, at rates between 2 and 20 radians per second. Pitch axis 'ocation varied from -0.25 to +0.75 chord and Reynolds number, based on chordlength, was held constant at 344,000. Peak lift and moment were seen to be primarily functions of pitch rate, while the angle at which dynamic stall

occurred was governed by pitch axis location. These results suggested that transient loading was relatively independent of instantaneous pitch angle.

Later experimental work by Ham (1972) facilitated formulation of a model describing the viscous interactions responsible for leading edge vortex initiation during constant rate pitch up. A convincing correlation was observed between laminar separation bubble kinematics and kinematics of the leading edge vortex shortly after initiation. This apparent relationship led to the conclusion that the leading edge vortex initiated when the laminar separation bubble burst under the influence of the local adverse pressure gradient.

High transient loading induced by unsteady separation was deemed detrimental to helicopter rotor blade operation. However, Silverstein and colleagues (1938), as well as Harper and Flanigan (1948), had convincingly demonstrated some of the benefits conferred upon fixed wing aircraft by unsteady separation resulting from constant rate pitching. The success of these efforts, coupled with progress in aircraft control system flexibility, motivated researchers in the seventies to once again investigate constant rate pitching as a means of aircraft performance enhancement.

Francis and coworkers (1983) undertook an experimental investigation designed to examine the effects of constant rate airfoil pitch motions, some of which involved sudden reversal in the pitch direction. Using pressure instrumented airfoils, the nondimensional pitch range between 0.001 and 0.2 was explored, with all motions initiated at zero pitch angle and amplitude variations extending to approximately 60 degrees. A lift impulse function, defined as the integration of instantaneous lift over the duration of the pitch motion, was adopted to quantify the sustained lift augmentation generated by

these various pitch motions. Results indicated that neither the highest pitch rates nor the largest amplitudes maximized the lift impulse function. Instead, lift impulse peaked when the maximum incidence angle closely approximated the angle at which leading edge separation would have occurred had the upward pitch continued unaltered.

Experiments involving constant rate pitching motions to large amplitudes have also been performed by Walker et al. (1985a, 1985b) and Helin et al. (1986). Results of these studies showed that, over a fourfold variation in Reynolds number, the unsteady separated flow structure was primarily dictated by nondimensional pitch rate. Specifically, greater nondimensional pitch parameter values permitted the airfoil to reach higher pitch angles before flow separation occurred, generated a higher suction peak, elicited a more energetic leading edge vortex and was associated with higher velocity reverse flows at the airfoil surface.

Graham and Strickland (1986) and Strickland and Graham (1986) pitched a NACA 0015 airfoil in a tow tank at nondimensional rates between 0.1 and 1.0, and at a Reynolds number of 100,000. In each case, the motion was begun at 0 degrees pitch angle and terminated when the airfoil had reached 90 degrees. Attributes of the resulting unsteady separated flow field were recorded using flow visualization, surface pressure data and load cell measurements. It was found that lift and drag coefficient data could be represented by simple trigonometric functions. Further, these simple trigonometric representations facilitated prediction of lift and drag coefficients over the entire experimental range of nondimensional pitch rate.

Jumper et al. (1987) stressed that the simplicity of the experimental

design facilitated insight into the mechanisms at work in the dynamic stall process. Jumper and colleagues pitched a pressure instrumented NACA 0015 airfoil about the midchord at constant rate for 20 different combinations of freestream velocity and pitch rate. This yielded lift, pressure drag and moment data as a function of instantaneous pitch angle for nondimensional pitch rates between 0.006 and 0.032. Comparison of these dynamic data to data collected at corresponding static angles of attack showed a postponement in both stall and flow separation at the airfoil quarterchord. The magnitude of these delays was found to collapse onto a single curve when plotted against nondimensional pitch rate. Jumper et al. asserted that this correlation established a systematic link between quarterchord separation and dynamic stall. In addition, unsteady separation was described as a process, emphasizing that different mechanisms were at work at different points in the unsteady separation event.

A study conducted by Helin et al. (1986) sought to not only understand unsteady separation generated by an airfoil pitching at constant rate, but to control certain aspects of flow field development. A NACA 0015 airfoil was pitched at constant rate from 0 to 60 degrees angle of attack, at nondimensional pitch rates of 0.4 and 0.8. In an attempt to exert control over flow field development, pitching was interrupted briefly at predetermined instantaneous pitch angles and then resumed. Flow visualization documented dramatic alterations to forced, relaxed and shedding flows in response to changes in the temporal aspects of the forcing functions. Leading edge vortices were seen to be controlled with respect to structure, dwell time and convection rate. Based upon these results, airfoil motion history changes were judged to hold significant potential for controlling the development of exploitable unsteady

separated flow fields.

In an effort to simulate unsteady separation experienced by helicopters in high speed forward flight or aircraft during post stall maneuvers, Lorber and Carta (1987) undertook a study encompassing Reynolds and Mach numbers representative of these scenarios. Reynolds numbers of 2,000,000 and 4,000,000 were employed, corresponding to Mach numbers of 0.2 and 0.4. An airfoil was pitched at constant rate which yielded nondimensional pitch rates between 0.001 and 0.020. The airfoil was instrumented with both pressure transducers and hotfilm anemometers, allowing detection of surface static pressures as well as the locations of boundary layer transition and separation. Results showed that leading edge vortex strength, as evidenced by suction peak magnitude, increased with more rapid pitch rate, and decreased with higher Mach number or when pitching was initiated close to the steady state stall angle. In addition, a small supersonic region occurred near the airfoil leading edge at Mach 0.4 and appreciably reduced the magnitude of the suction peak and force coefficient augmentation induced by unsteady separation.

In a recent investigation, Freymuth (1989) suggested prolonging the lift enhancements produced by unsteady separation through the use of separation control. To effect separation control in this study, the leading portion of an airfoil was replaced by a rotating cylinder. This rotating nose suppressed vorticity generation near the leading edge and inhibited dynamic stall near the leading edge while permitting the dynamic separation of vorticity from the trailing edge. As the modified airfoil was dynamically pitched to high angle at a nondimensional rate of 0.4, flow visualization showed that flow remained attached over a significant portion of the airfoil chord, even after pitching had

ceased. Also noteworthy was the absence of any leading edge vortex, although a prominent trailing edge vortex was generated.

This historical review has concentrated upon circumstances wherein airfoil temporal variation in pitch angle can be characterized as a sinusoid or ramp. Review of representative literature pertaining to this topic area reveals a broad and rapidly expanding knowledge base. However, substantial deficiencies exist in certain areas of this body of knowledge.

Several studies have employed flow visualization to document unsteady separated flow fields. However, few of these studies have examined a broad parameter range. In addition, researchers generally have failed to capitalize upon the discrete nature of unsteady separated flow fields, wherein distinct vortical structures are produced and reside which are particularly amenable to quantitative characterization. As such, for the most part, leading edge vortex kinematics have not been quantitatively characterized for a consistent set of circumstances over a broad parameter range.

Balances and load cells have been used to dynamically sense the forces and moments which a pitching airfoil generates due to unsteady separation. Such techniques have permitted direct determination of aerodynamic coefficients over a broad parameter range, and have facilitated assessment of application potential for chosen configurations undergoing specific kinematics. However, studies such as these have yielded minimum insight into the complex fluid dynamic mechanisms which give rise to the observed forces and moments. Force and moment coefficients have also been obtained through the use of pressure instrumented airfoils. While this method does record the signature of the leading edge vortex as it convects down the airfoil, it fails to reveal many

of the interactions responsible for leading edge vortex development and unsteady separation in general.

Anemometry, on the other hand, has been used to quantify fluid velocities in the unsteady separated flow field. However, the single point nature of these measurements and the difficulties inherent in velocity measurement on a pitching airfoil have conspired to set practical limits on the number of such measurements which can reasonably be performed. Accordingly, little anemometric data has been collected either in the boundary layer or in the potential flow region farther above the airfoil.

Focus of Current Experiments

Few studies have encompassed a wide parameter range and concentrated upon the crucial role of the leading edge vortex. Further, many investigations have not employed complementary measurement techniques or data reductions designed to characterize leading edge vortex behavior and reveal the part it plays in unsteady flows.

To better understand the physics responsible for unsteady separation, the current investigation considered the relatively simple circumstance of a flat plate pitching sinusoidally in a constant velocity freestream. A flat plate, compared to a conventional airfoil, focuses variations in static pressure nearer the leading edge and reduces the magnitude of these variations along the chord (McCullough and Gault, 1951). Sinusoidal pitching in a constant velocity freestream has been shown to elicit flow fields which are relatively well-behaved with regard to variations in reduced frequency parameter and mean pitch angle (Robinson and Luttges, 1984). Within the predominantly two-

dimensional region of the flow field along the plate centerline, flow visualization documented the kinematics of the leading edge vortex for reduced frequencies of 0.25, 0.5, 1.0, 2.0 and 3.5, and for mean pitch angles of 0, 5, 10, 20, 30 and 40 degrees. To satisfy the detailed examination of these parameters, pitch amplitude was held constant. Reynolds number was also held constant, since previous work has demonstrated that Reynolds number exercises minimal influence on the character of unsteady separation (Carr et al., 1977; Robinson, 1985). This portion of the study was designed to characterize leading edge vortex initiation, convection and growth. An intuitive physical model was invoked which attributed leading edge vortex behavior primarily to the influence of the overrunning freestream and attenuation of this influence by the inclined plate.

Inconsistencies between this model and experimental observations led to the conclusion that leading edge vortex development was significantly affected by influences originating in the boundary layer adjacent to the plate. To quantify the contribution of viscous interactions, particularly reverse flows, to leading edge vortex kinematics, surface hotwire anemometry was employed at reduced frequencies of 0.25, 0.5, 1.0 and 2.0, and at mean pitch angles of 0, 5, 10 and 20 degrees. Detailed data reductions involving both flow visualization and hotwire anemometry data were employed to clarify the physics responsible for leading edge vortex initiation, convection and growth.

CHAPTER III

VORTEX STRUCTURE

Introduction

The phenomenon of unsteady separation is universally characterized by the initiation and development large scale vortical structures in the neighborhood of a solid body. Presence of such structures is associated with radical alterations to the pressure distribution upon the body hosting the vortex which, in turn, subjects the body to greatly amplified aerodynamic forces and moments. Depending upon the circumstances surrounding the occurrence of unsteady separation, these amplified forces and moments may be considered beneficial or detrimental.

Exploitation of potential benefits or alleviation of possible detriments relies heavily upon understanding the physics responsible for unsteady separation. Since the leading edge vortex (LEV) is a prominent flow field entity, the role played by this structure may plausibly be presumed major and pivotal. In Chapter 4, vortex kinematics will be characterized in detail and some simplified fluid dynamic mechanisms will be postulated to account for these kinematics. Chapter 5 will systematically examine the contribution of surface flows to the observed kinematics.

Both vortex kinematics and surface flow data gathering were restricted to the centerline of the oscillating plate. In this region of the flow field, fluid

dynamic interactions and visualization of them were presumed simpler due to the minimization of three-dimensional effects. However, three-dimensionality has been shown to significantly influence unsteady separated flow field development (Adler and Luttges, 1985; Ashworth and Luttges, 1986; Freymuth, 1988c). Furthermore, in any unsteady flow field, observable streaklines are generally not coincident with streamlines (Prandtl and Tietjens, 1934). Thus, streakline behavior may not yield an accurate impression of the time varying velocity field. However, streaklines can accurately portray vorticity fields resulting from unsteady separation.

The investigations described in this chapter were designed to assess the role of three-dimensionality in flow field development and to validate the accuracy with which flow visualization portrayed the unsteady velocity field. Spanwise flow visualization using a novel smokewire technique confirmed the predominance of two-dimensionality in the vicinity of the plate centerline. In addition, hotwire anemometry corroborated the accuracy with which flow visualization indicated the position and spatial extent of leading edge vortices.

Experimental Methods

Experiments were conducted in the 40.6 cm x 40.6 cm wind tunnel at the University of Colorado. Unsteady separated flow in the vicinity of an oscillating flat plate was investigated using two different techniques of smoke-wire flow visualization in addition to hotwire anemometry. The flat plate was fabricated from solid aluminum, measured 30.5 cm x 15.2 cm x 0.64 cm, and had sharp leading and trailing edges.

Two test section configurations were employed in these tests. In the

first, the plate was centered in the unmodified test section, leaving 5.1 cm gaps between the ends of the plate and the test section walls. In the second configuration, the gap between the test section back wall and the plate end was closed by shortening the mounting shaft. A clear acrylic splitter plate measuring 122.0 cm x 40.6 cm x 0.64 cm, and having sharp leading and trailing edges was then installed in the test section parallel to the original walls. Longitudinal placement was such that the splitter plate leading edge was 30.5 cm upstream of the oscillating plate leading edge. Lateral orientation narrowed test section width to match the span of the oscillating plate, resulting in a sliding fit between the ends of the oscillating plate and the vertical surfaces at each end of the span.

The oscillating plate was mounted, at the quarterchord, on a 1.27 cm diameter steel shaft projecting through a flange mounted on the back wall of the test section. When viewed through the cast acrylic front wall and ceiling of the test section, this mounting configuration provided unobstructed visibility. Plate oscillation was driven by a gearmotor coupled to the mounting shaft through a crank linkage that allowed adjustments for both oscillation amplitude and mean pitch angle (MPA). A small disc magnet embedded in the rim of the linkage flywheel briefly closed a reed switch once for each flywheel revolution. A delay circuit furnished a time reference for any phase angle of the associated oscillatory motion.

Hotwire anemometry data was gathered using a Zenith model 241 microcomputer equipped with a model R1000 Rapid Systems 4x4 Digital Oscilloscope Peripheral. The Rapid Systems R1000 is capable of simultaneous data acquisition on four channels at sampling frequencies of up to 0.5 MHz,

with an analog bandwidth of 250 KHz. For this experiment, two channels were used, each of which was sampled at 2 KHz. The first channel took the linearized hotwire anemometer signal, while the second accepted the trigger pulse generated by the signal conditioning unit upon reed switch closure. Raw data from these two channels were stored on floppy disks for later reduction using Basic routines hosted on the Zenith microcomputer.

To minimize flow intrusion while retaining rigidity, the hotwire anemometer probe body was constructed of 1.65 mm outside diameter stainless steel hypodermic tubing and was 15.0 cm long. At the probe volume end, a pair of 0.30 mm diameter stainless steel needles bent at right angles projected 1.50 cm beyond the end of the hypodermic tubing to hold the hotwire element parallel to the probe body. For taking measurements, this probe was supported, parallel to the plate span, on a 0.35 cm in diameter steel mast, the lower end of which terminated in a 5 cm x 5 cm x 0.13 cm thick plate. This plate was affixed to the airfoil surface near the end of the plate span using double sided tape, which placed the probe element volume in a plane orthogonal to the oscillation axis and coincident with the airfoil centerline.

The hotwire element was constructed of 10 percent rhodium-platinum Wollaston wire having an element 5 microns in diameter. This probe element was operated in conjunction with a constant temperature hotwire anemometer unit equipped with a linearizing circuit. Overheat resistance ratio was set at 20 percent, which rendered the anemometer sensitive to flow speed variation and yielded acceptable resistance to element failure.

For visualization, smoke was introduced into the flow using a 0.013 cm diameter tungsten smoke wire successively mounted in two different

configurations. In the first configuration, the smokewire was mounted directly on the flat plate airfoil. The wire was stretched parallel to, and 0.25 cm ahead of, the plate leading edge over the 30.5 cm span. In the second configuration, the smokewire was stretched vertically along the test section centerline, approximately three chordlengths upstream of the oscillating plate leading edge. In either configuration, smokewire Reynolds number did not exceed 15.

In both configurations, the smokewire was lightly coated with a mixture of Rosco theatrical fog fluid and motor oil. Following a delay sufficient to allow the mixture to bead up on the wire, an electric current was passed through it. The resultant ohmic heating vaporized the mixture, yielding a dense, homogeneous sheet of smokelines lasting approximately three seconds. The smokelines were illuminated by a pair of high-intensity, stroboscopic arc-lamps having a seven microsecond flash duration. Stroboscopic illumination of the streaklines was phase-locked to plate oscillation, thus enabling the use of multiple-exposure photography (typically 4 to 6 exposures) to assess flow field structure reproducibility. The flowfield thus visualized was photographed through the test section side wall for the vertical wire configuration and through the ceiling in the horizontal wire configuration.

Top views of the leading edge vortex visualized using the horizontal smokewire were subjected to qualitative analysis, only. However, two quantities were measured from the vertical wire visualization for comparison with hotwire anemometry results. The first of the two was the height of the leading edge vortex core above the plate surface. The core was defined as the approximately circular region sparsely marked by, or apparently devoid of, visualizing medium and surrounded by diffuse smoke. The second of these two quantities was the

height of the outermost encircling streakline above the plate. The outermost encircling streakline was defined as the streakline farthest removed from the core which encircled a sufficient portion of the leading edge vortex circumference to apparently contact the plate surface in the vicinity of the vortex lower circumference.

Results

Spanwise Visualization of the Leading Edge Vortex

Spanwise visualization of the leading edge vortex using the horizontal smokewire was performed to ascertain the presence and extent of three-dimensionality in the unsteady flow field, and to assess the contribution of this three-dimensionality to leading edge vortex kinematics. To identify those leading edge vortex behaviors attributable to three-dimensionality, the flow circumstance obtained by installing the splitter plate in the test section was adopted as a two-dimensional reference. Reduced frequencies of 1.0 and 2.0, both at mean pitch angles of 10 degrees and oscillation amplitudes of 10 degrees, were judged representative of the parameter space which will be more extensively characterized in Chapters 4 and 5 using only the vertical smokewire in a test section having no splitter plate. All tests described in this chapter were conducted at a test section velocity of 5.0 ft/sec, corresponding to a Reynolds number based on plate chordlength of 13,000.

Top views of spanwise visualization using the horizontal smokewire are presented in Figures 3-1 through 3-4. Each sequence is composed of ten frames, wherein the plate undergoes a four degree pitch angle change from one frame to the next. In the left hand column, the uppermost frame (frame 1)

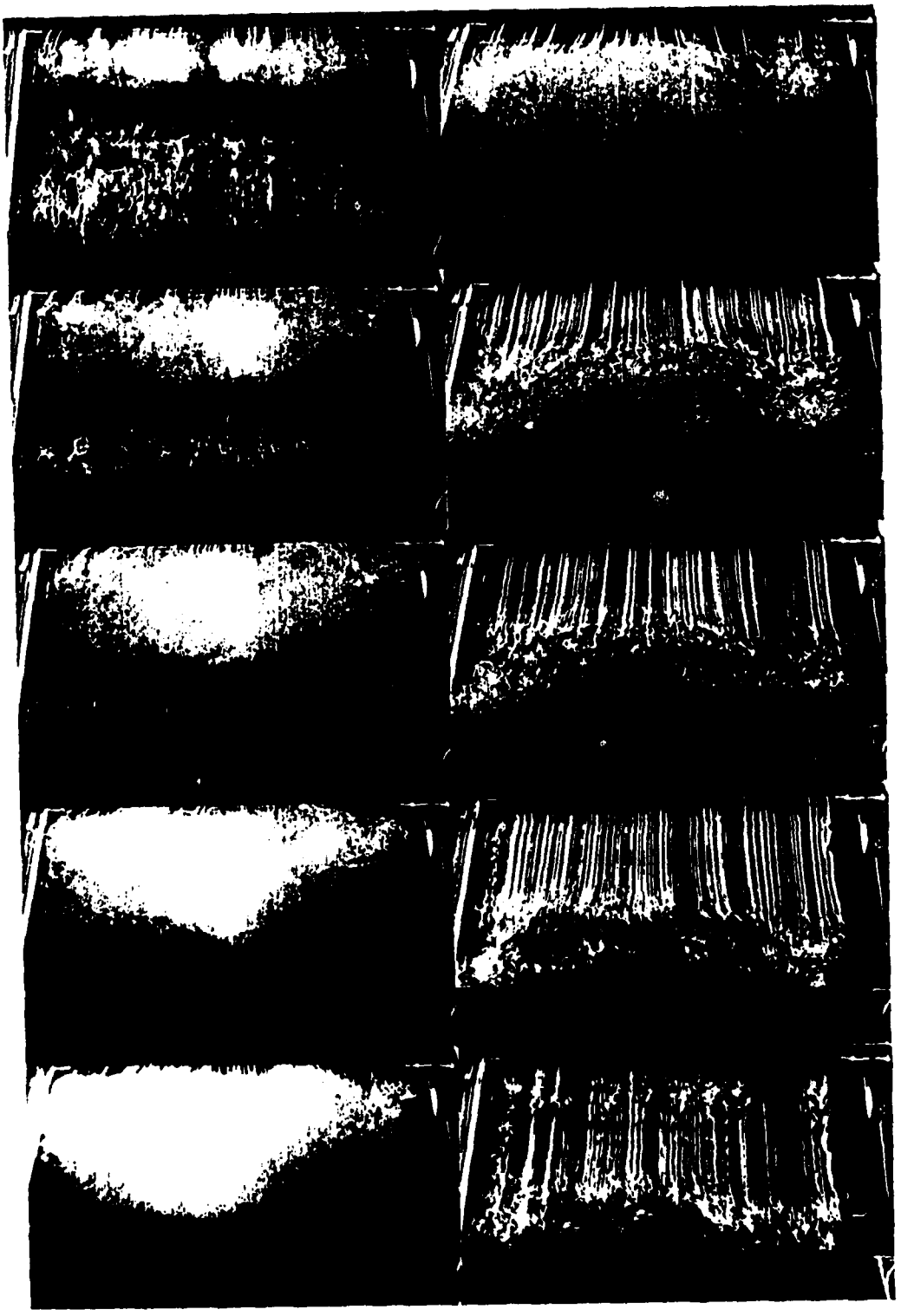

Figure 3-1. Top view of leading edge vortex development for K = 1.0, MPA = 10 degrees. Splitter plate installed in test section.

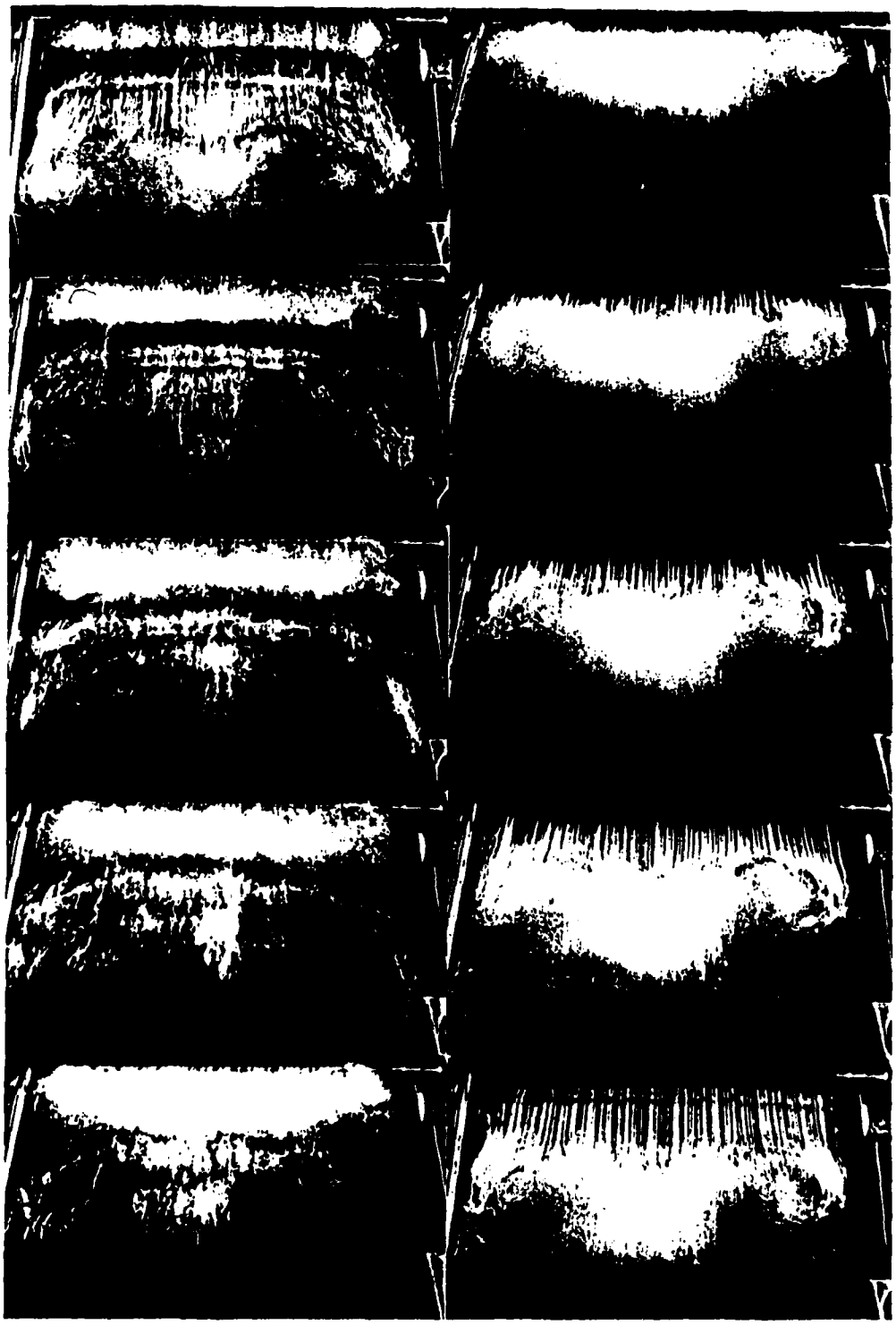

Figure 3-2. Top view of leading edge vortex development for K = 2.0, MPA = 10 degrees. Splitter plate installed in test section.

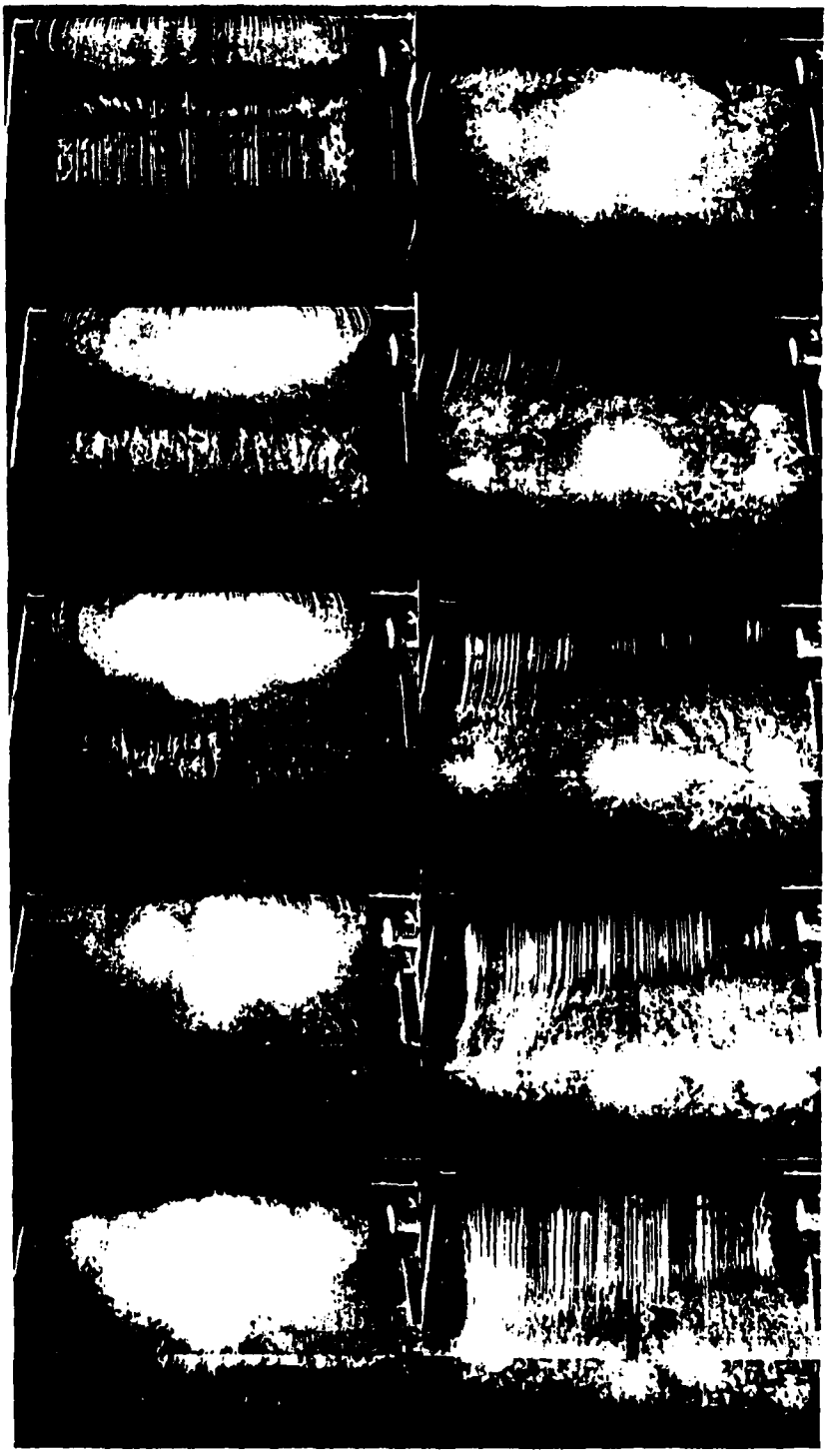

Figure 3-3. Top view of leading edge vortex development for K = 1.0, MPA = 10 degrees. Splitter plate removed from test section.

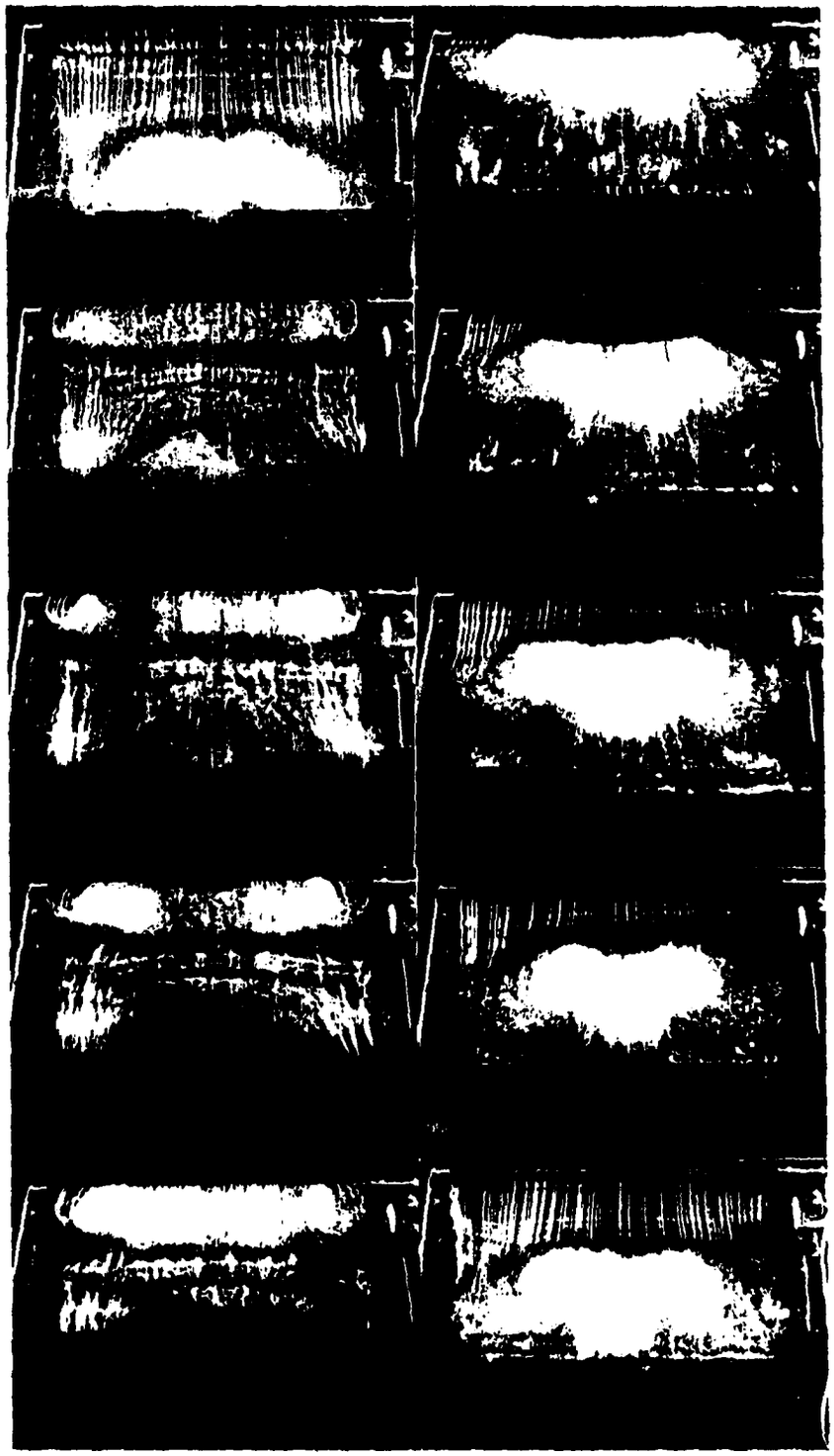

Figure 3-4. Top view of leading edge vortex development for K = 2.0, MPA ≈ 10 degrees. Splitter plate removed from test section.

corresponds to maximum upward pitch angle with the remaining frames (frames 2 through 5) in the column representing downward pitching. The top frame in the right hand column (frame 6) depicts the plate at maximum downward pitch angle, and subsequent frames (frames 7 through 10) document upward pitching motion. In each individual frame, the plate leading edge is near the top of the frame, with freestream proceeding from the top of the frame to the bottom.

Figure 3-1 shows a top view of leading edge vortex development for a reduced frequency of 1.0 and mean pitch angle of 10 degrees, with the splitter plate installed in the test section. Leading edge vortex presence is first apparent in frame 9 as an arching of the streaklines over approximately the first 10 percent chord. These arched streaklines retain integrity in the leading edge vortex vicinity, defining a vortex cross-section which is uniform along the span of the plate. In frame 10, streaklines in the downstream portion of the vortex begin to lose integrity. Leading edge vortex cross-section has grown, but appears to taper off in the outboard 10 percent of the plate span. In frames 1 and 2, the leading edge vortex is marked by dense, homogeneous smoke, except in the upstream portion of the vortex. Here, streaklines are seen to retain integrity prior to being rendered diffuse. Vortex cross-section continues to grow and remains generally uniform along the plate span, tapering over approximately the outboard 10 percent span of the plate.

In frames 3 through 5, vortex cross-section grows still larger, continues to be marked by dense, homogeneous smoke and tapers over approximately the outboard 10 percent of span. However, the vortex cross-section ceases to be generally uniform along the plate span. Instead, this uniformity is interrupted by two bulbous excrescences for which no internal structure is visible. In

frame 3, each of these perturbations is centered approximately 30 percent span inboard of the plate end and migrates toward the plate centerline in subsequent frames. In frame 5, these bulbous structures reach a location approximately 40 percent span inboard of the plate ends and begin to encroach upon the flow along the plate centerline which had previously appeared two-dimensional. The centroid of the leading edge vortex cross-section at the plate centerline is located at approximately 80 percent chord in frame 5. In frame 6, the leading edge vortex begins to be only sparsely marked by diffuse smoke, precluding further characterization.

Figure 3-2 shows a top view of leading edge vortex development for a reduced frequency of 2.0 and mean pitch angle of 10 degrees, with the splitter plate installed in the test section. The leading edge vortex is initially seen in frame 9 in the form of arched streaklines over approximately the first 5 percent chord. These arched streaklines retain integrity in the leading edge vortex vicinity and show uniform a vortex cross-section across the plate span. In frame 10, leading edge vortex cross-section has grown and continues to be uniform along the span length. The integrity of streaklines in the vortex vicinity also continues to be preserved.

In frames 1 through 5, the leading edge vortex tends to be marked by dense, homogeneous smoke, except in the upstream portion of the vortex. Here, streaklines retain integrity prior to being rendered diffuse. Vortex cross-section continues to grow, remaining generally uniform along the plate span and showing no tendency to taper toward the outboard region of the plate. This uniformity in leading edge vortex cross-sectional is, however, disrupted by the appearance in frame 1 of bulbous excrescences in the vortex at approximately

20 percent span inboard of the plate ends. Over the following four frames, these structures grow in size while the apparent structure area centroids remain approximately 20 percent span from the plate ends. In frames 1 through 5, no internal structure can be seen for these excrescences.

In frames 6 through 10, leading edge vortex cross-section grows still larger and continues to be marked by dense, homogeneous smoke. The excrescences contained in the vortex structure also continue to grow and migrate from 20 percent inboard of the plate end in frame 6, to nearly 30 percent in frame 10. In so doing, they encroach upon the apparently two-dimensional flow near the plate centerline. However, as the leading edge vortex passes the plate trailing edge, two-dimensional flow around the plate centerline appears to be preserved in a region which is approximately 25 percent span wide. During this time, the perturbations occurring in the leading edge vortex reveal a pronounced rotational character.

Figure 3-3 shows a top view of leading edge vortex development for a reduced frequency of 1.0 and mean pitch angle of 10 degrees, with the splitter plate removed from the test section. The leading edge vortex is first observed in frame 10. At this time in the cycle, the streaklines maintain integrity over much of the leading edge vortex circumference, and show minor loss of cohesiveness only in the downstream portion of the vortex. Leading edge vortex cross-section appears uniform across the span except near the ends of the plate, where vortex cross-section appears to taper beginning approximately 10 percent span inboard of the ends of the plate. In frame 1, the leading edge vortex cross-sectional area has grown over much of the central span, but the tapering now extends inboard from the plate ends approximately 20 percent

span. Streaklines now lose cohesiveness approximately half way over the vortex circumference.

In frames 2 through 5, vortex cross-sectional area continues to grow, but this growth is confined to progressively narrower regions of the span as the tapering effect observed previously advances farther inboard. Also present, but smaller than when the splitter plate was installed, are excrescences in the leading edge vortex. Although the visualization reveals no inner detail in these structures, migration of these structures toward the plate centerline is evident. In frame 5, with the leading edge vortex area centroid has reached the 73 percent chord station. At this point in the cycle, progressive vortex cross-section tapering and excrescence inboard migration inboard have conspired to nearly disrupt two-dimensional flow along the plate centerline. Following frame 5, smoke visualizing the leading edge vortex is too diffuse to permit further analysis.

Figure 3-4 shows a top view of leading edge vortex development for a reduced frequency of 2.0 and mean pitch angle of 10 degrees, with the splitter plate removed from the test section. The leading edge vortex is first evident in frame 1, where the streaklines tend to retain integrity over much of the vortex circumference and lose cohesiveness only near the downstream portion of the vortex. Vortex cross-sectional area appears constant across a major portion of the span, but begins to taper approximately 10 percent inboard of the plate ends.

In frames 2 through 5, leading edge vortex cross-sectional area grows steadily, the vortex no longer being marked by discrete streaklines but by dense, homogeneous smoke instead. During this time period, tapering of the leading

edge vortex cross-section progress inboard to approximately 20 percent span inboard of the plate ends. Also during this portion of the cycle, the vortex excrescences which are first evident in frame 2 at approximately 20 percent span inboard of the plate ends, grow in size and migrate inboard toward the plate centerline. In frame 5, these structures are located approximately 30 percent inboard of the plate ends.

In frame 6, both the vortex and the excrescences within it have continued to grow perceptibly. In addition, flow visualization now reveals a rotational internal structure within the excrescences. The effect of vortex tapering combined with that of excrescence growth and inward migration has left a region of apparently two-dimensional flow in the plate center which is approximately 30 percent span wide and centered about the plate centerline. In frames 7 through 10, this two-dimensional region narrows as the excrescences continue to grow and migrate inward toward the plate centerline. In frame 10, just prior to the leading edge vortex passing the trailing edge, these structures have reached a location which is approximately 40 percent span inboard of the plate ends. At this time, the region of two-dimensional flow in the plate center extends outward approximately 10 percent on either side of the plate centerline.

Figures 3-5 and 3-6 exhibit histories of leading edge vortex chordwise position and cross-sectional area, respectively. For both of these graphs, zero radians corresponds to maximum upward pitch angle. Reduced frequencies of 1.0 and 2.0, both at a mean pitch angle of 10 degrees, were investigated, first in the unmodified test section and then in conjunction with the splitter plate. The resulting flow field was visualized using a smokewire stretched vertically in a plane parallel to the test section centerline and which passed through the plate

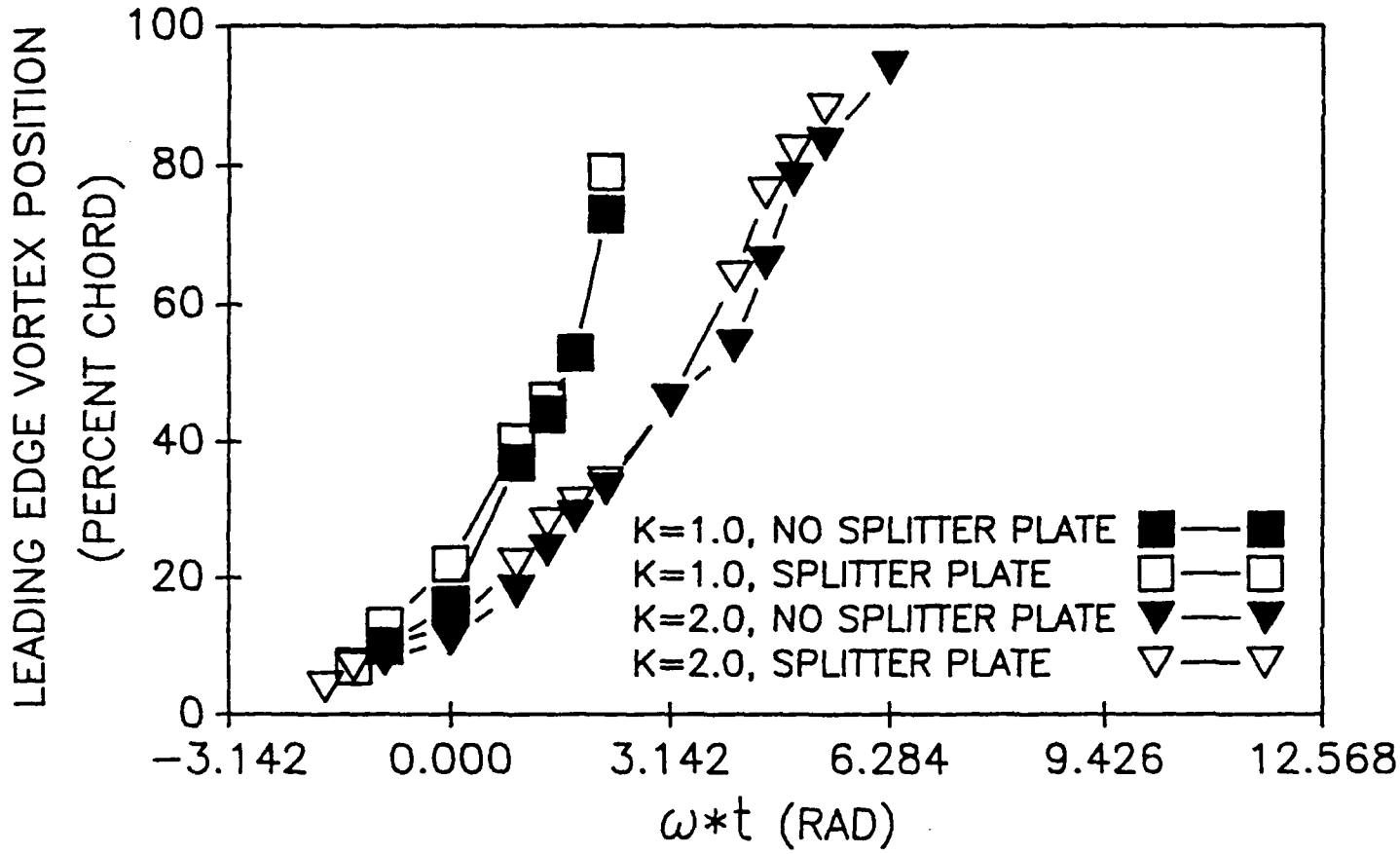

Figure 3-5. Leading edge vortex chordwise position histories for K = 1.0 and 2.0, MPA = 10 degrees. Test section with and without splitter plate.

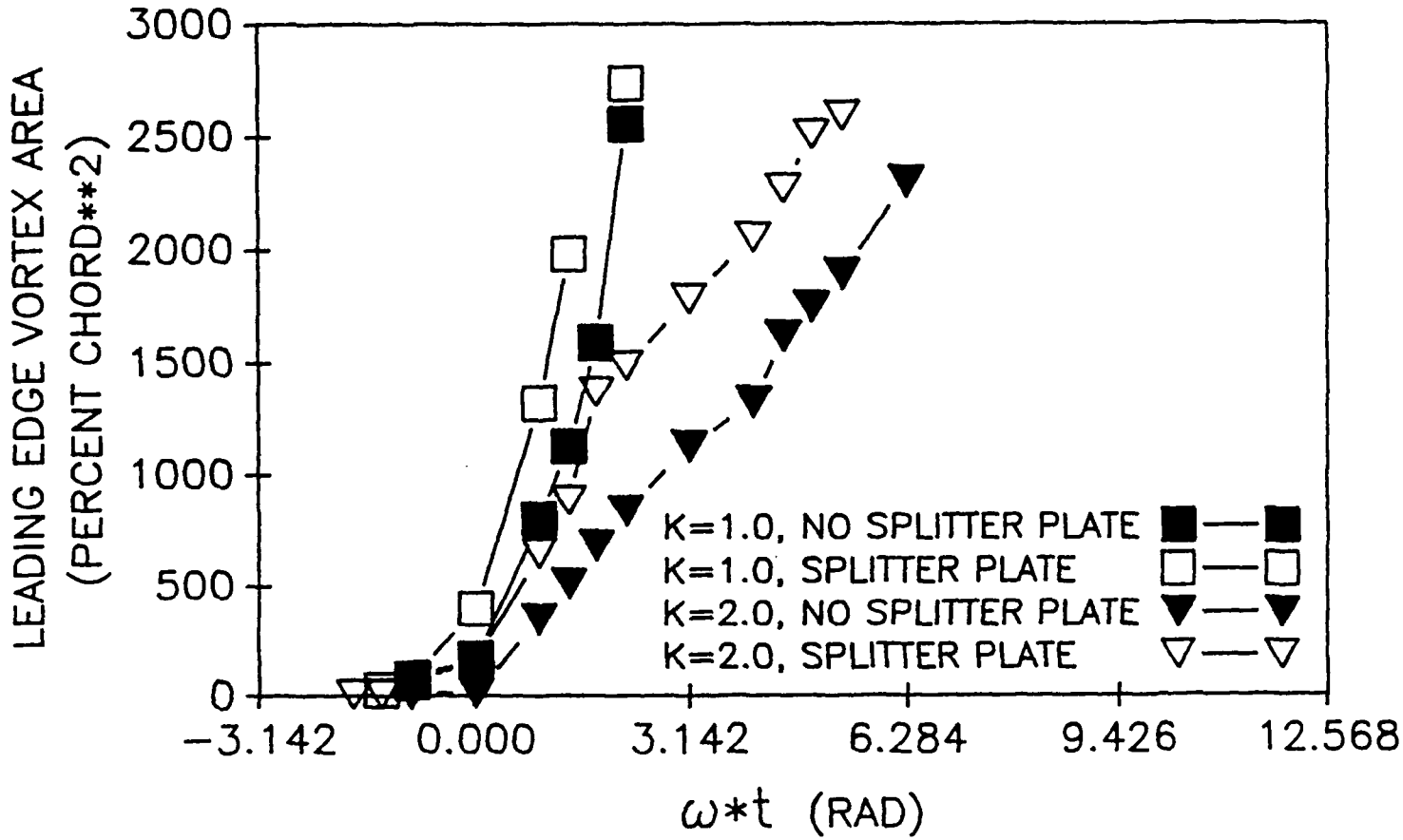

Figure 3-6. Leading edge vortex cross-sectional area histories for K = 1.0 and 2.0, MPA = 10 degrees. Test section with and without splitter plate.

centerline.

For both reduced frequencies dealt with in Figure 3-5, introduction of the splitter plate prompted leading edge vortex initiation 19 milliseconds (corresponding to 6 and 12 percent of the oscillation cycle for reduced frequencies of 1.0 and 2.0, respectively) earlier in the cycle and 3 percent chord farther forward on the plate than was recorded for the same parameter values in the unmodified test section. Following initiation, vortex convection was such that, at a given time in the pitching cycle, the leading edge vortex was observed farther back on the plate for the splitter plate case than for the unmodified test section.

A linear least squares fit was applied to the data in Figure 3-5 to determine the leading edge vortex average convection velocity. For a reduced frequency of 1.0, this convection velocity was found to be 38.8 percent of freestream in the absence of the splitter plate and 37.1 percent of freestream when the splitter plate was installed. For a reduced frequency of 2.0, average convection velocity was determined to be 51.2 percent of freestream in the unmodified test section and 47.5 percent of freestream with the splitter plate in place.

Figure 3-6 shows leading edge vortex growth histories for reduced frequencies of 1.0 and 2.0, both at a mean pitch angle of 10 degrees. As with the convection histories in Figure 3-5, these test conditions were repeated twice, once with the splitter plate in the test section and once without. Information concerning time of leading edge vortex initiation in Figure 3-6 is identical to that contained in Figure 3-5. However, in Figure 3-6, information regarding chord station at which initiation occurred has been replaced by vortex cross-

sectional area just following initiation. After vortex initiation, Figure 3-6 shows that, for any specific time during the pitching cycle, leading edge vortex cross-sectional area is consistently greater when the splitter plate is installed in the test section.

A linear least squares fit was applied to the vortex area histories displayed in Figure 3-6 to determine the leading edge vortex average growth rate. For a reduced frequency of 1.0, average cross-sectional area growth rate was 14,818 percent chord squared per second in the unmodified test section and 15,642 percent chord squared per second when the splitter plate was installed. For a reduced frequency of 2.0, average vortex growth rate was determined to be 13,241 percent chord squared per second in the absence of the splitter plate and 15,893 percent chord squared per second with the splitter plate in place.

Spanwise visualization showed that leading edge vortex tapering as well as excrescence growth and migration rendered the vortex three-dimensional progressively farther inboard as it convected. However, three-dimensionality never encroached upon the vortex in the plate centerline region until the vortex had convected past the three-quarter chord station. Using the centerline visualization technique employed to obtain the data which will be presented in the following chapters, leading edge vortex kinematics along the plate centerline were compared for the two and three-dimensional cases. This comparison showed that vortex initiation, convection and growth were not significantly different for the two and three-dimensional circumstances.

Anemometric Corroboration of Visualization

For purposes of anemometric characterization of the leading edge

vortex, reduced frequencies of 1.0 and 2.0, and a mean pitch angle of 20 degrees were chosen as representative of the parameter space to be dealt with in Chapters 4 and 5. Hotwire anemometry was used to measure velocities within the leading edge vortex as the core passed through 20, 40, 60 and 80 percent chord stations. Velocity measurements were performed at 0.25 cm increments along a line perpendicular to the plate surface and passing through the plate center line at each of these four chord stations.

Each of Figures 3-7 through 3-10 contains flow visualization photographs and corroborative hotwire anemometry for reduced frequencies of 1.0 and 2.0, both at a mean pitch angle of 20 degrees. Heights of the vortex core and of the outermost streakline encircling the vortex have been measured from the visualization photographs and transferred to the corresponding anemometric data plots.

Figures 3-7 and 3-8 contain vortex velocity profiles which exhibit considerable qualitative similarity. Beginning just above the plate surface, flow velocity begins to decline in nonlinear fashion, decreasing at a progressively greater rate as height above the plate rises. This trend continues until a minimum velocity between 10 and 60 percent of freestream is reached. Then, velocity increases with height in a manner which is approximately linear, until a maximum velocity which is greater than twice freestream velocity is attained. Subsequent height increases bring velocity decreases which assume a decidedly nonlinear character, with height increases being associated with ever smaller decreases in velocity.

In Figures 3-7 and 3-8, flow visualization indicates that the leading edge vortex possesses a strongly circulatory character. Close correspondence

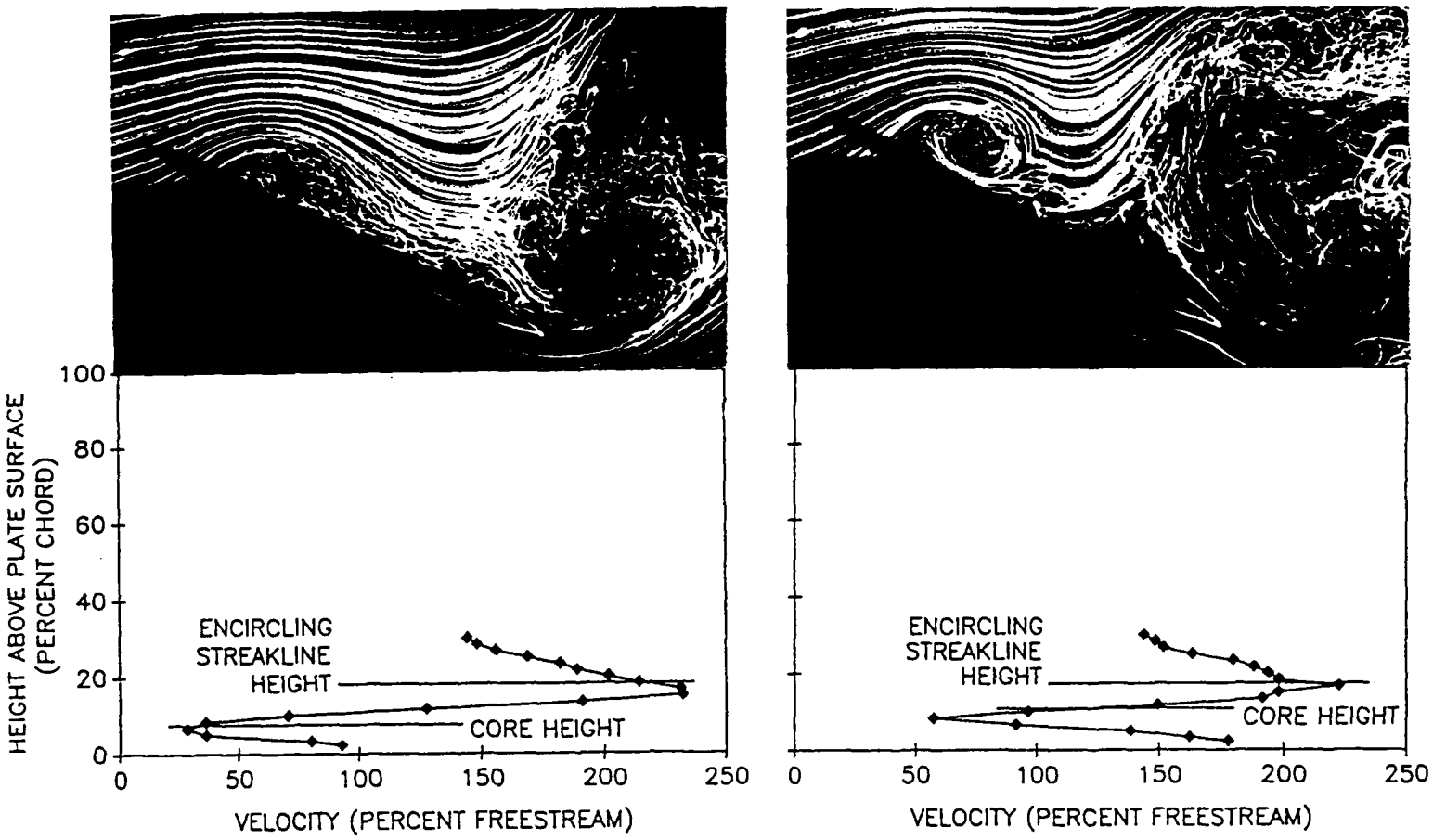

Figure 3-7. Flow visualization and vertical velocity profile for leading edge vortex located at 0.20 chord. K = 1.0, MPA = 20 degrees (left side) and K = 2.0, MPA = 20 degrees (right side).

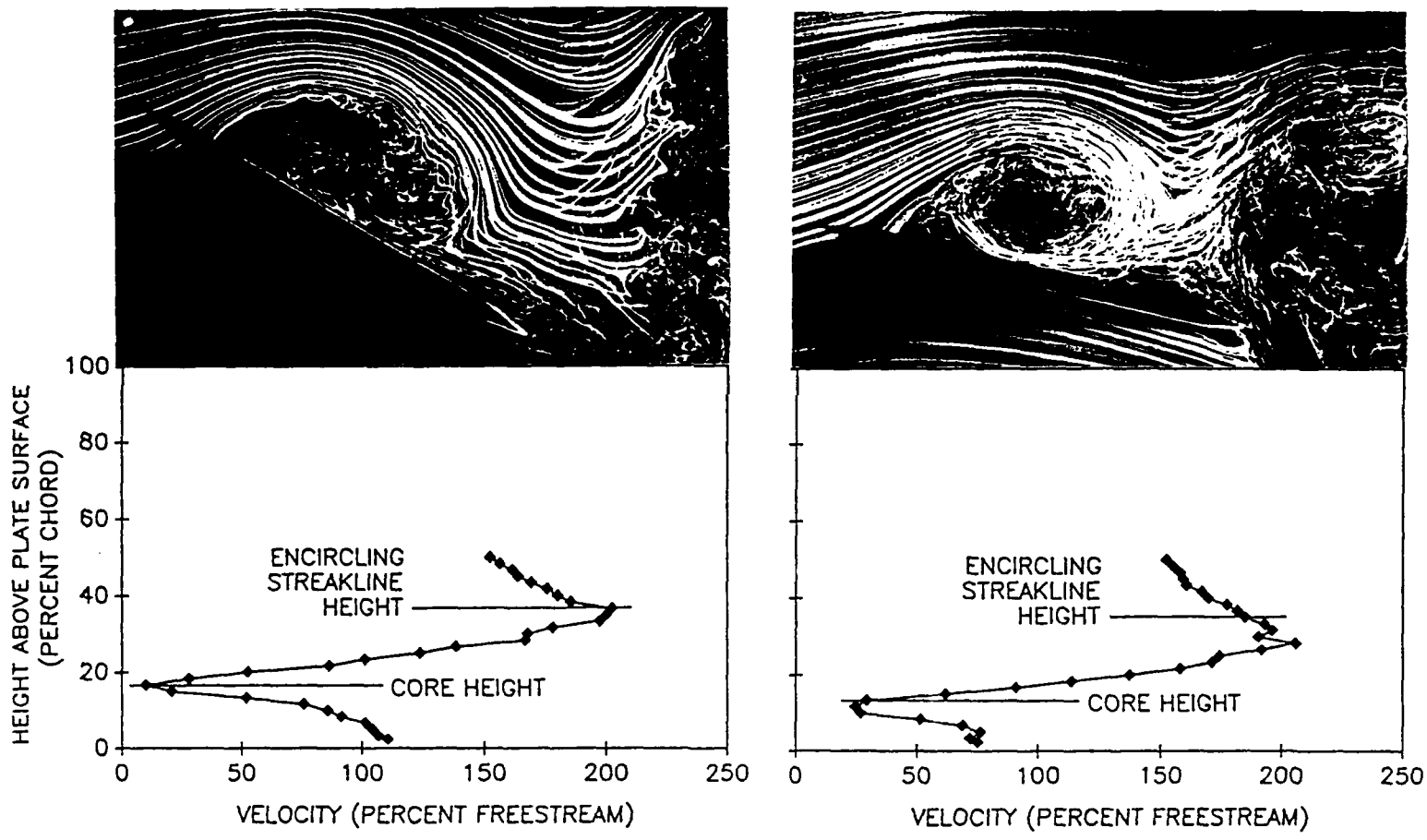

Figure 3-8. Flow visualization and vertical velocity profile for leading edge vortex located at 0.40 chord. K = 1.0, MPA = 20 degrees (left side) and K = 2.0, MPA = 20 degrees (right side).

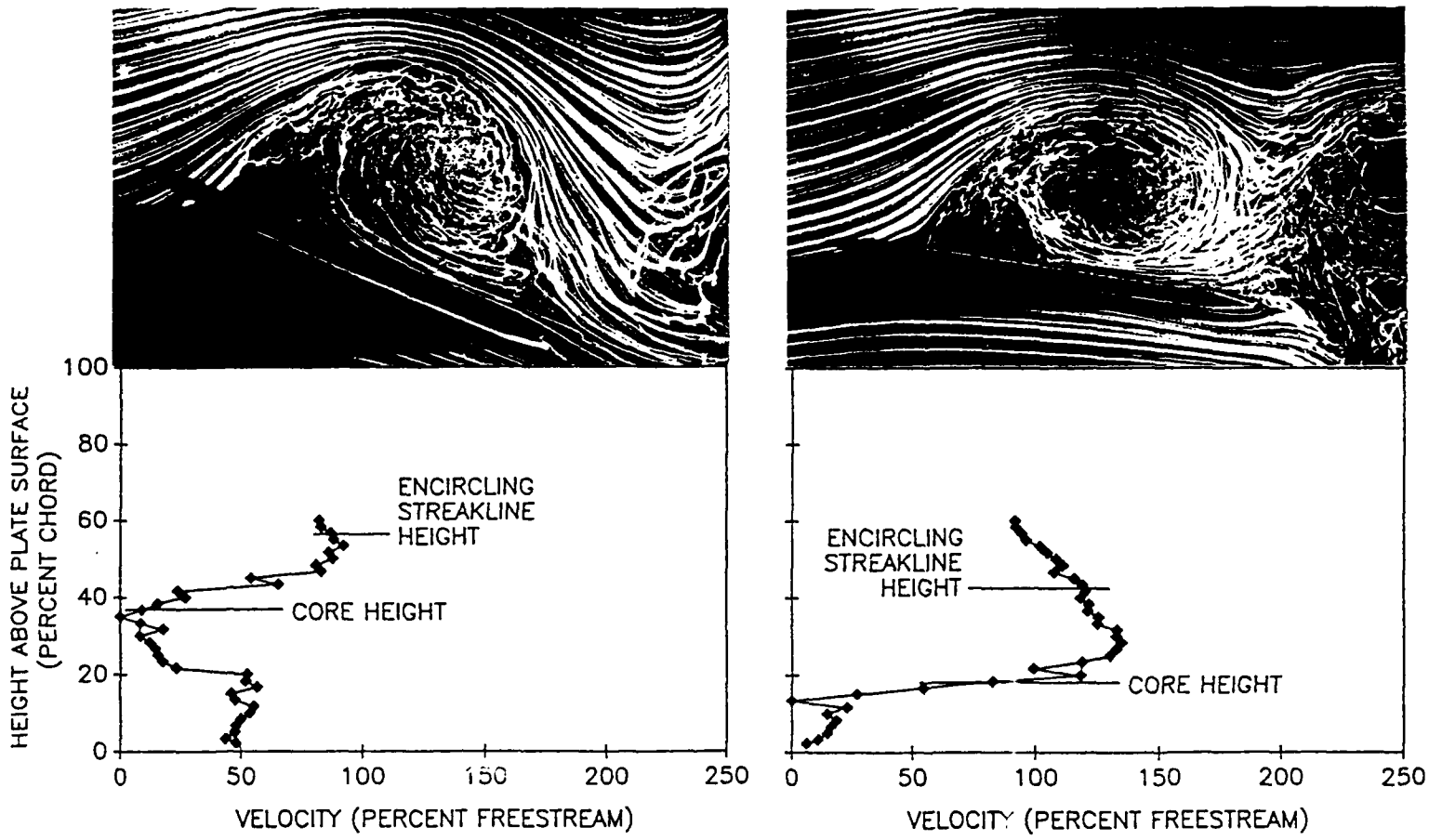

Figure 3-9. Flow visualization and vertical velocity profile for leading edge vortex located at 0.60 chord. K = 1.0, MPA = 20 degrees (left side) and K = 2.0, MPA = 20 degrees (right side).

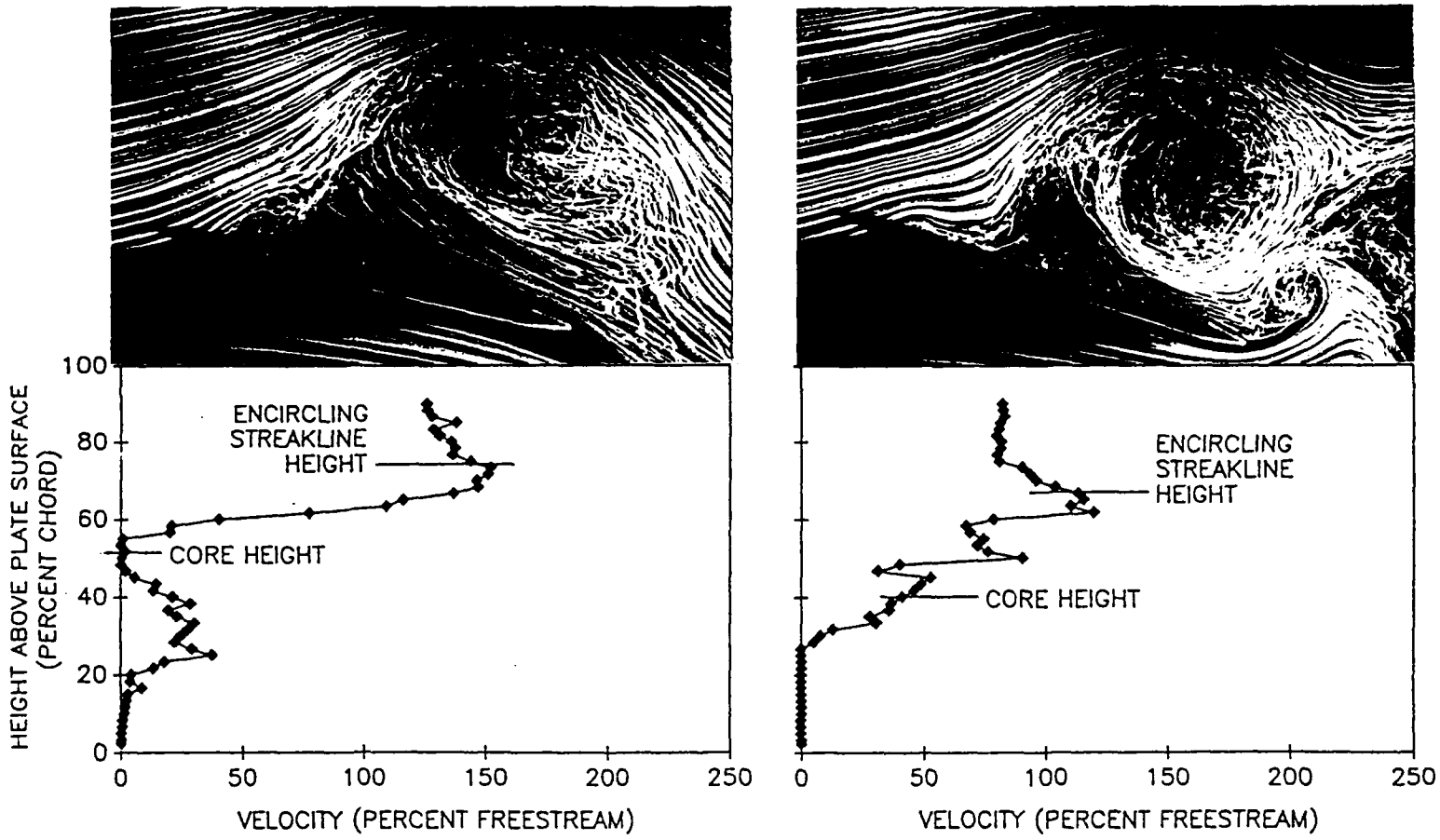

Figure 3-10. Flow visualization and vertical velocity profile for leading edge vortex located at 0.80 chord. K = 1.0, MPA = 20 degrees (left side) and K = 2.0, MPA = 20 degrees (right side).

exists between vortex core height as measured from visualization and the height of the velocity minimum observed in the anemometric velocity profiles. In these same figures, the height of the outermost encircling streakline in the visualization generally agrees well with the height of the velocity maximum which occurs in the velocity profiles.

The velocity profiles presented in Figure 3-9 differ considerably from those in Figure 3-7 or 3-8. Beginning at the plate surface, velocity remains approximately constant with rising height before decreasing to zero percent of freestream in a generally nonlinear fashion with further increases in height. After reaching zero, velocity begins to increase with greater height above the plate surface. For a reduced frequency of 1.0, this increase is not generally linear, although a linear subinterval does exist. In contrast, the velocity increase for a reduced frequency of 2.0 is strongly linear. Following attainment of maximum velocity, a decrease in velocity occurs with additional increases in height. This portion of the velocity profile is irregular and cannot be categorized as linear.

As in previous figures, flow visualization again suggests that the leading edge vortex has a strong circulatory component. For a reduced frequency of 1.0, close correspondence exists between the heights of the vortex core and the outermost encircling streakline as measured from visualization, and the heights of the velocity minimum and maximum, respectively, observed in the anemometric velocity profiles. However, for the reduced frequency of 2.0, disparities existed between these visualization and anemometric parameters.

The velocity profiles shown in Figure 3-10 display a character which is more complex than that of profiles presented previously. For the case of

reduced frequency of 1.0, velocity remains at or close to zero over the first 20 percent chord above the plate surface. Then, velocity increases with greater height, reaching a local maximum of approximately 40 percent freestream before irregularly declining once again to zero at approximately 50 percent chord above the plate surface. After attaining this minimum, velocity grows in generally linear fashion with height until velocity reaches a maximum of 150 percent freestream. The subsequent velocity decline is nonlinear and becomes progressively slower at greater height.

For the reduced frequency 2.0 case in Figure 3-10, velocity near the plate surface remains zero until a height of 30 percent chord is attained. This is followed by a nonlinear increase and then a decline to a local velocity minimum. Subsequently, velocity once again grows, this time in a linear manner, before undergoing a nonlinear decline, which is then followed by a linear increase to a maximum value of 120 percent of freestream. At this point, velocity decreases irregularly to 80 percent freestream and remains approximately constant with further height increases.

Flow visualization performed with the leading edge vortex at 80 percent chord again indicates that the vortex continues to be strongly circulatory. For the reduced frequency of 1.0 case, excellent agreement exists between the heights of the leading edge vortex core and outermost encircling streakline, and, respectively, the heights of the velocity minimum and maximum in the velocity profile. The reduced frequency of 2.0 case shows good correspondence between outermost encircling streakline height and the maximum in the velocity profile. Core height also shows reasonable spatial proximity to the least of two local minima.

CHAPTER IV

VORTEX KINEMATICS

Introduction

The processes at work in the vicinity of an airfoil undergoing unsteady separation are numerous and diverse, and interact in ways that can obscure the underlying fluid-dynamic mechanisms giving rise to the observed flow. The simultaneous temporal and spatial evolution of the unsteady flow field further hinders understanding by rendering each of several experimental variables nonlinear, discontinuous and generally ambiguous. Previous investigations have dealt with airfoils undergoing sinusoidal pitch oscillation such that reduced frequency parameter and mean pitch angle effects are known to be relatively well-behaved for sinusoidal pitching (Robinson and Luttges, 1984).

Within these investigations, however, pitching motions that carry the lifting surface through zero pitch angle remain relatively unstudied. This situation has persisted in spite of indications that the associated hysteresis and pressure influences are likely to be critical underlying factors in the genesis of unsteady flows (Francis and Keesee, 1985). In addition, most experimental studies have not encompassed a broad range of reduced frequency parameters where test results could be subjected to comparable analyses. Many studies have dealt exclusively with symmetric airfoil sections (Graham and Strickland, 1986; Helin et al., 1986; Jumper et al.,

1986; McAlister et al., 1978). Airfoils may be an impediment to physical understanding, though, because of the introduction of a prominent pressure gradient over much of the chord. The present study employed a flat plate, which, compared to an airfoil, focuses variations in static pressure nearer the leading edge and reduces the magnitude of these variations along the chord (McCullough and Gault, 1951). The flat plate was oscillated sinusoidally through zero pitch angle, for a broad range of reduced frequency parameters. Comparative evaluations included 0, 5, 10, 20, 30 and 40 degree mean pitch angles (MPA).

The current investigation corroborates the finding that high values of reduced frequency parameter yield high leading edge vortex (LEV) convection rates, and that high mean pitch angles reduce it. As with vortex convection velocity, leading edge vortex growth rate is also quite sensitive to reduced frequency parameter and mean pitch angle. Ancillary shedding structures were prominent in these tests. The interactions between forced flow field structures and those flow structures arising from inherent flow instabilities are used to aid in the physical interpretation of the initiation and development of unsteady separation. Also, the data analyses were carried out in a manner that emphasizes the specific role of underlying physical support mechanisms.

Experimental Methods

Experiments were conducted in the 40.6 cm x 40.6 cm wind tunnel at the University of Colorado. Two-dimensional, unsteady separated flow in the vicinity of an oscillating flat plate was investigated using smoke-wire flow visualization. The flat plate was fabricated from solid aluminum, measured

30.5 cm x 15.2 cm x 0.64 cm, and had sharp leading and trailing edges. The plate was mounted, at the quarterchord, on a 1.27 cm diameter steel shaft projecting through a flange mounted on the back wall of the test section. When viewed through the front cast acrylic wall of the test section, this mounting configuration provided unobstructed visibility.

The plate was driven by a gearmotor coupled to the mounting shaft through a crank linkage that allowed adjustments for both oscillation amplitude and mean pitch angle. A small disc magnet embedded in the rim of the linkage flywheel briefly closed a reed switch once for each flywheel revolution. A delay circuit furnished a time reference for any phase angle of the associated oscillatory motion.

Smoke was introduced into the flow using a 0.013 cm diameter tungsten smoke wire stretched vertically along the test section centerline, approximately three chordlengths upstream of the plate leading edge. The wire was lightly coated with a mixture of Rosco theatrical fog fluid and motor oil. Following a delay sufficient to allow the mixture to bead up on the wire, an electric current was passed through it. The resultant ohmic heating vaporized the mixture, yielding a dense, homogeneous sheet of smokelines lasting approximately three seconds. The smokelines were illuminated by a pair of high-intensity, stroboscopic arc-lamps having a seven microsecond flash duration. Stroboscopic illumination of the streaklines was phase-locked to plate oscillation, thus enabling the use of multiple-exposure photography (typically 4 to 6 exposures) to assess flow field structure reproducibility.

Quantitative raw data extracted from the multiple-exposure photographs consisted of leading edge vortex initiation time, length, height and chordwise

position, trailing edge vortex initiation time, length and height, and ancillary structure wavelength. Boundaries for both leading and trailing edge vortices were clearly defined at high values of reduced frequency parameter or elevated mean pitch angle. At these conditions, streaklines encircled a sufficient portion of the vortex perimeter to visualize the upper, lower, upstream and downstream vortex borders. In this case, length and height were measured along the major and minor axes of an approximate ellipse described by the outermost encircling streakline.

As reduced frequency parameter value or mean pitch angle decreased, the streaklines encircled progressively shorter lengths of both the leading and trailing edge vortex perimeter. In the case of the leading edge vortex, streaklines retreated from, and left unvisualized, first the upstream vortex border, then the lower border, and finally the downstream one. When no encircling streakline was present upstream or downstream, the vortex border was taken to be the outermost streakline appearing to make contact with the plate surface. In the absence of an encircling streakline at the vortex lower border, the plate surface was considered the lower vortex border. Here, vortex length and height were defined as the maximum lengths measurable, parallel and perpendicular to the plate, within the confines of the outermost streakline. In the case of the trailing edge vortex, streaklines retreated from, and left unvisualized, first the upstream vortex border, and then, infrequently, the upper border. When no encircling streakline was present at the upstream or upper border of the trailing edge vortex, these borders were visually extrapolated. As with the leading edge vortex, vortex length and height were defined as the maximum lengths measurable, parallel and perpendicular to the plate, within the

confines of the outermost encircling streakline.

Leading edge vortex chordwise position was measured relative to the vortex center. At higher reduced frequency parameter values, the leading edge vortex core was conspicuous, thus providing an unambiguous reference point for measurement. As reduced frequency parameter value decreased, the vortex core became less apparent. In the absence of a definite vortex core, the vortex center location was defined to be the approximate centroid of the vortex cross-sectional area, this area being bounded as described above. Trailing edge vortex position was not measured since this vortex remained relatively stationary in the vicinity of the plate trailing edge during development.

Ancillary vortical structure wavelength was defined to be the distance between adjacent vortical structures rotating in the same sense. This distance was measured between corresponding points on adjacent structures. If visible, the cores of the vortical structures were chosen as measurement reference points. However, any repeatable, identifiable feature common to a train or street of structures constituted a satisfactory reference point. Although flow history might have been encoded in major flow structures, the dynamic, consistent perseverance and growth of these structures from one phase angle to the next suggested that flow history was not a major contaminant in the present flow visualizations.

Results

The independent variables explored in this investigation were reduced frequency parameters of 0.25, 0.5, 1.0, 2.0, and 3.5, as well as mean pitch angles of 0, 5, 10, 20, 30 and 40 degrees. Pitch amplitude was held constant at

10 degrees above and below mean angle. Within the range of independent variables examined, the unsteady flow field induced by the oscillating flat plate remained qualitatively similar, exhibiting the same principal flow structures throughout the entire test variable range. However, the observable attributes of the individual structures, as well as spatial and temporal relationships between multiple structures and the oscillating plate, were seen to vary dramatically as independent variables changed. A quantitative description of the influence exercised by the independent variables will be deferred until later in this section. As a basis for this subsequent discussion, each of the principal flow structures briefly will be discussed.

Qualitative Descriptions of Structures

Leading edge vortices. Among the flow structures elicited in the vicinity of the plate as it underwent unsteady separation, the most prominent was the leading edge vortex. The leading edge vortex developed over approximately the first 20 percent chord, and usually just prior to plate maximum pitch angle. Consistent with previous reports, higher reduced frequency parameters delayed leading edge vortex emergence to later in the pitching cycle. In contrast, elevated mean pitch angles seemed to hasten emergence.

Details of leading edge vortex initiation and early development for a reduced frequency parameter value of 1.0, and mean pitch angles of 0 and 10 degrees, are shown in Figure 4-1. With pitch-up already having begun in the 0 degree case (left column), no significant smokeline disturbance was evident about the plate leading edge. Immediately downstream, however, the smokeline

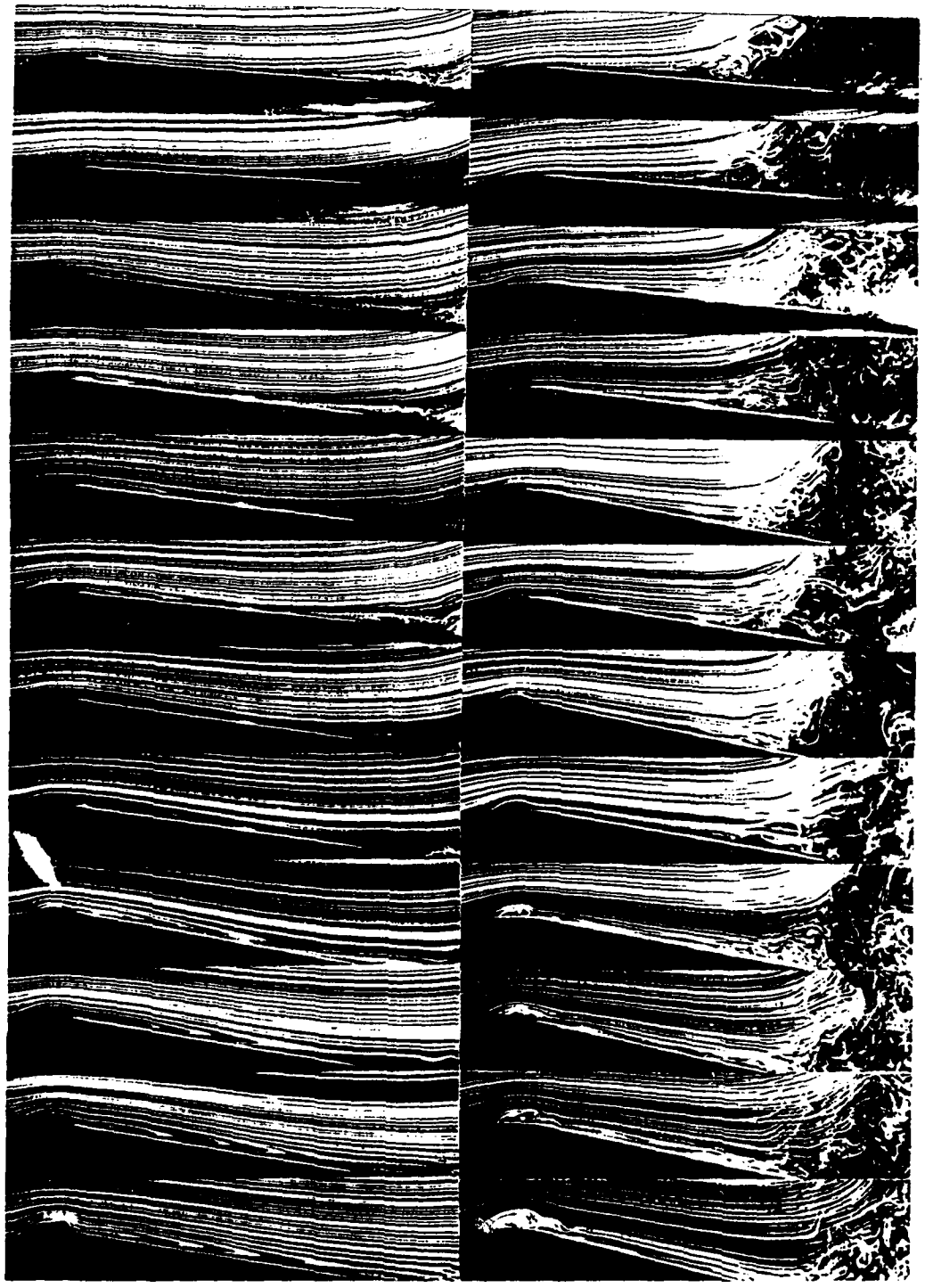

Figure 4-1. Leading edge vortex initiation for K = 1.0, MPA = 0 degrees (left column), and K = 1.0, MPA = 10 degrees (right column). Time elapsed between frames is 0.005 sec.

nearest to the plate in the leading edge region radically altered direction while maintaining integrity. This occurrence indicated the presence of reverse flow on the plate surface, and is discussed in more detail below.

Soon (subsequent frames), the smokeline closest to the plate leading edge was displaced slightly from the surface, but reapproached it a few percent chord downstream. As the plate continued to pitch up, this smokeline was driven increasingly farther from the plate. At the same time, this smokeline was drawn ever closer to the immediate downstream plate surface. As pitch-up continued, this smokeline eventually appeared to intersect the plate surface. Shortly thereafter, a well-defined vortex formed, indicating that leading edge vortex initiation had occurred.

The process of leading edge vortex initiation for the 10 degree mean angle case (right column) was qualitatively similar to that observed in the 0 degree case. The 10 degree increase in mean pitch angle, however, altered the values of several crucial physical parameters associated with the nascent leading edge vortex. Higher mean angle caused initiation to occur sooner in the oscillation cycle, and also drove the initiation site closer to the plate leading edge. In addition, increased mean angle yielded a larger, less elongated leading edge vortex.

After the leading edge vortex emerged, it began to convect away from the leading edge in a predominantly chordwise direction. Chordwise motion was accompanied by a velocity component which caused the leading edge vortex to migrate away from the plate. Each combination of reduced frequency and mean angle resulted in different convection and growth rates, as well as varying tendencies to migrate away from the plate surface and

to lose cohesiveness. In addition, for all such combinations of independent variables, the vortex exhibited varying instantaneous rates of convection and growth during residence on the plate. Figures 4-2 and 4-3 show the chordwise position and cross-sectional area histories for a typical leading edge vortex, respectively. Leading edge vortex cross-sectional shape also varied with time and chordwise position, depending upon reduced frequency and mean angle.

In general, average vortex convection rate climbed in response to higher reduced frequency parameter values, and fell as mean pitch angle was increased. Average vortex growth rate displayed nonmonotonic behavior with respect to reduced frequency parameter values, increasing with higher reduced frequency up to a reduced frequency of 1.0. Beyond, average vortex growth rate decreased with rising reduced frequency. In contrast, average growth rate seemed to increase monotonically with higher mean angle. Increased reduced frequency seemed to minimize the tendency of the vortex to migrate away from the plate surface, while higher mean angles appeared to have the opposite effect. Higher reduced frequencies and mean angles both seemed to result in more prolonged retention of vortex cohesiveness. The attributes of a typical mature leading edge vortex were vividly displayed by phase-locked, multiple flash photography. This technique superimposes, and therefore visually averages and reinforces, repeatable events phase-locked to the plate motion. Conversely, random occurrences appear diffuse due to the low probability of image superposition occurring to yield a coherent composite image.

Examination of a phase-locked, multiple flash photographic image depicting a mature leading edge vortex reveals clearly observable differences between the vortex itself and the overrunning flow. The overrunning flow is

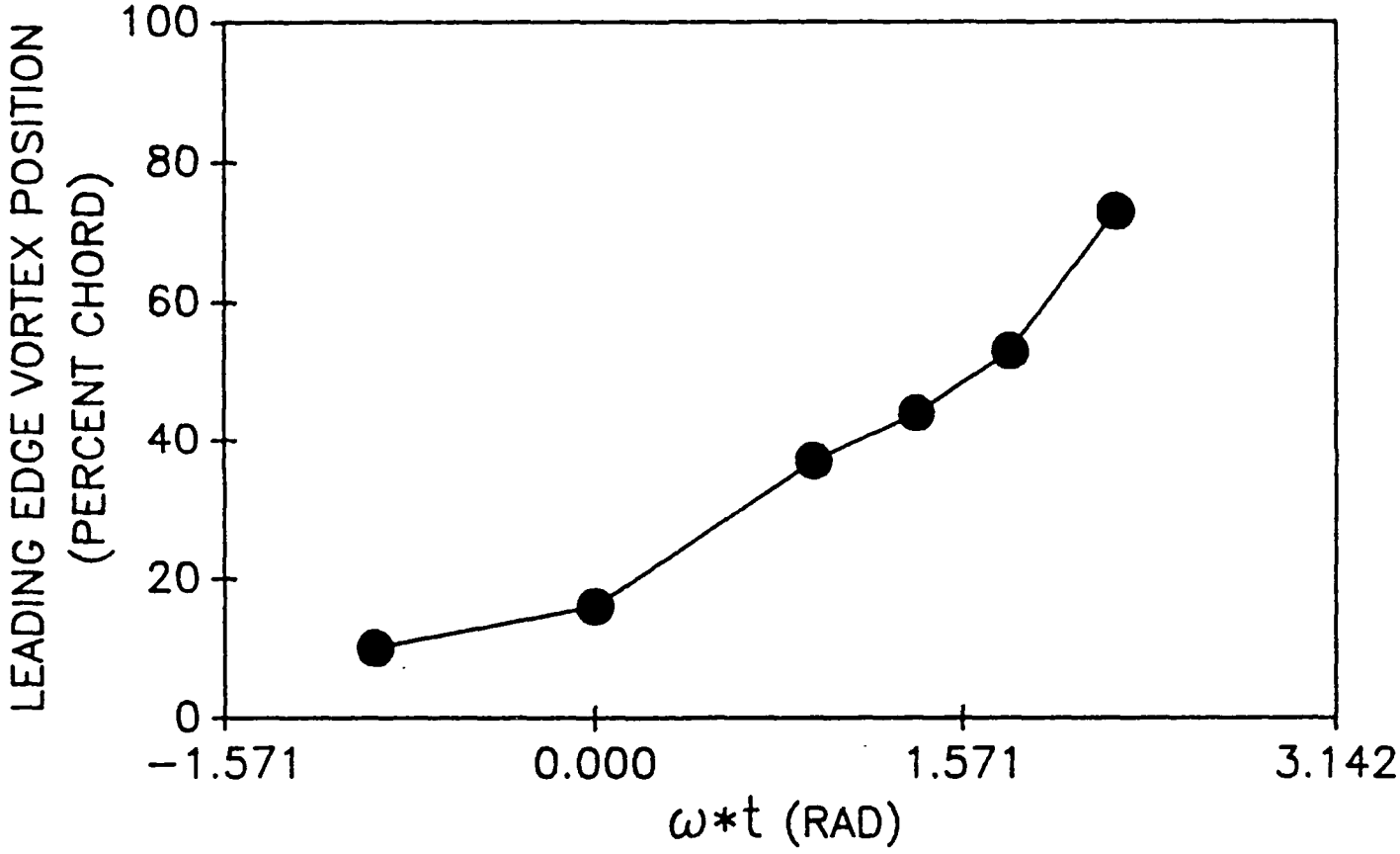

Figure 4-2. Leading edge vortex chordwise position history for K = 1.0, MPA = 10 degrees.

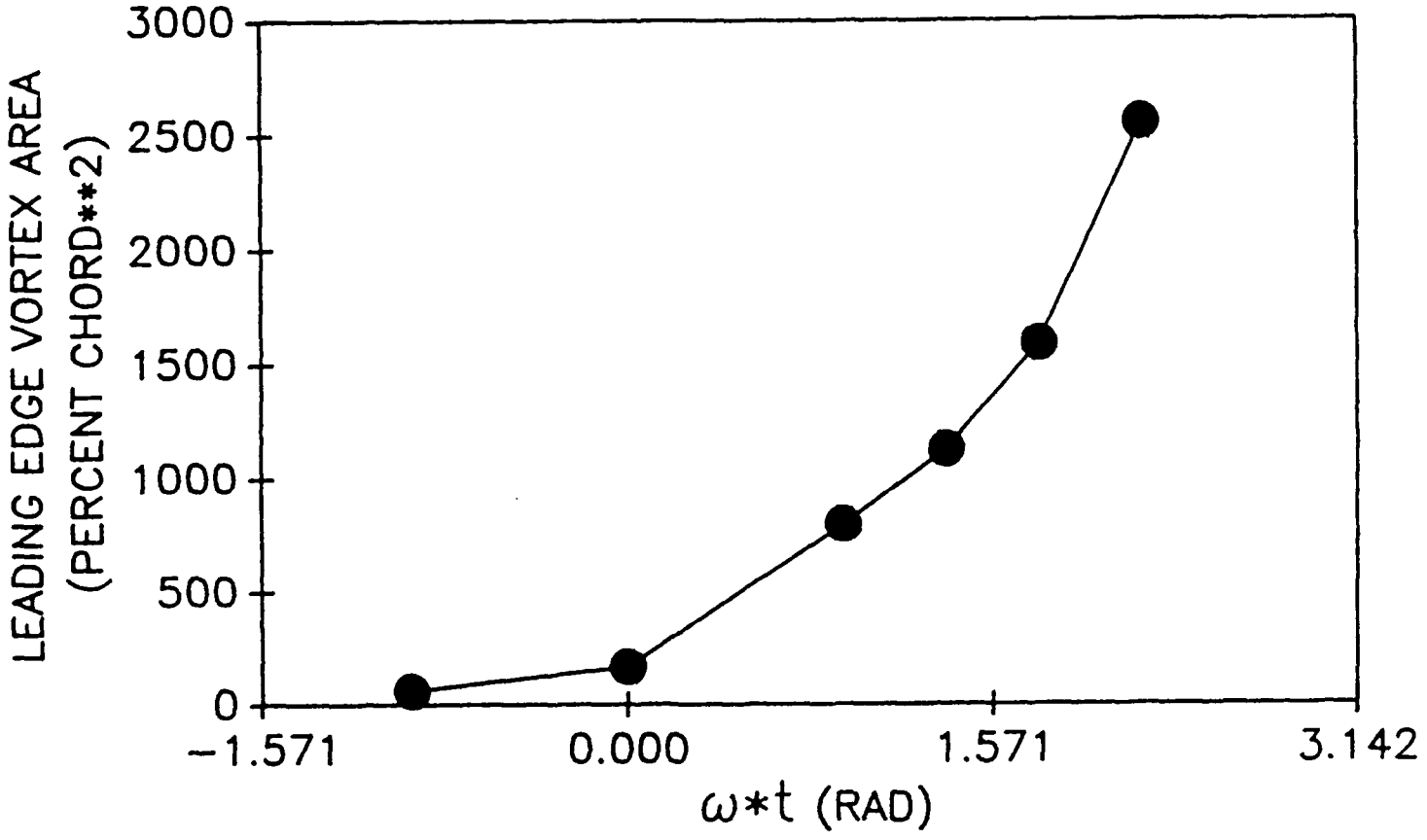

Figure 4-3. Leading edge vortex cross-sectional area history for K = 1.0, MPA = 10 degrees.

characterized by relatively well-defined streaklines which, though visibly displaced by the presence of the vortex, retain spatial integrity for some distance downstream of the vortex. Such streakline images suggest that the overrunning flow is predominantly laminar in nature. The interior of the vortex, in contrast, can be distinguished by the diffuse smoke traces marking the flow within it. Such a diffuse image implies that the flow there possesses a significant random velocity component, and probably can be considered largely turbulent in nature.

At the downstream boundary of the vortex, some of the streaklines underwent radical deformation and loss of definition as the overrunning flow was entrained downward into the downstream elements of the vortex. In this region, it is especially important to bear in mind that the flow field under consideration is unsteady, and that the smoke streaklines marking the flow do not necessarily coincide with streamlines. As such, the smokelines are not guaranteed to lie parallel to the local velocity vector. On the other hand, continuing dynamic alterations in flow structures temporally show the absence of simple convecting flow histories.

Trailing edge vortices. The trailing edge vortex also appeared to play a crucial role in the process of unsteady separation, becoming appreciably larger and more persistent at mean pitch angles of 20, 30 and 40 degrees. At initiation, the trailing edge vortex manifested itself just downstream of the plate trailing edge as a localized flexure in streaklines which otherwise generally appeared straight. Subsequently, this localized flexure assumed a strongly rotational character. As the vortex grew in size, rotational sense opposite that of the leading edge vortex soon became apparent.

As with leading edge vortices, higher reduced frequency seemed to yield more cohesive trailing edge vortices. Trailing edge vortex shedding was accompanied by rapid loss of cohesiveness. Shedding occurred as the leading edge vortex on the opposite surface approached the neighborhood of the trailing edge, or when a convecting leading edge vortex on the same surface displaced the resident trailing edge vortex. Such shedding events were followed quickly by flow separation from the opposite surface of the plate.

Reverse flow. In addition to the vortical structures already discussed, flow visualization also indicated the presence of reverse flows. These were evidenced by streaklines that abruptly underwent radical bending toward the upstream direction while retaining integrity. Reverse flow most often occurred on the suction surface as instantaneous pitch angle approached maximum amplitude. Elevated mean angle seemed to hasten the onset of reverse flow. The relatively well-defined streaklines initially characterizing the reverse-flow region were often disrupted a after short time, and assumed a diffuse, chaotic appearance. The relation of reverse flow to increased reduced frequency parameter values is more complicated and is related to a special set of spatial considerations. Details of these spatial relations are given below.

The streakline behavior just described is an indicator of when reverse flow commenced and what spatial characteristics it possessed at that time. However, as previously discussed in connection with vortical structures, the relationship between streamlines and streaklines becomes ambiguous in unsteady flow fields. As such, flow visualization provides accurate information concerning reverse flow at inception, but provides little detailed information

beyond that point in time.

Ancillary structures. Ancillary vortical structures were observed on the plate trailing edge and in the immediate wake of the plate at varying times in the oscillation cycle for mean pitch angles of 0, 5 and 10 degrees. Such structures depended, once again, upon reduced frequency and mean pitch angle. At low values of reduced frequency parameter, successive vortices possessing alternating rotational senses were shed in a manner reminiscent of a conventional vortex street. For 5 and 10 degree mean pitch angles, these vortex streets displayed a noticeable asymmetry, with somewhat larger ancillary vortices being shed from the lower surface of the plate.

At higher values of reduced frequency parameter, the ancillary structures generally appeared as trains of vortices exhibiting the same rotational sense, with each vortex resembling the others in terms of size, wavelength and cohesiveness. In addition, ancillary structures were shed from both plate surfaces for the 0 and 5 degree mean pitch angle cases, but from only one surface for the 10 degree mean angle case. Ancillary structures shed from the upper and lower surfaces appeared quite similar for the 0 degree mean angle case, but prominent asymmetries were observed in the 5 degree mean angle case. In the 5 degree mean angle case, at a reduced frequency parameter value of 1.0, ancillary structure shedding from the plate upper surface was of greater duration, and yielded structures exhibiting significantly more repeatability and longer cohesiveness retention than those shed from the lower surface. The same was true for the lower surface at reduced frequency parameter values of 2.0 and 3.5, at the same mean pitch angle. Ancillary structures representative of those observed throughout the experimental variable range are depicted in Figure 4-4.

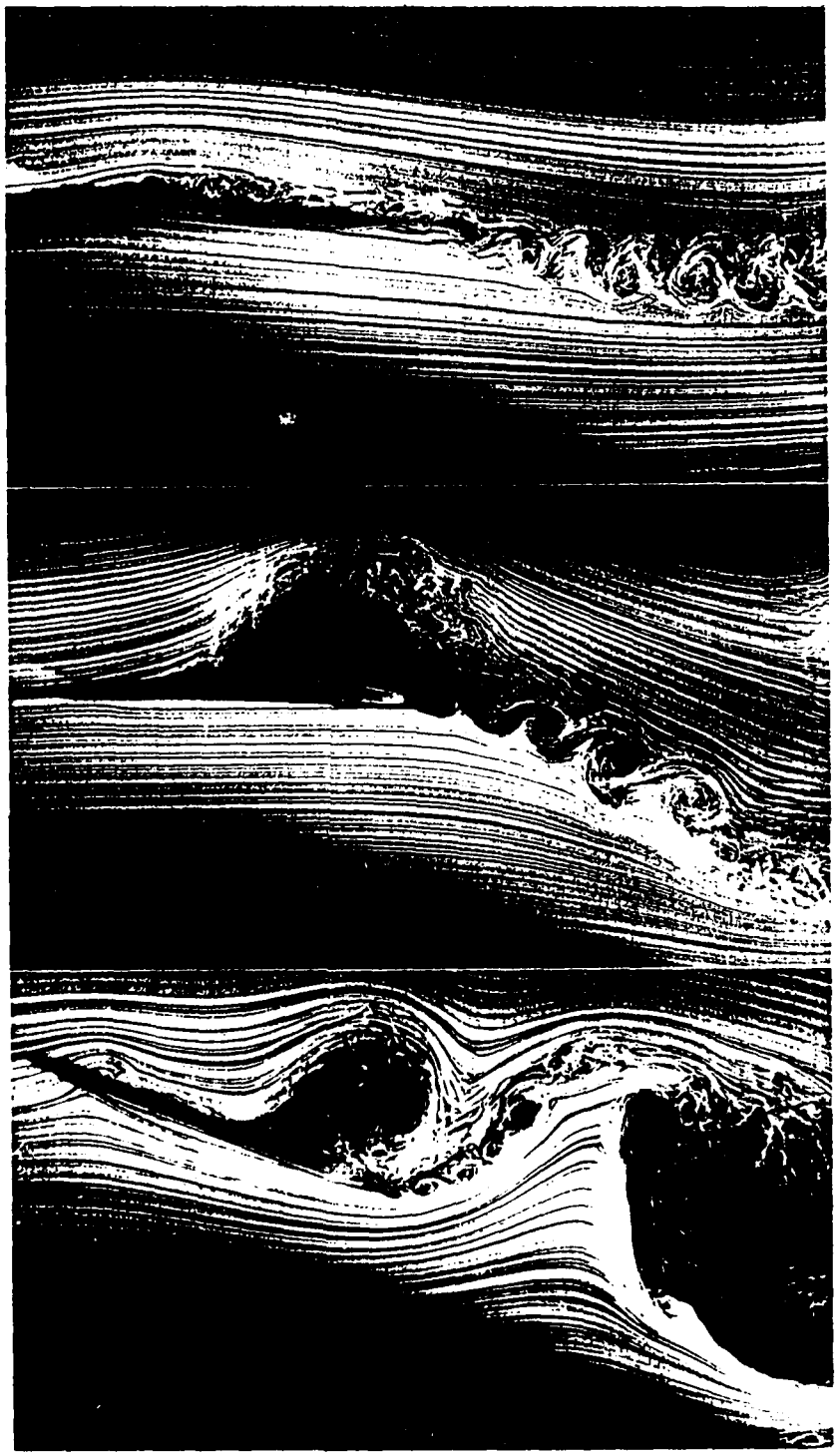

Figure 4-4. Representative ancillary structures. K = 0.5, MPA = 0 degrees (top); K = 1.0, MPA = 10 degrees (center); K = 2.0, MPA = 10 degrees (bottom).

Initiation of ancillary structure shedding, for low values of reduced frequency parameter, occurred a short time after the mature leading edge vortex and any related residual structures had convected off the plate, leaving both surfaces devoid of mature vortical structures. Shedding persisted until the leading edge vortex with an adjacent downstream reverse-flow region had convected sufficiently to place the downstream boundary of the vortex in the neighborhood of the trailing edge. At this point, ancillary structure shedding ceased and was supplanted by turbulent flow. At higher reduced frequency parameter values, ancillary structure shedding initiated as the downstream boundary of the reverse-flow region associated with the leading edge vortex, reached the vicinity of the plate trailing edge. Shedding then appeared to cease as a leading edge vortex convected into the region of the trailing edge from either surface of the plate.

Quantitative Characterizations of Structures

Leading edge vortex. Turning to quantifications of the above structures, the leading-edge vortex initiation site and time, as well as size and shape, were actively influenced by variations in reduced frequency and mean pitch angle. Photography did not generally reveal the precise moment of leading edge vortex formation, and exhaustive characterization of this event was precluded. In spite of this limitation, the available data disclosed the following trends.

Increasing either reduced frequency or mean angle tended to drive the formation site closer to the plate leading edge. At initiation, leading edge vortex size was ever smaller with increasing reduced frequency, and was larger

with higher mean angle. An increase in reduced frequency yielded a less elongated nascent vortex, as did greater mean pitch angle. Vortex formation, measured relative to the plate oscillation cycle phase angle, appeared to be delayed to later in the cycle by increasing reduced frequency, but hastened by higher mean angle. These trends in leading edge vortex initiation time are shown graphically in Figure 4-5. The foregoing characteristics of the nascent leading edge vortex demonstrate that this phenomenon can be looked upon as a collection of contributing factors all of which move the flow to a specific threshold point of vortex initiation.

The mature leading edge vortex, on the other hand, is a constantly evolving entity of an inherently time-varying nature. As such, the detailed position and size histories of the mature leading edge vortices are critically important to understanding the underlying physical mechanisms from which they derive. Figures 4-6 and 4-7 show the position history of the convecting leading edge vortex across reduced frequency and mean pitch angle ranges. Notably, instantaneous convection velocity varies as the maturing vortex passes over the oscillating plate. The convecting vortex undergoes more rapid and numerous instantaneous velocity variations as reduced frequency increases. In addition to the information obtained by examining the details of each individual vortex position history, comparisons can be made between the individual histories. Figures 4-6 and 4-7 show that increasing reduced frequency yields a corresponding increase in average leading edge vortex convection rate.

Application of a linear least-squares fit to the convection data presented in Figures 4-6 and 4-7 provided an accurate, consistent measure of average vortex convection velocity. Using this measure, average convection

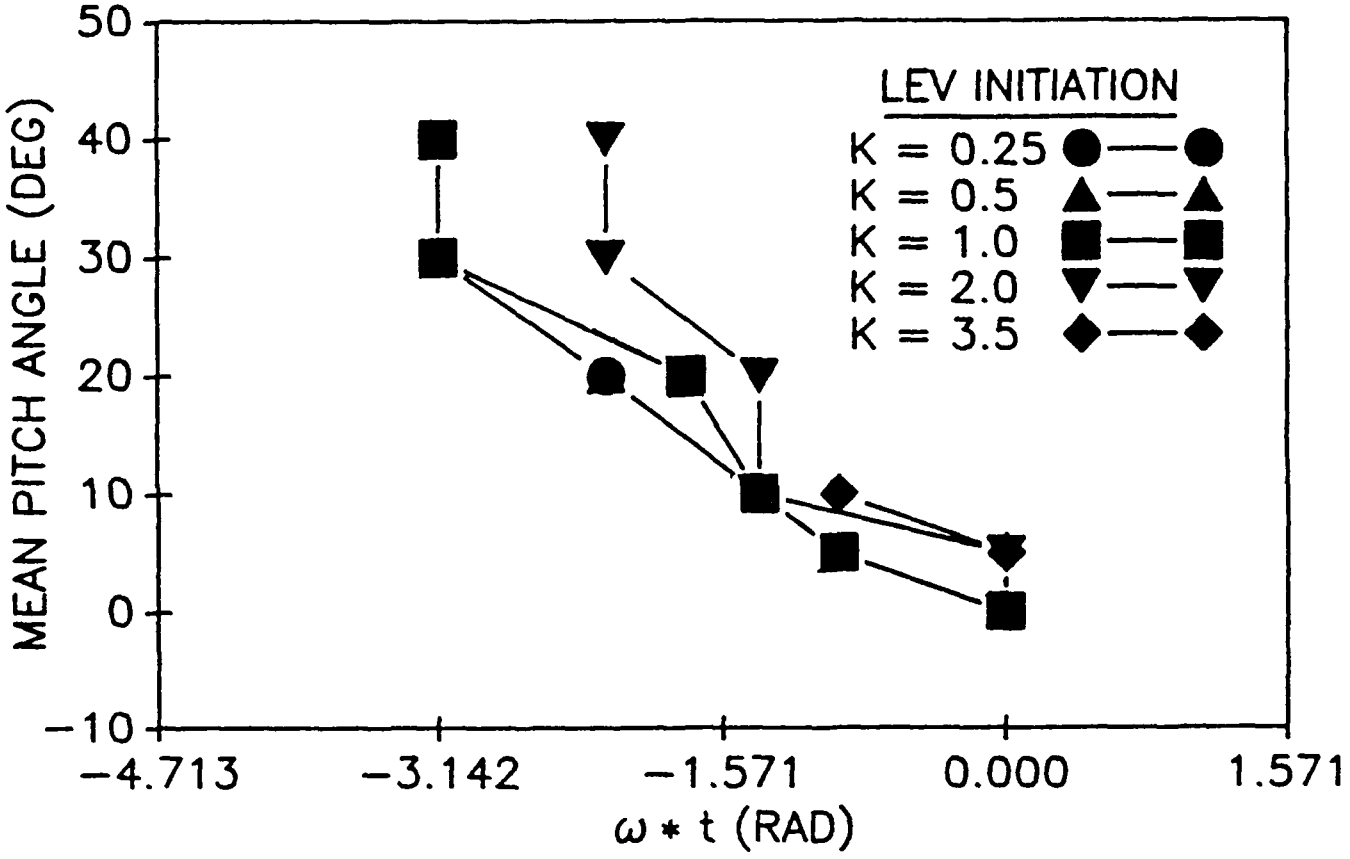

Figure 4-5. Leading edge vortex initiation time for experimental range of K and MPA.

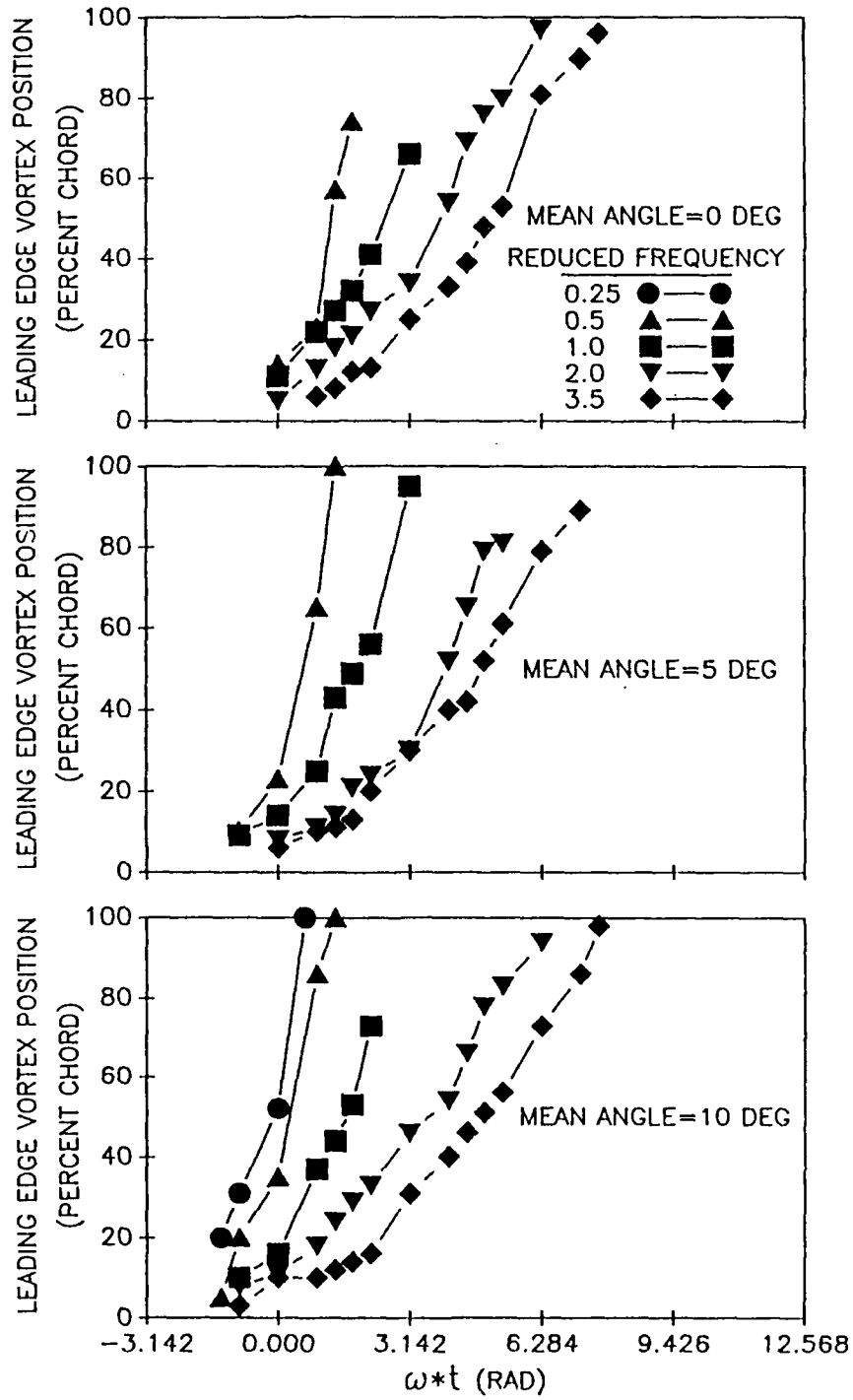

Figure 4-6. Leading edge vortex chordwise position histories for experimental range of K and MPA = 0, 5 and 10 degrees.

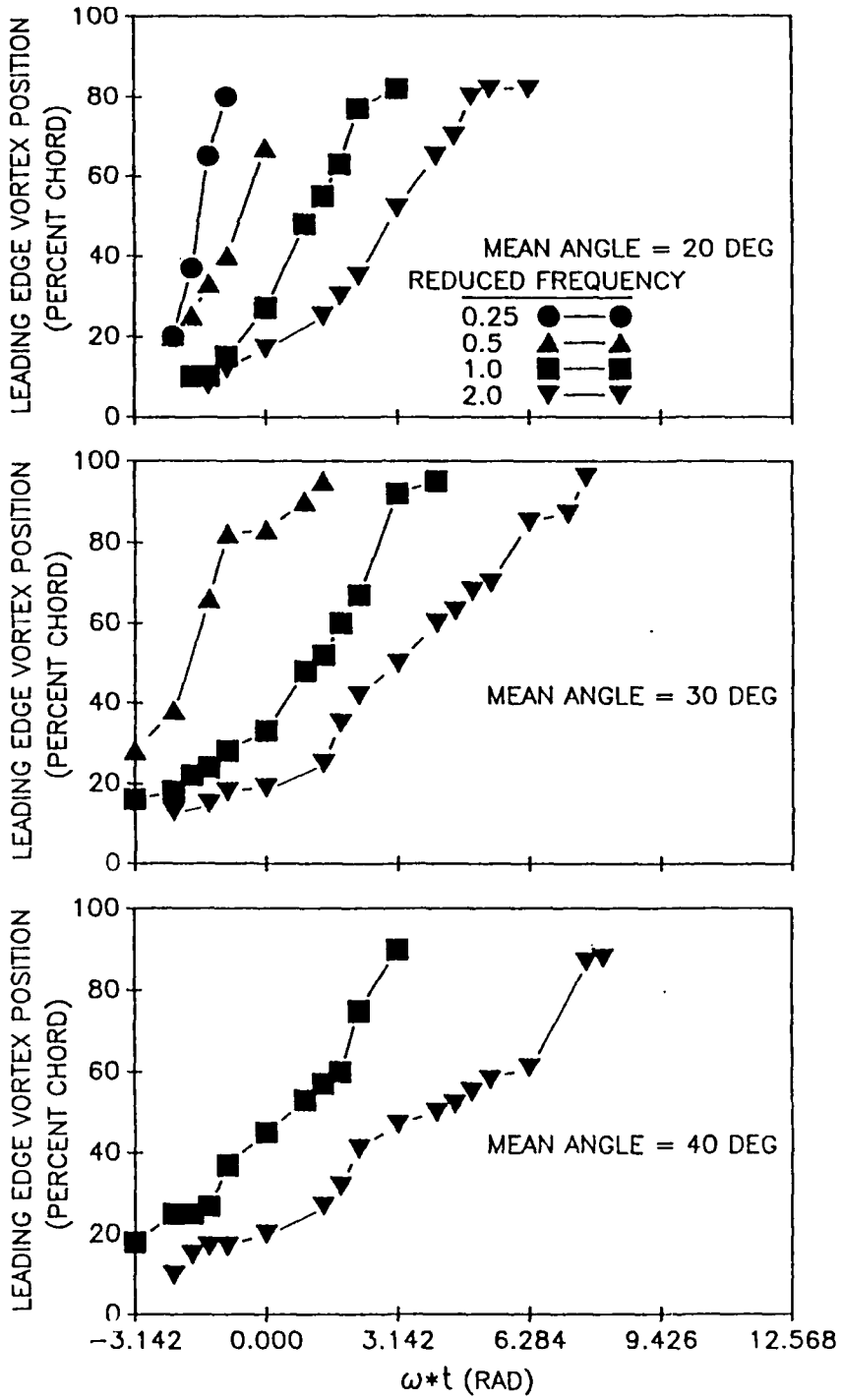

Figure 4-7. Leading edge vortex chordwise position histories for experimental range of K and MPA = 20, 30 and 40 degrees.

velocity was computed for all combinations of reduced frequency and mean angle. The results, presented in Figure 4-8, lend quantitative support to the trends noted previously in Figures 4-6 and 4-7.

As the maturing leading edge vortices convect down the surface of the plate, they simultaneously exhibit variations in cross-sectional area. Detailed quantitative characterization of this size variation is crucial in attempting to unravel the underlying mechanisms giving rise to the flow field. Thus, leading edge vortex growth was studied in much the same way as was convection.

Figures 4-9 and 4-10 show the cross-sectional area history of the developing leading edge vortex for the range of reduced frequencies and mean pitch angles included in this study. Viewed individually, these histories show that instantaneous growth rate fluctuates during the entire lifespan of the vortex. However, in most cases, the history does not behave in a radically nonlinear manner. This is especially true at lower reduced frequencies.

A linear least-squares fit was also applied to the vortex growth data presented in Figures 4-9 and 4-10 in order to obtain average growth rates for each of the experimental cases. Figure 4-11 summarizes these results, and supplies information which is not immediately available in Figures 4-9 and 4-10. Figure 4-11 highlights the nonmonotonic behavior of average vortex growth rate with respect to reduced frequency, not indicated by Figures 4-9 and 4-10.

Trailing edge vortex. Trailing edge vortex behavior was decidedly different from that of the leading edge vortex. In addition to the conspicuous and universal opposition in rotational senses, other dissimilarities existed between the two types of vortices. At mean pitch angles of 0, 5 and 10 degrees, the trailing edge vortex was generally smaller than the leading edge

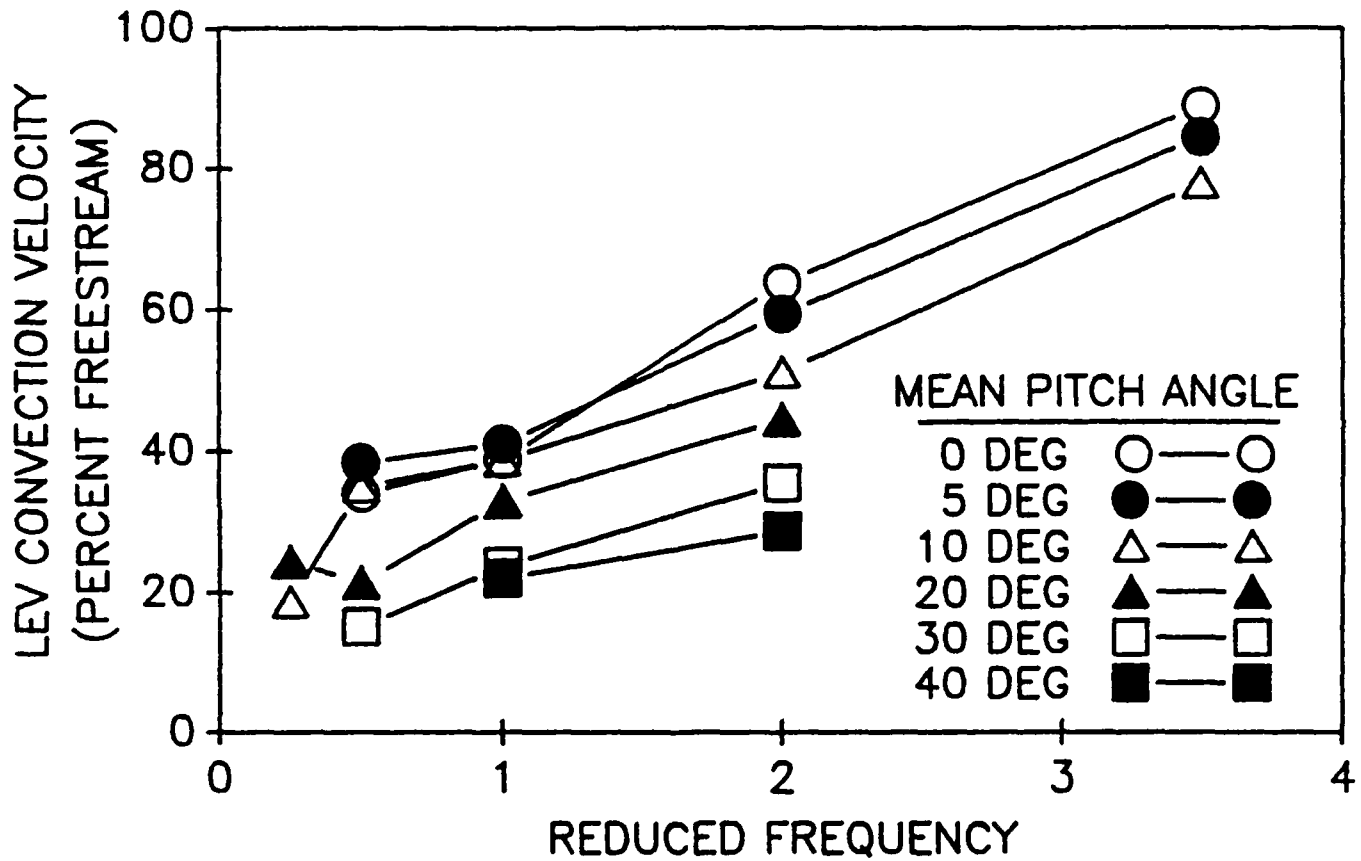

Figure 4-8. Average leading edge vortex convection rate vs. K.

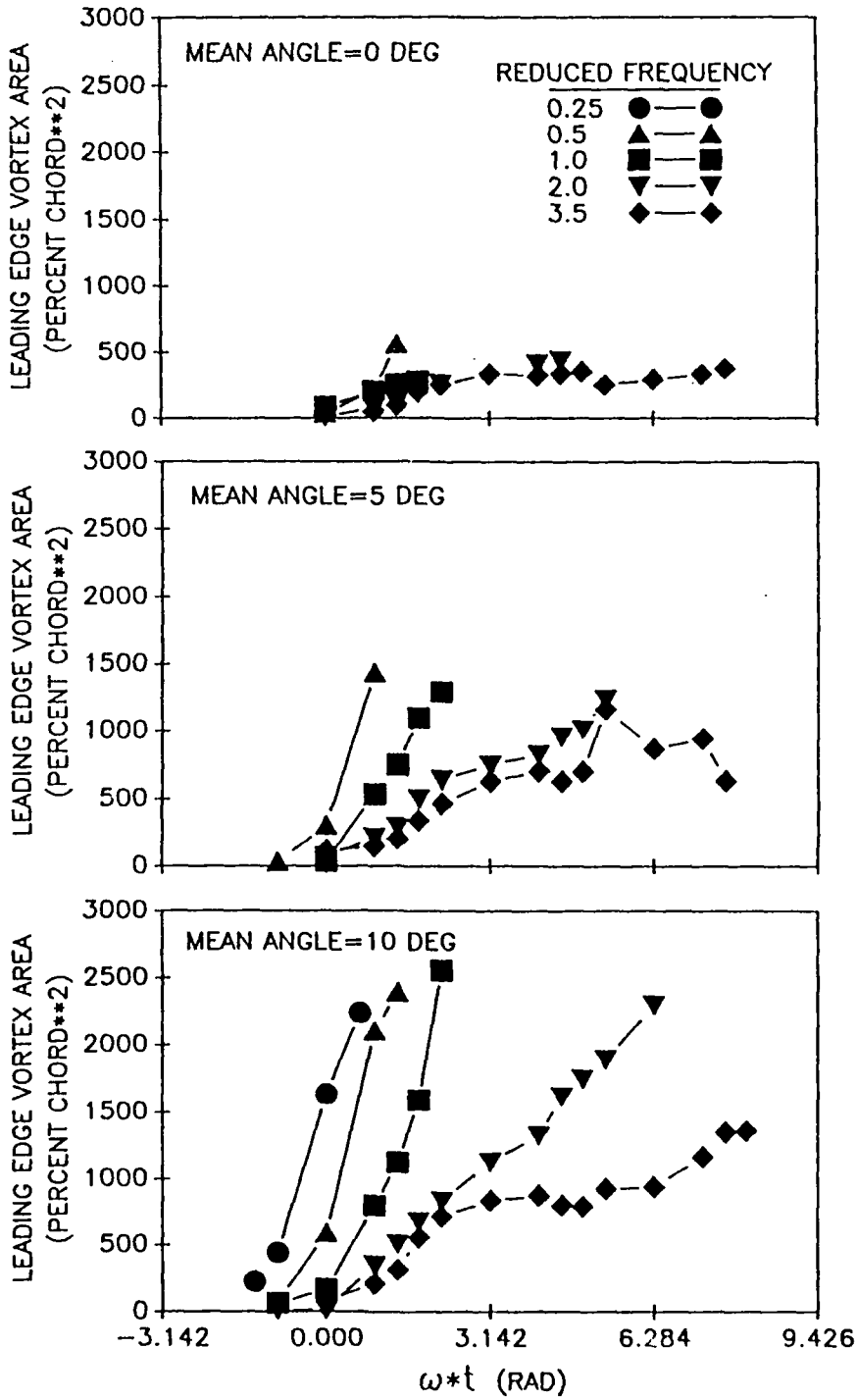

Figure 4-9. Leading edge vortex cross-sectional area histories for experimental range of K and MPA = 0, 5 and 10 degrees.

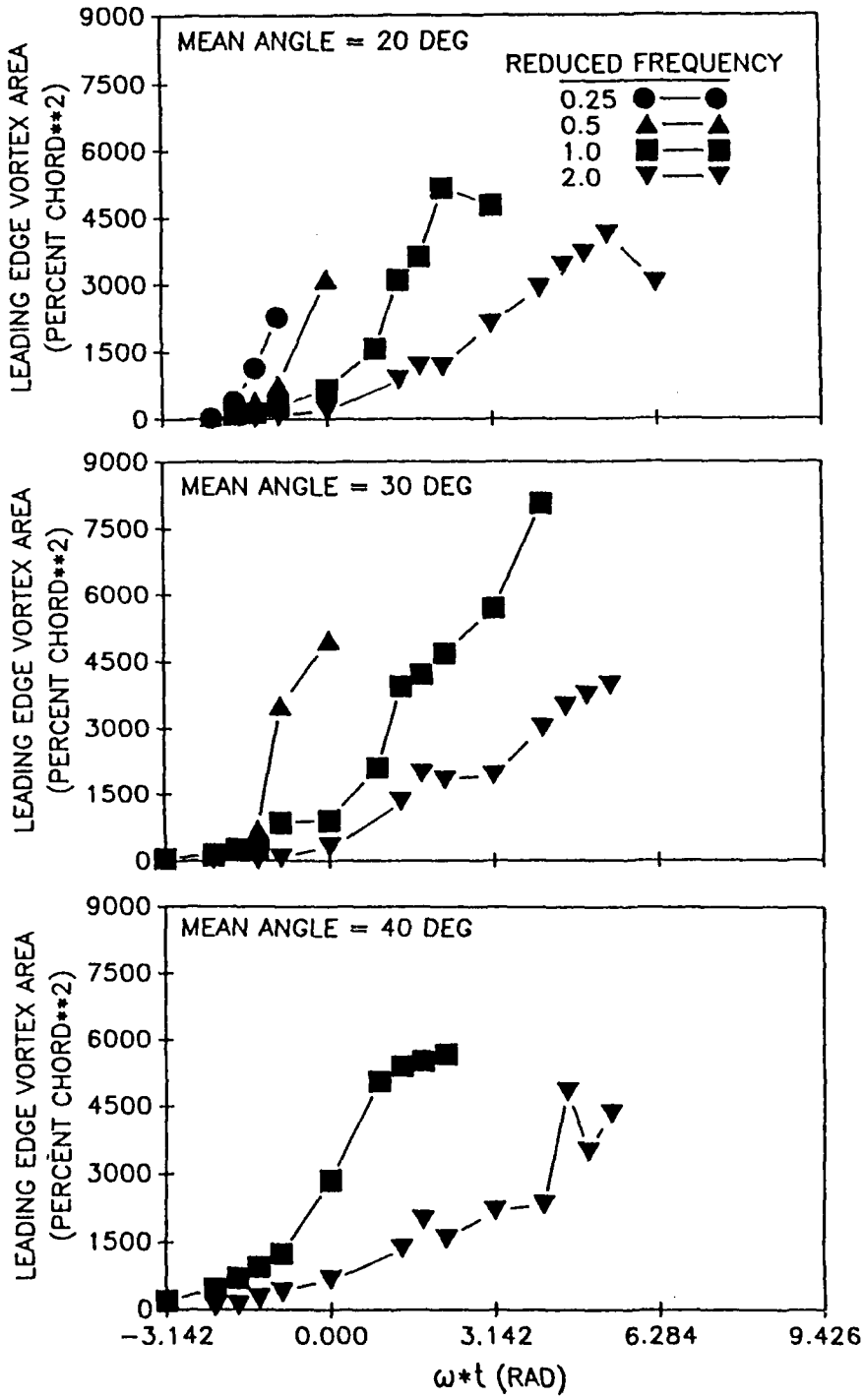

Figure 4-10. Leading edge vortex cross-sectional area histories for experimental range of K and MPA = 20, 30 and 40 degrees.

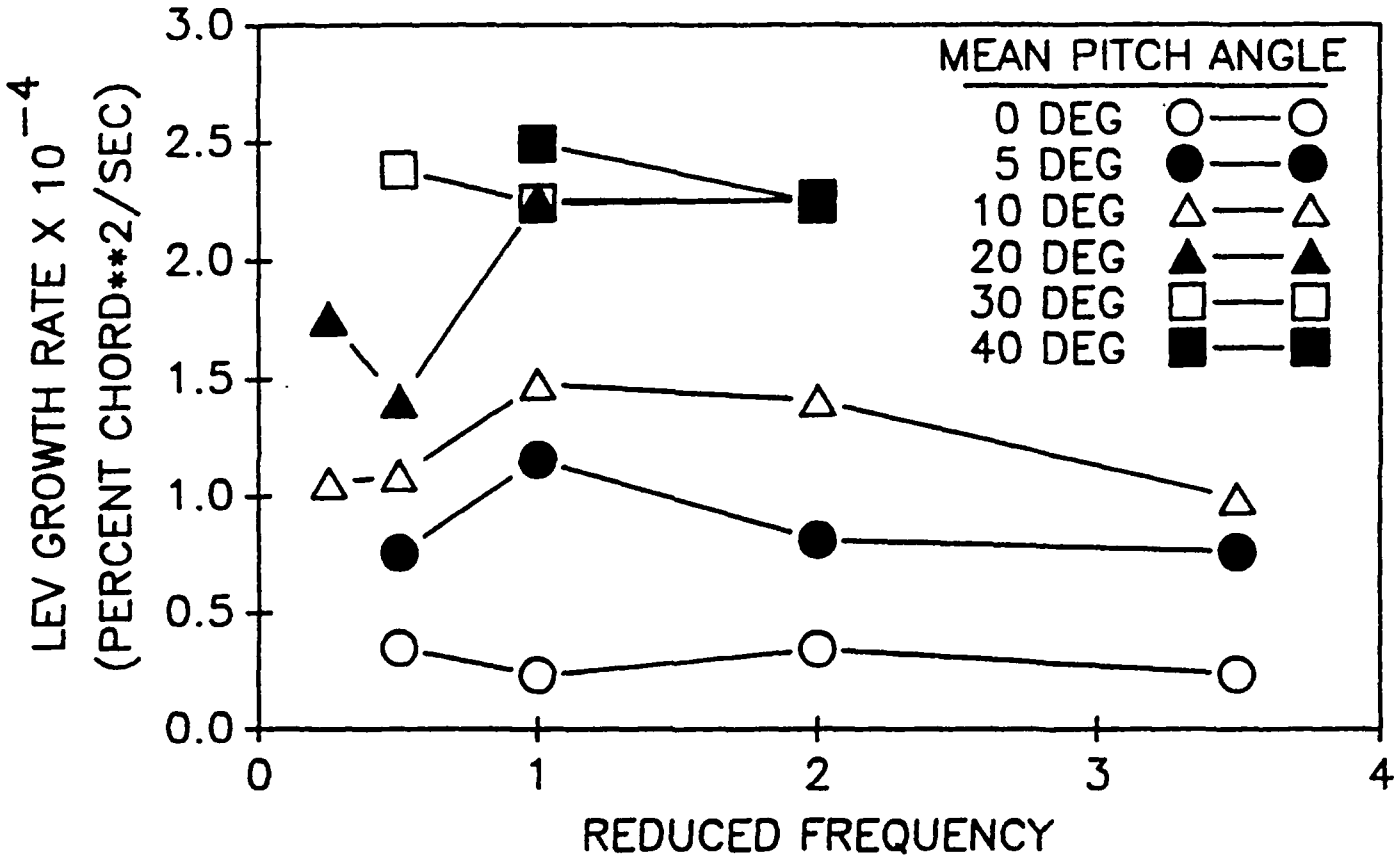

Figure 4-11. Average leading edge vortex cross-sectional area growth rate vs. K.

vortex and persisted for a shorter period of time. However, at mean pitch angles of 20, 30 and 40 degrees, trailing edge vortex size and persistence were comparable to that of the leading edge vortex.

In spite of size and persistence duration dissimilarities, trailing edge vortex initiation was observable throughout the most of the experimental range of reduced frequency and mean pitch angle. As such, initiation phase angle could be determined to the degree of accuracy permitted by the photographic procedure, which was not intended to capture the precise moment of vortex initiation. Trailing edge vortex initiation data are presented graphically in Figure 4-12. Leading edge vortex initiation data are also shown for purposes of comparison. The graph horizontal axis is consistent with time histories presented previously in that zero radians corresponds to maximum upward plate pitch angle.

Trailing edge vortex initiation, in comparison to that for the leading edge vortex, displayed a less orderly response to variations in reduced frequency and mean pitch angle. Lower reduced frequency generally elicited trailing edge vortex initiation earlier in the cycle. This alteration was most pronounced at elevated mean pitch angles, where more than a half cycle difference was observed between initiation phase angle for reduced frequency parameter values of 0.25 and 2.0. For reduced frequency parameter values of 0.25 and 0.5, higher mean pitch angle consistently yielded earlier trailing edge vortex initiation. In contrast, for reduced frequency parameter values of 1.0 and 2.0, increases in mean pitch angle resulted in nonmonotonic variation of trailing edge vortex initiation.

Due to limitations in trailing edge vortex size and persistence at mean

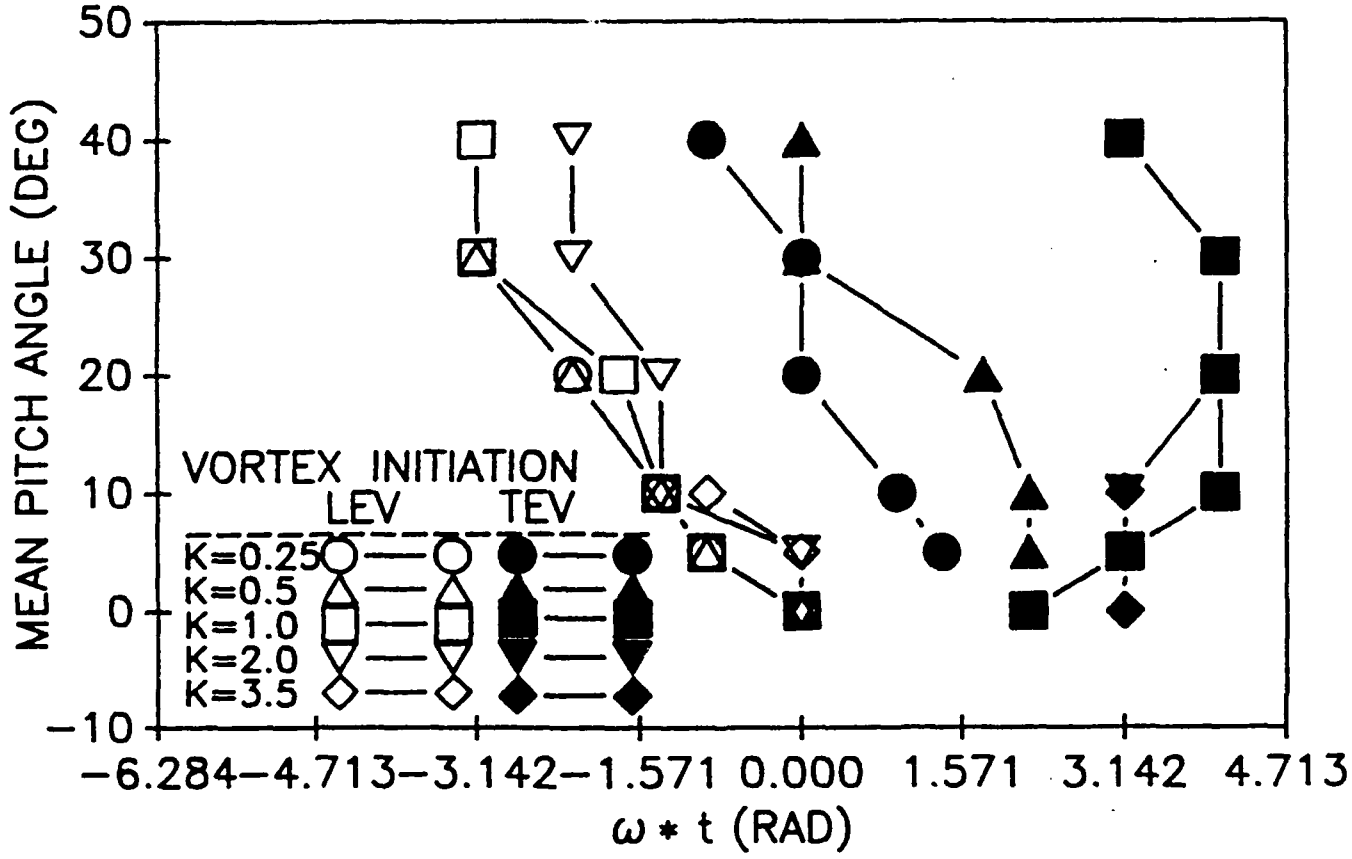

Figure 4-12. Leading and trailing edge vortex initiation time for experimental range of K and MPA.

pitch angles of 0, 5 and 10 degrees, characterization of this structure could not be carried out with the same degree of detail permitted for the leading edge vortex. However, at mean pitch angles of 20, 30 and 40 degrees, trailing edge vortex size and persistence were comparable to that of the leading edge vortex and trailing edge vortex growth was amenable to quantitative documentation.

Trailing edge vortex growth histories are presented graphically in Figure 4-13. Individual histories showed instantaneous vortex growth rate variation during the life of the trailing edge vortex, with greater variation in instantaneous growth rate generally occurring at higher mean pitch angles. In addition, at higher mean pitch angles the trailing edge vortex generally persisted for a greater portion of the cycle, but attained smaller maximum cross-sectional area. These trends in persistence and maximum size were most pronounced at higher reduced frequency parameter values.

A linear least squares fit was applied to the cross-sectional area histories presented in Figure 4-13 to obtain average growth rates for each individual case. These results are presented in Figure 4-14 and show that the average growth rate of the trailing edge vortex generally decreased monotonically with increasing mean pitch angle. Trailing edge vortex growth rate behaved nonmonotonically with respect to reduced frequency, exhibiting an apparent minimum at a reduced frequency of 0.5 and increasing at both higher and lower reduced frequencies.

A definite phase relationship was observed between the shedding times of the leading and trailing edge vortices. At low reduced frequency, the trailing edge vortex was shed after the leading edge vortex. High reduced

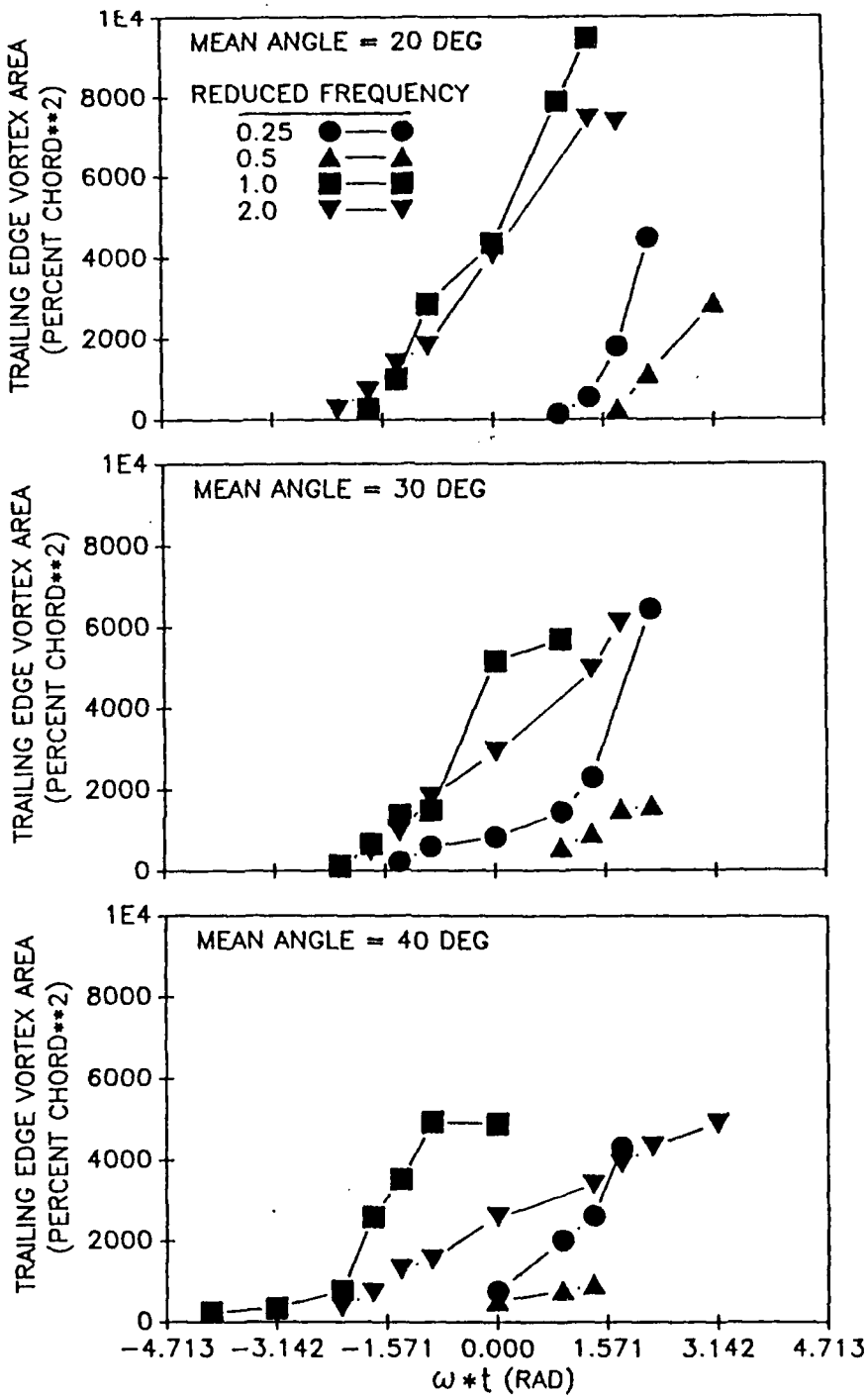

Figure 4-13. Trailing edge vortex cross-sectional area histories for K = 0.5, 1.0, 2.0 and MPA = 20, 30, 40 degrees.

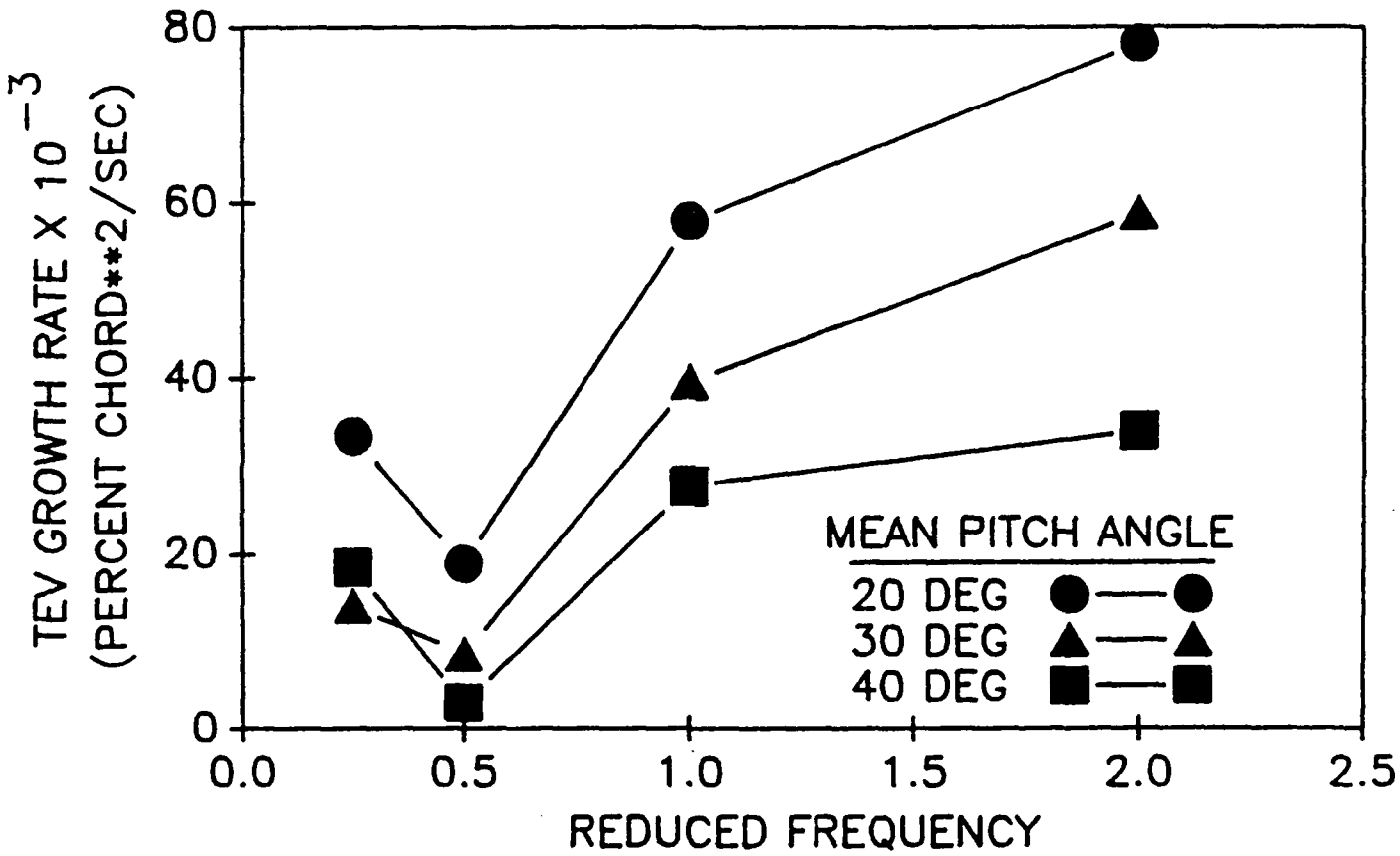

Figure 4-14. Average trailing edge vortex cross-sectional area growth rate vs. K.

frequency gave rise to the opposite sequence of events, with the trailing edge vortex being shed before the leading edge vortex. Variations in mean pitch angle seemed to have no discernible effect upon this phase relationship.

Ancillary structures. The ancillary structures, though vortical in character, differed fundamentally from structures discussed previously. The principal distinction was that all other structures developed in close proximity to the oscillating plate, whereas the ancillary structures developed fully only in the wake. In contrast to the trailing edge vortices, which were largest and most persistent at elevated mean pitch angles, the ancillary structures were evident only at the lower mean pitch angles of 0, 5 and 10 degrees. Increasing either reduced frequency or mean pitch angle appeared to slow the convection rate of these structures.

Wavelengths of these ancillary structures varied nonmonotonically with reduced frequency parameter, growing to a maximum at a reduced frequency of 1.0, and then decreasing for higher reduced frequencies. At reduced frequencies of 1.0 and below, wavelength consistently grew with higher mean angle. At higher reduced frequencies, however, no clear trend is evident with respect to mean angle. These results are presented graphically in Figure 4-15.

Data set partitioning. To gain a more thorough physical understanding of each independent variable, reduced frequency and mean pitch angle were decomposed into differing constituents for a more detailed examination. These decomposed variables were assessed with regard to influences produced in the elicited flows.

The numerator of the expression for reduced frequency contains two terms. The first term is angular frequency, and implies that plate sinusoidal

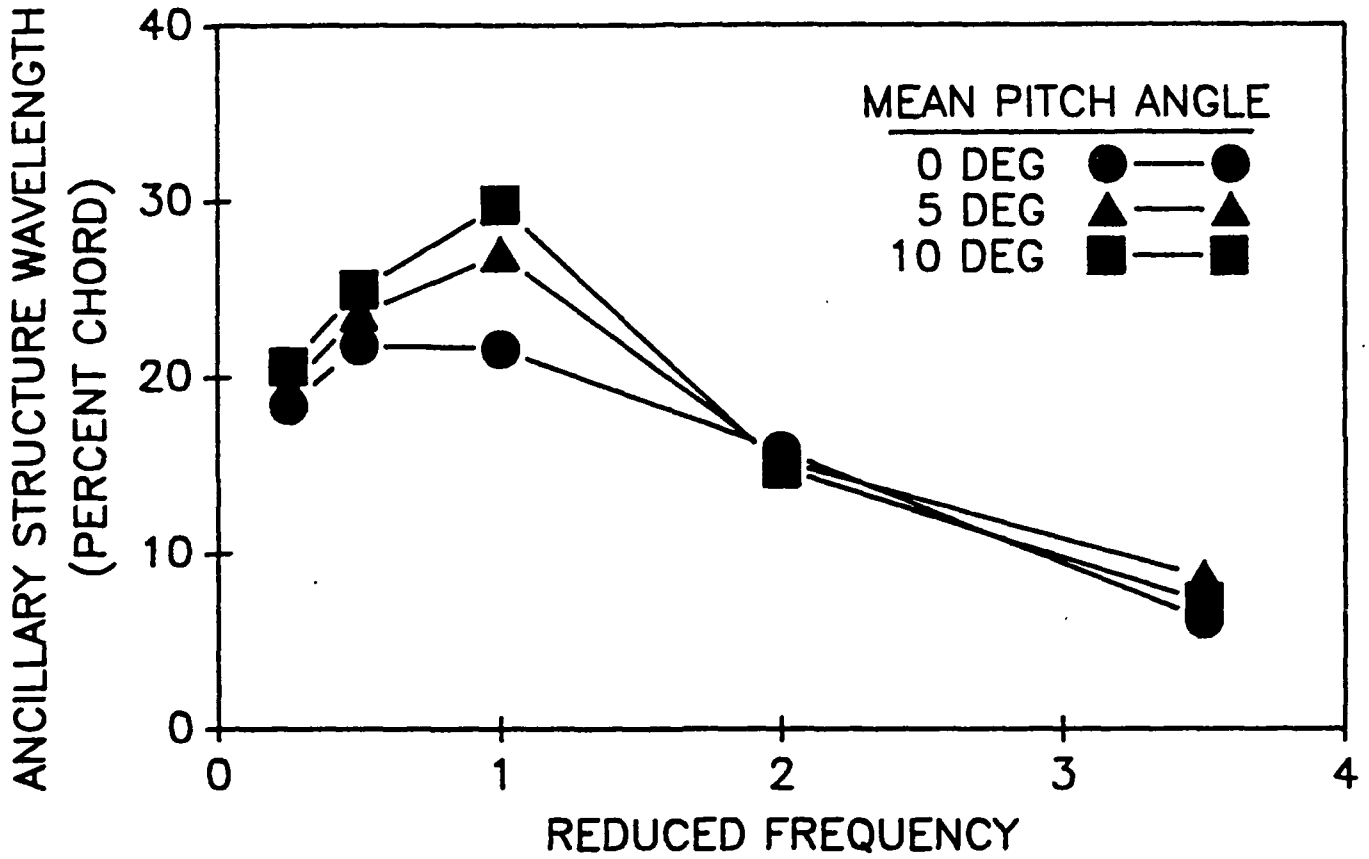

Figure 4-15. Ancillary structure wavelength vs. K.

pitching motion possesses not only a characteristic rate, but that both the sign and magnitude of this rate vary with time. All experiments here used a quarterchord pitch axis. Plate instantaneous pitch rate can assume both positive and negative values. The second term in the numerator is a characteristic length, and can be viewed as an index of flow element and flow structure locations with respect to plate geometry. The denominator can, quite simply, be considered an indicator of the influence exercised by the freestream.

Mean pitch angle, the other experimental independent variable, directly governs the maximum depth of the region on the plate suction surface shielded from the freestream. In addition, this quantity determines when in the oscillation cycle the shielding effect transitions to the opposite plate surface, and, in conjunction with angular frequency, governs the instantaneous rate at which this depth varies, as well. The mean pitch angle also relates to the amount of an oscillatory cycle occurring above or below plate static stall angle.

The foregoing physical decomposition of variables led to alternative ways of examining those data presented above. Both reduced frequency and mean angle are physically linked to both instantaneous pitch angle and pitch rate. The data sets were, accordingly, partitioned into two subsets: (1) one set corresponding to pitch-up data recorded prior to the plate maximum pitch angle, and (2) one corresponding to data acquired during pitch-down. Partitioning was applied to both leading edge vortex position and cross-sectional area histories. For small reduced frequency parameter values and large mean pitch angle, vortex initiation occurred as the plate pitched away from zero angle, but prior to it reaching maximum pitch angle. As reduced frequency was increased or mean angle reduced, initiation was delayed to higher

instantaneous pitch angles. At sufficiently high reduced frequency or low mean angle, vortex initiation was delayed until the maximum pitch angle had been attained and the plate rotational sense had reversed.

Vortex initiation occurred on both plate surfaces for the zero mean angle cases despite the fact that pitch angle did not exceed 10 degrees. Leading edge vortex initiation took place only on the upper surface of the plate for mean angles greater than zero, with one exception. This exception appeared at a reduced frequency of 3.5 and mean angle of 5 degrees, when a small leading edge vortex was observed on the lower surface of the plate.

The data sets for both the leading edge vortex position and cross-sectional area histories were partitioned into two subsets in the manner previously described. Due to the dependency of leading edge vortex initiation on reduced frequency and mean angle, not all test cases yield a vortex or a vortex history prior to the attainment of maximum pitch angle. A linear least-squares fit was applied to each of these subsets to arrive at average rates of vortex convection and growth both prior to and following the attainment of maximum pitch angle. The results are summarized in Figures 4-16 and 4-17.

For each combination or reduced frequency and mean pitch angle, average convection velocity during pitch-up was generally lower than that during pitch-down, aside from the case corresponding to reduced frequency 0.5 and 30 degree mean pitch angle. The vortex growth rate plot suggests the same trend, although the case corresponding to reduced frequency of 0.25 and 10 degree mean angle constitutes a notable exception.

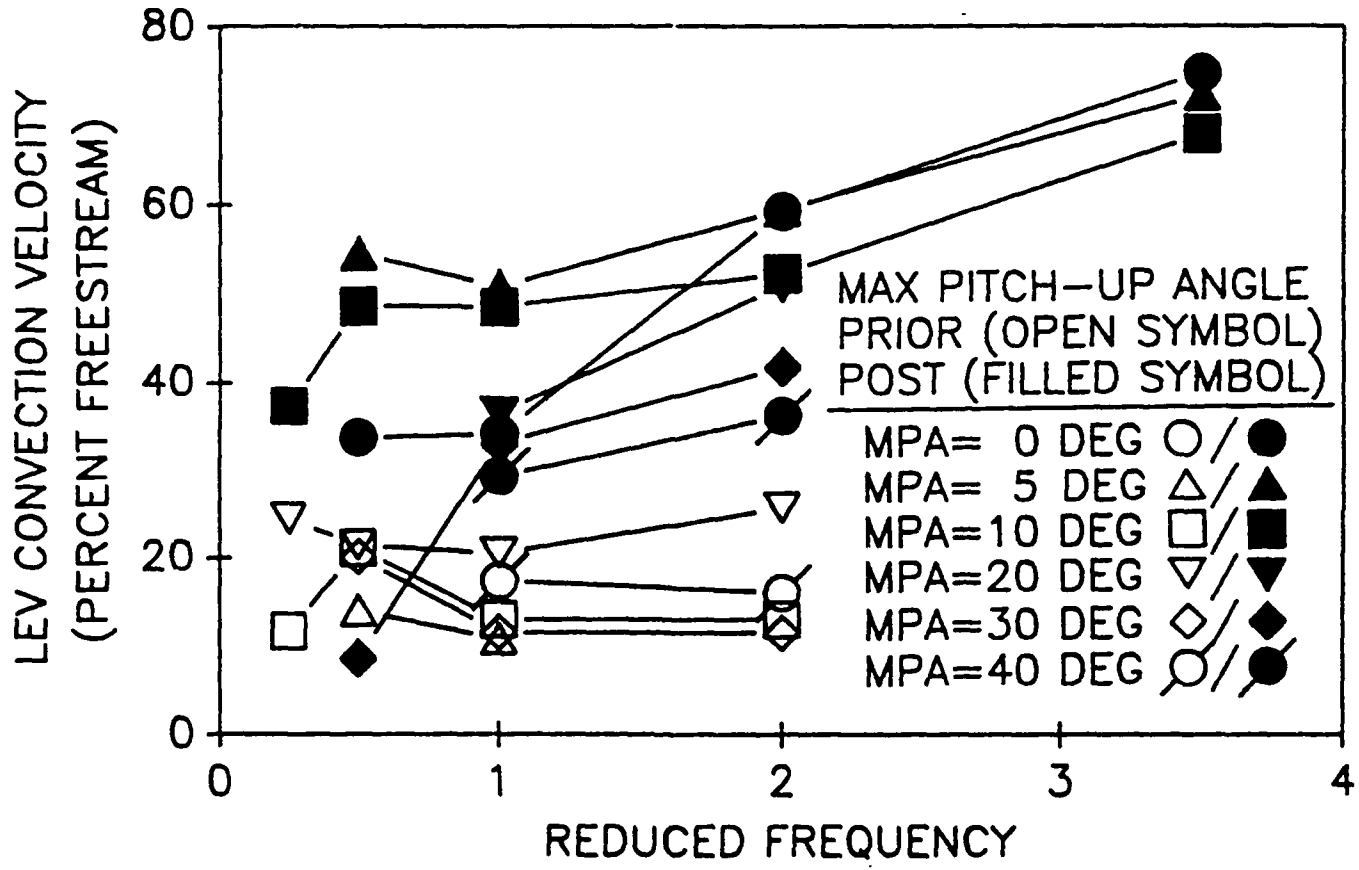

Figure 4-16. Average leading edge vortex convection rate vs. K, before and after plate reaches maximum upward pitch angle.

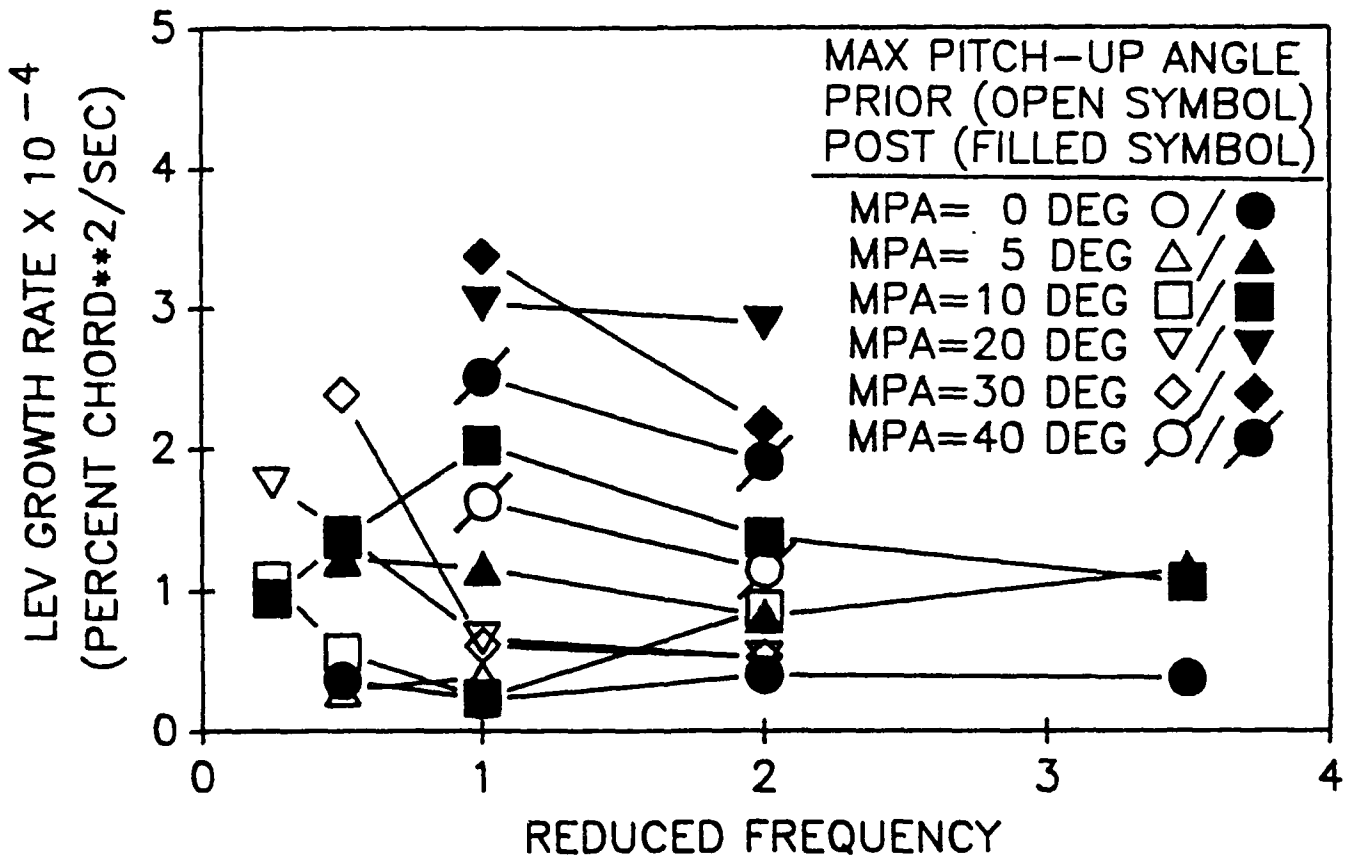

Figure 4-17. Average leading edge vortex cross-sectional area growth rate vs. K, before and after plate reaches maximum upward pitch angle.

CHAPTER V

SURFACE FLOWS

Introduction

Unsteady separated flows continue to be the subject of intense study. Much of this enduring strong interest derives from the radical air vehicle performance enhancements thought to be attainable by exploiting unsteady separation. If feasible, these performance enhancements will ensue from augmented aerodynamic coefficients, which, in turn, will depend predominantly upon the behavior of large scale vortical structures in a three-dimensional flow environment.

As a precursor to rigorous understanding of the fluid dynamics responsible for three-dimensional unsteady separation, diverse investigations encompassing an extensive parameter space have documented the kinematics of unsteady separated flow structures under two-dimensional conditions. Resulting characterizations of flow structure behavior affirm the effect exercised by the potential flow field upon the large scale vortical structures peculiar to unsteady separation (Luttges and Kennedy, 1988). However, convincing evidence exists that the kinematics of these large scale structures are also actively influenced by boundary layer flows, including reverse flows (Schreck and Luttges, 1988).

That reverse flows are present during steady state airfoil stall has been well documented. McCullough and Gault (1951) identified three distinct

varieties of airfoil stall. In the first type of stall, trailing edge stall, reverse flow was observed to extend upstream from the airfoil trailing edge to the turbulent separation point. The second and third types, leading edge and thin airfoil stall, displayed localized regions of reverse flow not contiguous with the airfoil trailing edge.

For the case of oscillating airfoils, Carr, et. al. (1977) observed reverse flows which were assigned to one of three categories of stall somewhat different from those of McCullough and Gault. In trailing edge stall on a cambered airfoil, flow reversal was observed to progress up the airfoil from the trailing edge as angle of attack increased. Flow reversal onset was delayed to higher angles of attack at increased values of reduced frequency parameter. For leading edge bubble-bursting stall on a sharp leading edge airfoil, reverse flow was initially detected near the airfoil leading edge. This zone of reversal then spread downstream, where it merged with reverse flow which had begun to move forward from the trailing edge earlier in the airfoil pitching cycle. The third category of stall, originally defined by Carr, et. al. in this study, was that of turbulent leading edge separation and was observed on a NACA 0012 airfoil. Here, reverse flow progressed forward on the airfoil from the trailing edge to approximately 0.40 chord. Then, flow reversal advanced almost instantaneously to the airfoil leading edge.

Many previous investigations in the area of two-dimensional unsteady separated flow have employed symmetric airfoil sections. However, for simplicity, the current study used a flat plate. A flat plate, compared to an airfoil, focuses variations in static pressure nearer the leading edge and reduces the magnitude of these variations along the chord. Another measure intended

to simplify the physical circumstance was sinusoidal pitch oscillation of the plate. Such forcing functions are known to elicit relatively well behaved flow fields amenable to the study of the physics underlying unsteady separation (Robinson and Luttges, 1984).

In this experiment, hotwire anemometer measurements were taken in the unsteady boundary layer surrounding the sinusoidally oscillating flat plate. These measurements were accomplished throughout an extended range of reduced frequency parameter values and mean pitch angles. Existing flow visualization pertaining to the same reduced frequencies and mean pitch angles provided data characterizing leading edge vortex initiation, convection and cross-sectional area growth. Hotwire and leading edge vortex kinematics data sets were then compared. The subsequent data analyses were carried out in a manner designed to highlight the physical support mechanisms responsible for unsteady separation.

Experimental Methods

Experiments were conducted in the 40.6 cm X 40.6 cm wind tunnel at the University of Colorado. Two-dimensional, unsteady separated flow proximal to an oscillating flat plate was investigated using tandem element hotwire anemometry. The flat plate was fabricated from solid aluminum, measured 30.50 cm x 15.20 cm x 0.64 cm, and tapered to sharp leading and trailing edges over the forwardmost and rearmost 1.52 cm. The plate was mounted, at the quarterchord, on a 1.27 cm diameter steel shaft projecting through a flange mounted on the back wall of the test section.

The plate was driven by a gearmotor coupled to the mounting shaft

through a crank linkage that allowed adjustments for both oscillation amplitude and mean pitch angle. A small disc magnet embedded in the rim of the linkage flywheel briefly closed a reed switch once during each flywheel revolution. Flywheel construction permitted the rim containing the disc magnet to be rotated independently of the flywheel hub, if desired. This feature allowed reed switch closure to be moved to any selected time in the plate oscillation cycle. Flywheel rim orientation relative to the hub was adjusted such that reed switch closure occurred when the plate reached maximum upward pitch angle. Upon detection of switch closure, a signal conditioning unit generated an electrical pulse suitable for oscilloscope triggering.

Data gathering was performed by a Zenith model 241 microcomputer equipped with a model R1000 Rapid Systems 4x4 Digital Oscilloscope Peripheral. The Rapid Systems R1000 is capable of simultaneous data acquisition on four channels at sampling frequencies of up to 0.5 MHz, with an analog bandwidth of 250 KHz. For this experiment, two channels, each sampled at 2 KHz, were used for the two elements of the tandem element hotwire anemometer. A third channel, also sampled at 2 KHz, accepted the trigger pulse generated by the signal conditioning unit upon reed switch closure. Raw data from these three channels were stored on floppy disks for later reduction using Basic routines hosted on the Zenith microcomputer.

The hotwire anemometer probe body employed a gooseneck configuration to suspend the probe volume above the plate surface. To minimize flow intrusion and still retain the necessary degree of structural integrity, the gooseneck was fabricated of small diameter stainless steel hypodermic tubing. The end of the gooseneck opposite the probe volume

terminated in a thin stainless steel plate which was mounted flat on the oscillating plate surface using thin double-sided adhesive tape. The probe mounting plate was separated from the probe volume by a distance of 3.50 cm.

At the probe volume end of the gooseneck, two pairs of 0.30 mm diameter stainless steel needles projected 1.30 cm downward beyond the end of the hypodermic tubing to carry the hotwire elements. The orientation of the needle points was such that the hotwire elements, when soldered thereon, were supported in tandem configuration. That is, elements were parallel to each other and separated by a distance of 1.75 mm. With the probe properly affixed to the plate, the hotwire elements occupied a plane parallel to the plate surface, with the two tandem elements separated from each other by 1.75 mm in the streamwise direction. The hotwire elements consisted of Wollaston wire having 10% rhodium-platinum elements 5 microns in diameter.

Each of the two hotwire probe elements was operated in conjunction with one of two independent constant temperature hotwire anemometer units equipped with linearizing circuits. Overheat resistance ratios of both anemometer circuits were set at 10 percent. This rendered the anemometers sensitive to variations in flow temperature as well as velocity. Thus, the hotwire element immersed in the thermal wake of the other experienced less cooling, which yielded output signals of reduced magnitude.

As such, reverse flow was considered to have been detected when the signal associated with the element nearest the plate trailing edge assumed a magnitude greater than that of the element closest to the leading edge. This assumption was explicitly tested, as seen below. Obviously, the anemometer indicating the correct local flow speed was that which showed the highest flow

speed, this anemometer being exposed to flow unaffected by the other hotwire element wake.

Results

Hotwire Anemometry Data

Measurement system characteristics. Data presented in Chapter III affirm the two-dimensionality of the flow along the plate centerline over a major portion of the chord. Also in evidence was the symmetry of the flow field about the centerline. In this experiment, hotwire data were collected along the plate centerline. Thus, the local flow velocity vector was expected to conform to that of previous observations and to lie in a plane perpendicular to both hotwire elements.

With the probe properly installed on the plate, the probe element plane was parallel to the plate surface, and the individual elements were parallel to the plate axis of rotation. The probe element plane was never located more than 1.0 mm above the surface. Still, due to the complex nature of unsteady separation, flow tangency at the plate surface was no guarantee of flow parallel to the plate at the height of the probe element plane. Thus, flow continuously parallel to the element plane was equally uncertain.

The flow reversal detection capability of the probe in the presence of such a type of flow angularity needed to be verified. This was accomplished by first suspending the probe in the center of the otherwise empty test section, with test section velocity set at 5 ft/sec. The probe was then rotated about an axis parallel to the elements, varying the angle between the element plane and the test section centerline.

With the element plane parallel to the test section centerline and the hotwire elements oriented vertically, velocity sensed by the upstream anemometer was approximately 35 percent greater than that sensed by the downstream one. The element plane was then rotated about an axis parallel to the hotwire elements, to an angle of 15 degrees with respect to the test section centerline. In this orientation, the upstream anemometer sensed a velocity which still exceeded by nearly 10 percent that sensed by the downstream one. In this manner, it was determined that the probe was capable of detecting flow reversal provided the fluid velocity vector remained within approximately 15 degrees of the probe element plane. These results were consistent with those reported for other tandem element probes of similar design (Eaton, et al., 1979; Mahler, 1982; Shivaprasad and Simpson, 1982)

Frequency response of each constant temperature hotwire anemometer was set such that anemometer bandwidth was approximately 0.5 kHz. Velocity fluctuations of interest in the experimental results exhibited frequencies which were at least one order of magnitude lower than the 0.5 kHz cutoff frequency. As such, results confirmed that this bandwidth was wide enough to detect all frequencies pertinent to the phenomenon under investigation. At the same time, bandwidth was sufficiently narrow to exclude undesirable electromagnetic interference.

The linearized anemometer signals were sampled by the Rapid Systems digital oscilloscope peripheral unit at a frequency of 2kHz. With both anemometer bandwidths set at 0.5 kHz, digital sampling occurred at a frequency four times that of the highest frequency of interest. As such, the 2 kHz

sampling rate easily met the Nyquist criterion.

Both linearized hotwire anemometer signals were digitally sampled at 2 kHz over 20 consecutive plate oscillation cycles. The timing mark, consistently generated at plate maximum upward pitch angle by reed switch contact closure, was also sampled at 2 kHz. Using this timing mark to insure phase coherency between cycles, the 20 individual cycles were ensemble averaged to yield a representative time history of flow velocity magnitude over a single cycle.

Through ensemble averaging, time varying components of the discretized anemometer signal were significantly attenuated unless phase coherent with plate oscillation. These random components arose predominantly from such sources as turbulence, electromagnetic interference and discretization error.

The independent variables explored in this investigation were reduced frequency parameter values of 0.25, 0.5, 1.0 and 2.0, and, for the three highest reduced frequencies, mean pitch angles of 0, 5, 10 and 20 degrees. Only mean pitch angles of 10 and 20 degrees were investigated for the reduced frequency parameter value of 0.25. Pitch amplitude was held constant at 10 degrees. For each reduced frequency/mean angle combination the probe was placed successively at each of 10 chord stations in the measurement region located along the plate centerline. Test section velocity was 10.0 ft/sec for the reduced frequency of 0.25 and 5.0 ft/sec for all other reduced frequencies.

The 10 chord stations where the probe was placed were located at 7.5, 15, 22.5, 30, 40, 50, 60, 70, 80 and 92.5 percent chord. Chord stations were chosen at 7.5 and 92.5 percent chord in order to examine the flow on the tapered leading and trailing segments of the plate. Remaining stations were

arrayed in a manner intended to yield slightly improved spatial resolution in the forward portion of the plate. Here, recently formed leading edge vortices were still relatively compact and cohesive, as suggested by flow visualization.

Individual chord station flow velocity histories. For each combination of reduced frequency parameter and mean pitch angle, the probe was successively positioned at each of 10 chord stations on the plate centerline. Probe element plane height above the plate surface was 1.0 mm for the upper surface cases and 0.5 mm for those on the lower surface. Data collected at individual chord stations over 20 plate pitch cycles were then ensemble averaged to produce an individual history of the flow velocity at each chord station. In addition to recording the time varying flow velocity at the chord station, each flow history also documented episodes of flow reversal. Variations in reduced frequency parameter, mean pitch angle and chord location were all observed to strongly influence individual flow history character.

Across the experimental range of reduced frequency and mean pitch angle, directional surface flow anemometry was performed at a fixed height above each plate surface. As such, detailed boundary layer profile characterizations were not performed. However, this methodology was consistent with, and rendered feasible, the experimental objective of ascertaining the role of surface flows in vortex kinematics over a broad parametric range. To fulfill this objective, it was sufficient that the anemometry provide a consistent index of flow speed and direction within the boundary layer.

That the anemometric measurements done at a height of 1.0 mm above the plate upper surface were representative of boundary layer behavior was

verified by performing identical measurements at heights of 0.5 mm and 1.5 mm above the plate upper surface. These additional measurements were done at the same 10 chord stations and for reduced frequencies of 1.0 and 2.0 and at mean pitch angles of 0 and 10 degrees. On the lower surface, supplemental anemometry was done at heights of 0.75 mm and 1.0 mm, for a more restricted set of chord stations, reduced frequencies and mean pitch angles.

These additional tests showed that measurements performed higher in the boundary layer than 1.0 mm on the upper surface, and higher than 0.5mm on the lower surface, would have failed to detect flow reversal episodes of significant speed and duration. Alternatively, anemometry done at heights lower than these would have recorded events which were qualitatively similar to those observed at 1.0 mm (upper surface) and 0.5 mm (lower surface). However, velocity magnitudes, being appreciably lower, would have significantly reduced signal to noise ratio of the measurement system.

Figure 5-1 shows three pairs of flow speed histories selected from the airfoil upper surface (K = 2.0, MPA = 10 degree case), which constitute three individual flow velocity histories. One complete plate pitching cycle, beginning at maximum upward plate pitch angle, is presented in each graph. The plot having symbols superimposed on it corresponds to the fore probe element, that element nearest to the plate leading edge. Aft element response is depicted by the uninterrupted solid line.

The top graph in Figure 5-1 shows the 7.5 percent chord flow history. For most of the cycle, the velocity history assumed a generally sinusoidal appearance. Late in the cycle, though, sinusoidal appearance was appreciably perturbed as flow reversal occurred. Interestingly, flow speed did not appear to

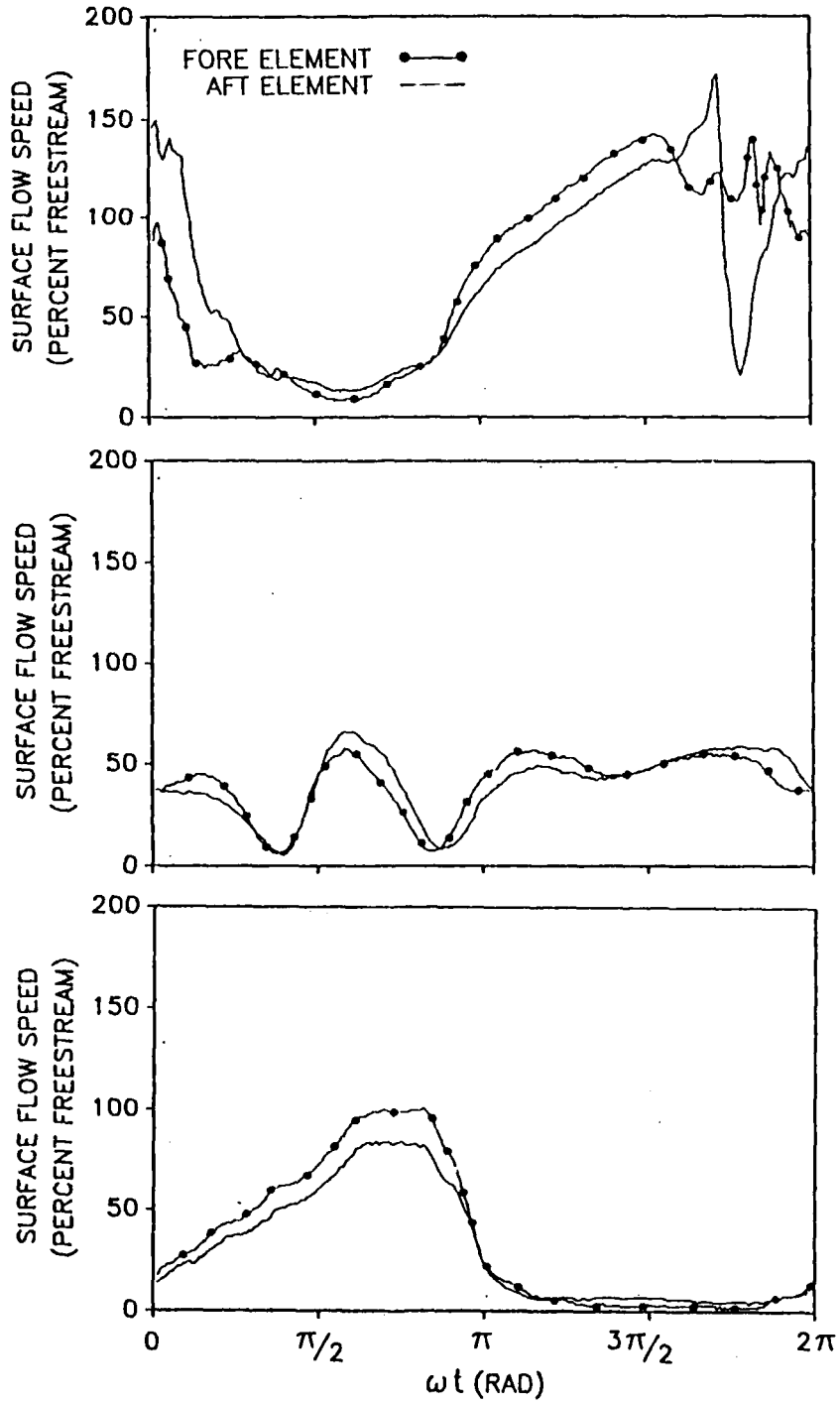

Figure 5-1. Individual chord station flow velocity histories of K = 2.0, MPA = 20 degrees, upper surface. Chord stations are (from top) 7.5 percent, 30 percent and 92.5 percent. Probe element plane located 1.0 mm above plate surface.

decrease to zero prior to reversal. Also, flow reversal did not initiate and then persist uninterrupted. Rather, it appeared intermittently, and later ceased when flow speed was approximately 20 percent of the freestream value.

The middle graph in Figure 5-1 depicts the flow velocity history at 30 percent chord. While overall velocity history did not exhibit a discernible sinusoidal appearance, two episodes of flow reversal were apparent. The first began just prior to quarter cycle, when flow speed decreased to approximately 6 percent freestream. Following this, reverse flow speed built steadily to a peak value of 68 percent freestream, and then decreased steadily to approximately 10 percent freestream, when downstream flow resumed. Using existing leading edge vortex kinematics data, this flow reversal occurrence was linked to passage of the leading edge vortex. The second episode of flow reversal initiated at approximately three-quarters cycle and persisted until the cycle was completed. Flow speed did not appear to decrease below 40 percent freestream at any time during this occurrence. This episode was not associated with any observed vortical structures.

The bottom graph in Figure 5-1 shows the flow velocity history at 92.5 percent chord. As at the 7.5 percent chord station, the flow velocity history took on a sinusoidal appearance, albeit a somewhat more distorted one near the trailing edge. The sinusoidal behaviors common to the 7.5 and 92.5 percent chord stations appeared to be approximately one half cycle out of phase. An extended episode of flow reversal began just following midcycle and persisted until just prior to cycle completion. Reverse flow speed throughout this occurrence did not exceed 6 percent freestream.

High resolution smokewire flow visualization was performed in the 7.5

percent chord neighborhood, for the time late in the cycle at which flow reversal first occurred. These flow visualization photographs are presented in Figure 5-2. The upper photograph corresponds to a time approximately 0.005 sec prior to the time at which the two plots intersect. The lower photograph coincides with the time when the two plots intersect. The 7.5 percent chord position is denoted in both plates by the white arrow.

The upper photograph shows a thickening of the boundary layer in the plate leading edge region. Streakline orientation at 7.5 percent chord suggests the flow velocity vector was displaced approximately 7 degrees from parallel to the plate surface. In the lower photograph, a vortex has initiated just downstream of the leading edge. At 7.5 percent chord, the outermost streakline encircling the vortex appears to stagnate and split into two branches on the plate surface. One branch extends upstream of the bifurcation point, and the other stretches downstream.

Figure 5-3 shows three pairs of flow speed histories chosen from the lower surface K = 2.0, MPA = 5 degree case, which constitute three individual flow velocity histories. The top graph shows flow velocity history at 7.5 percent chord, the middle one corresponds to 30 percent and the bottom graph deals with 92.5 percent chord. As before, one complete cycle, beginning at maximum upward plate pitch angle, is presented in each graph. The plot having symbols superimposed on it corresponds to the fore probe element, that element nearest to the plate leading edge. Aft element response is depicted by the uninterrupted solid line.

All three velocity histories in Figure 5-3 display general appearances that are decidedly sinusoidal in nature. Similar to the upper surface, a phase

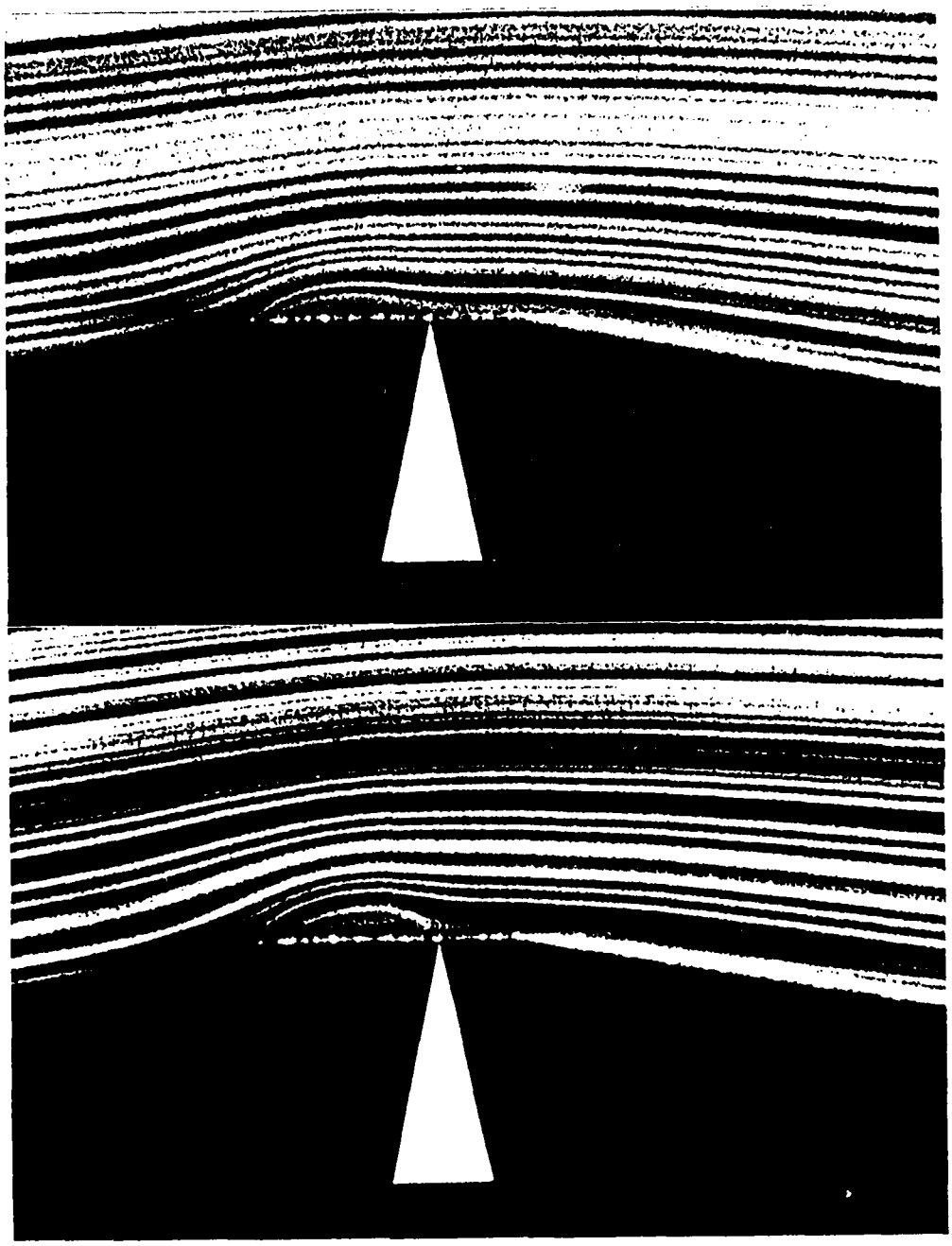

Figure 5-2. Flow visualization of plate leading edge region during leading edge vortex initiation. Time elapsed between frames is 0.005 sec. 7.5 percent chord station is indicated by white arrows.

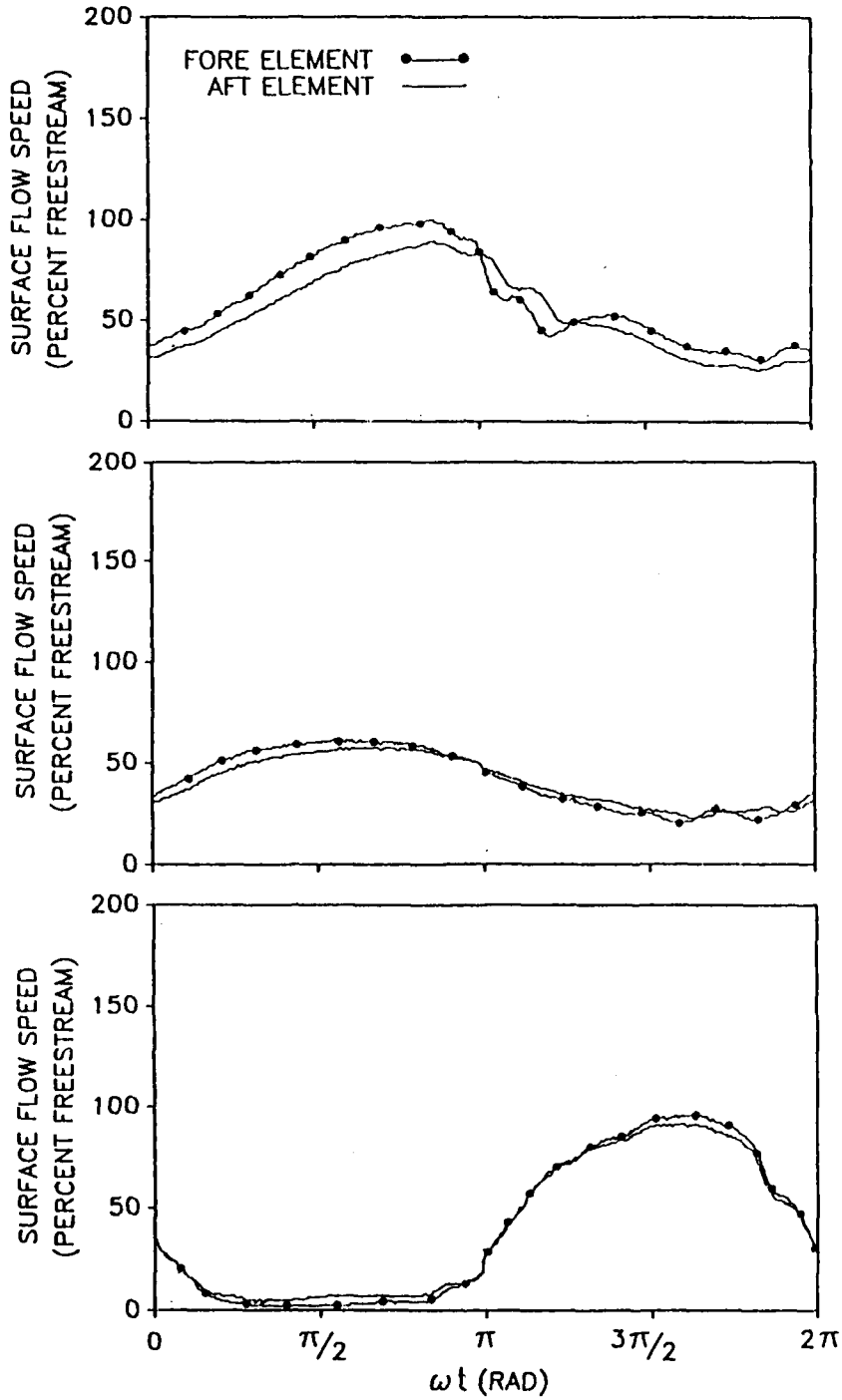

Figure 5-3. Individual chord station flow velocity histories of K = 2.0, MPA = 5 degrees, lower surface. Chord stations are (from top) 7.5 percent, 30 percent and 92.5 percent. Probe element plate located 0.5 mm above plate surface.

shift of approximately one-half cycle existed between the 7.5 and 92.5 percent chord stations. In addition, the lower surface flow history at 30 percent chord exhibited sinusoidal behavior which was nearly in phase with the 7.5 percent chord flow history. Magnitudes of the sinusoidal flow histories were comparable for 7.5 and 92.5 percent chord. Magnitude of the 30 percent chord station history was approximately half that of those at 7.5 and 92.5 percent.

As these are lower surface velocity histories, sinusoidal character was not disrupted by the presence of leading edge vortices. However, flow reversal was observed on the plate lower surface. Reversal initiated at 7.5 and 30 percent chord as the plate began to pitch up. Reverse flow then persevered for approximately one-sixth cycle at 7.5 percent chord and approximately one-third cycle at 30 percent chord. Flow speed decreased neither prior to nor following these instances of flow reversal. Although these observations may seem physically inconsistent, the ensuing discussion will clarify the compatibility between these and other experimental results.

Plate surface flow reversal histories. Individual chord station flow velocity histories contained flow reversal information as well as flow speed data. Flow reversal was defined as having occurred whenever flow speed sensed by the aft hotwire element exceeded that sensed by the fore element. Microcomputer based software routines were designed to detect fulfillment of this reversal criterion, and then employed to identify episodes of flow reversal in each individual chord station flow history. This was accomplished and the resulting data compiled for all 10 chord stations on both sides of the plate, for each combination of reduced frequency and mean pitch angle.

This data reduction yielded upper and lower surface flow histories

similar to those shown in Figures 5-4 and 5-5. The 10 discrete chord stations lie along the graph vertical axis, with plate leading edge corresponding to the top of the graph. Pitch oscillation cycle increases to the right on the horizontal axis, and two complete cycles are depicted in each history. Pitch oscillation cycle begins at plate maximum upward pitch, consistent with the convention used previously. At any given chord station, the temporal occurrence of flow reversal episodes is indicated by the presence of horizontal traces. Time during the cycle at which the leading edge vortex passed the chord station is indicated by the open square plotting symbols.

Evaluation of the four reversal histories in Figure 5-4 in absolute terms was not attempted. However, comparisons between the four demonstrate qualitatively the influence of variations in reduced frequency and mean pitch angle. At a reduced frequency of 0.5, increasing the mean pitch angle from 5 degrees to 20 degrees substantially increased the duration of flow reversal over the entire plate chordlength. For a reduced frequency of 2.0, increasing mean pitch from 5 degrees to 20 degrees yielded an increase in reverse flow duration over the forward portion of the plate, and a reduction in duration on the rear portion.

In all four histories displayed in Figure 5-4, flow reversal appears to be closely related to the leading edge vortex. At a reduced frequency of 0.5, for both mean pitch angles, flow reversal generally extended one chord station or more upstream and downstream of the leading edge vortex location. At K = 0.5, increasing the mean pitch angle from 5 degrees to 20 degrees broadened the extent of the flow reversal in both the upstream and downstream directions.

For the reduced frequency of 2.0, at mean pitch angles of both 5 and

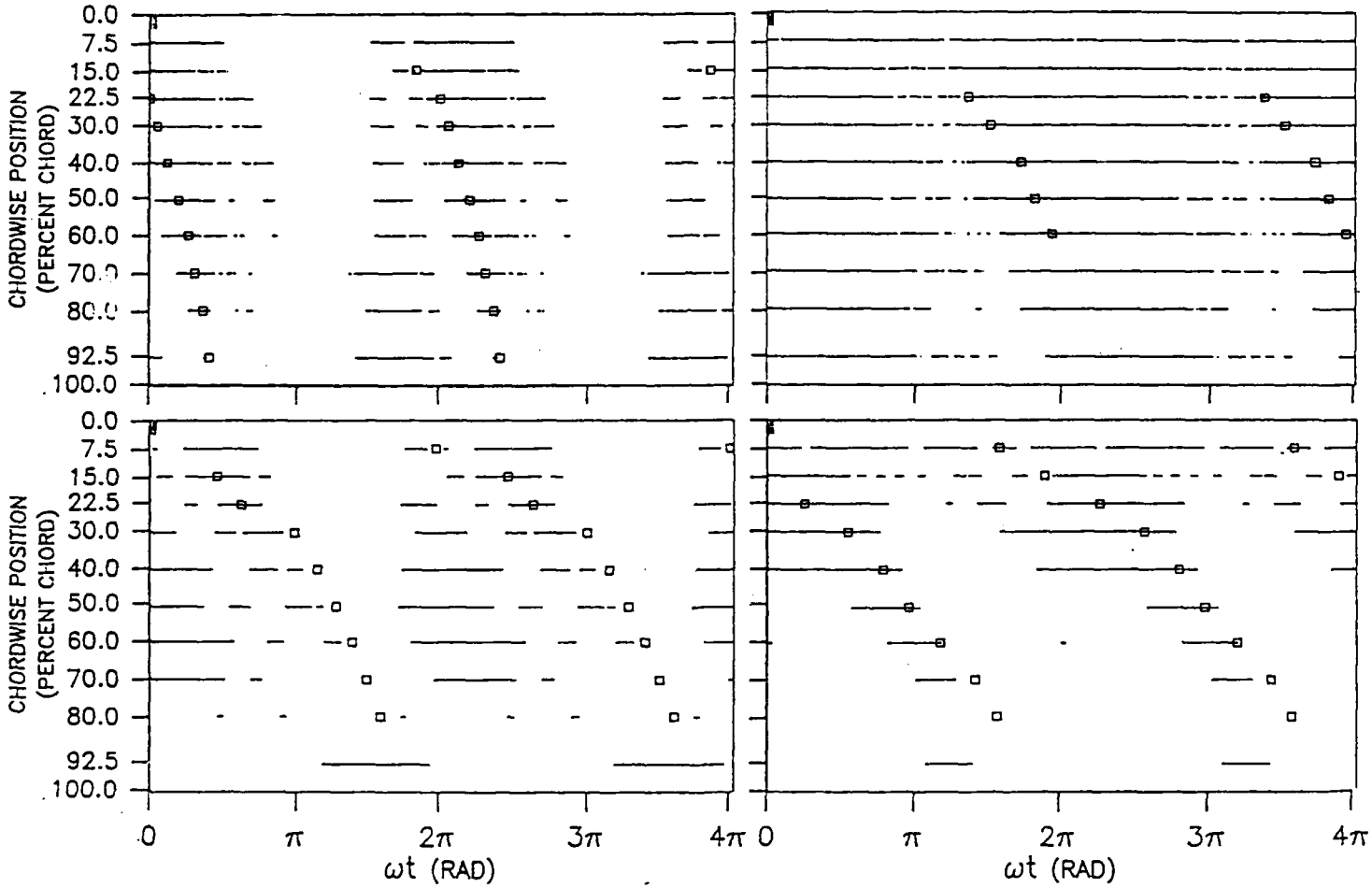

Figure 5-4. Upper surface flow reversal histories over two cycles. Conditions are (upper left) K=0.5, MPA=5 degrees; (upper right) K=0.5, MPA = 20 degrees; (lower left) K=2.0, MPA=5 degrees· (lower right) K=2.0, MPA=20 degrees. Horizontal lines show flow reversal. Arrival of LEV area centroid at chord station shown by open square.

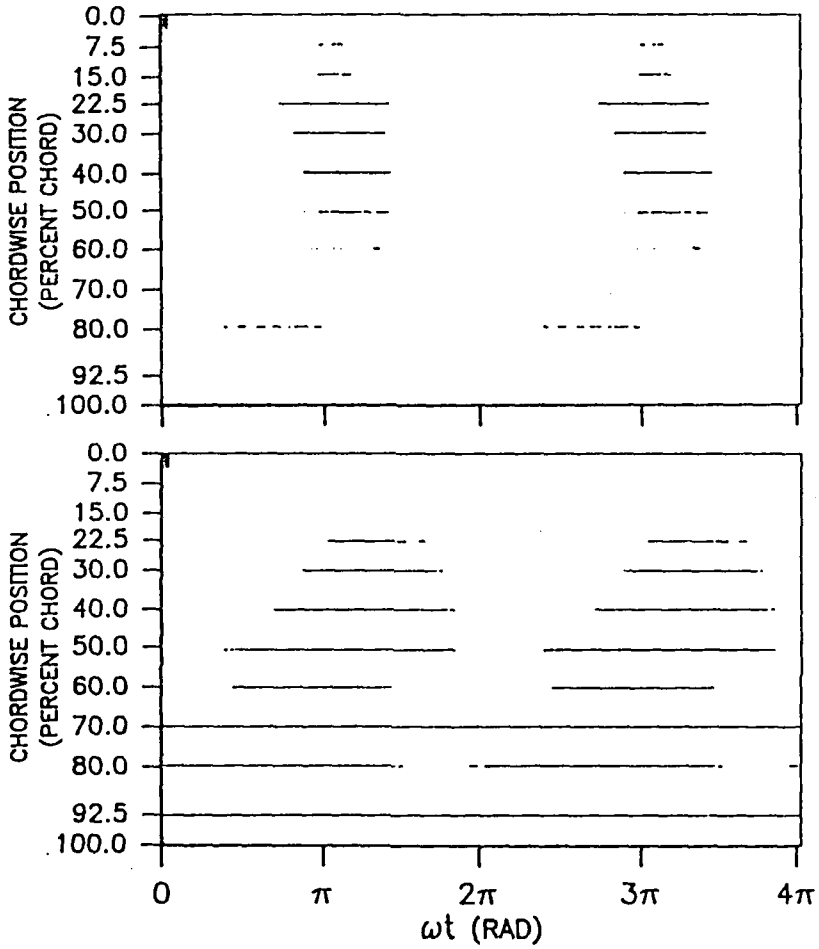

Figure 5-5. Lower surface flow reversal histories over two cycles. Conditions are (from top) K = 0.5, MPA = 5 degrees; K = 2.0, MPA = 20 degrees. Horizontal lines indicate presence of flow reversal.

20 degrees, reverse flow typically extended both upstream and downstream of the leading edge vortex when the vortex resided in the forward portion of the plate. As the leading edge vortex convected toward the trailing edge, reverse flow upstream of the vortex typically ceased, and flow reversal downstream of the leading edge vortex was diminished in spatial extent.

The precise time and location of leading edge vortex initiation was not isolated in this investigation. However, the chord station and time at which the leading edge vortex initially appears in the data are reasonable estimates of the actual location and time of initiation. Using this approximation, two crucial observations can be made concerning reverse flow and leading edge vortex initiation in Figure 5-4. First, flow reversal was not observed which extended uninterrupted from the plate trailing edge to the initiation site prior to leading edge vortex initiation. Second, in the two histories shown for reduced frequency of 2.0, no reverse flow was observed downstream of the initiation site prior to leading edge vortex initiation.

Figure 5-5 shows flow reversal histories for the lower plate surface. Once again, two complete cycles are shown, and the first cycle begins when the plate reaches maximum upward pitch angle. It is remarkable that flow reversal occurs on a surface that is never inclined away from the oncoming freestream flow. As reduced frequency and mean pitch angle are increased from 0.5 and 5 degrees to 2.0 and 20 degrees, flow reversal duration is prolonged and broadened in spatial extent. Over the entire experimental parameter range, duration and spatial extent of flow reversal on the plate lower surface generally increased in response to both greater reduced frequency and higher mean pitch angle.

Correlations Between Vortex Kinematics and Surface Anemometry

To clarify the physics underlying unsteady separation, correlations were sought between physical parameters thought to be strongly interdependent. Such an interdependence was postulated to exist between local surface flow average velocity and leading edge vortex instantaneous convection velocity, and also between local surface flow average velocity and leading edge vortex instantaneous cross-sectional area growth rate.

Local surface flow average velocity was defined as the time average of the velocities sensed at two adjacent chord stations while the leading edge vortex cross-sectional area centroid convected from the first of these chord stations to the second. Leading edge vortex instantaneous convection velocity was computed as the quotient of distance between two adjacent chord stations and time elapsed as the vortex convected from the first of these chord stations to the second. Leading edge vortex instantaneous cross-sectional area growth rate was defined as the quotient of cross-sectional area growth occurring between two adjacent chord stations and time elapsed as the vortex convected from the first of these chord stations to the second.

Local surface flow average velocities were computed from local surface flow histories according to the above definition. Actual computations were performed by a microcomputer based software routine. Leading edge vortex instantaneous convection velocities and instantaneous growth rates were derived from existing leading vortex kinematics data. Local surface flow average velocity, leading edge vortex instantaneous convection velocity and leading edge vortex instantaneous growth rate were calculated for each pair of adjacent chord

stations through which the leading edge vortex passed, across the entire experimental range of reduced frequency and mean pitch angle. Local surface flow average velocity was plotted against vortex instantaneous convection velocity and the result is presented in Figure 5-6. In like manner, vortex instantaneous growth rate was plotted against local surface flow average velocity. This result is presented graphically in Figure 5-7.

A linear least-squares fit was applied to the data in Figure 5-6 to disclose the correlation between local surface flow average velocity and leading edge vortex instantaneous convection velocity. Faster reverse flows were clearly associated with decreased leading edge vortex instantaneous convection velocities, and faster downstream flows corresponded to increased leading edge vortex instantaneous convection velocities. In addition, data points showed broader dispersion about the linear fit at negative local surface flow average velocities than at positive local surface flow average velocities.

As with the convection data in Figure 5-6, a linear least-squares fit was applied to the growth data in Figure 5-7. In doing so, a correlation was also revealed in these data. Faster reverse flows were definitely related to higher leading edge vortex instantaneous growth rates, and faster downstream flows were observed in connection with decreased vortex instantaneous growth rates. Wider dispersion of data points around the linear fit occurred at negative local surface flow average velocities than at positive velocities.

In addition to surface flows, the oncoming freestream also influences leading edge vortex kinematics. The projected frontal area of the inclined plate was adopted as an index of attenuation of freestream influence, since projected frontal area is related to the volume shielded from the freestream by the

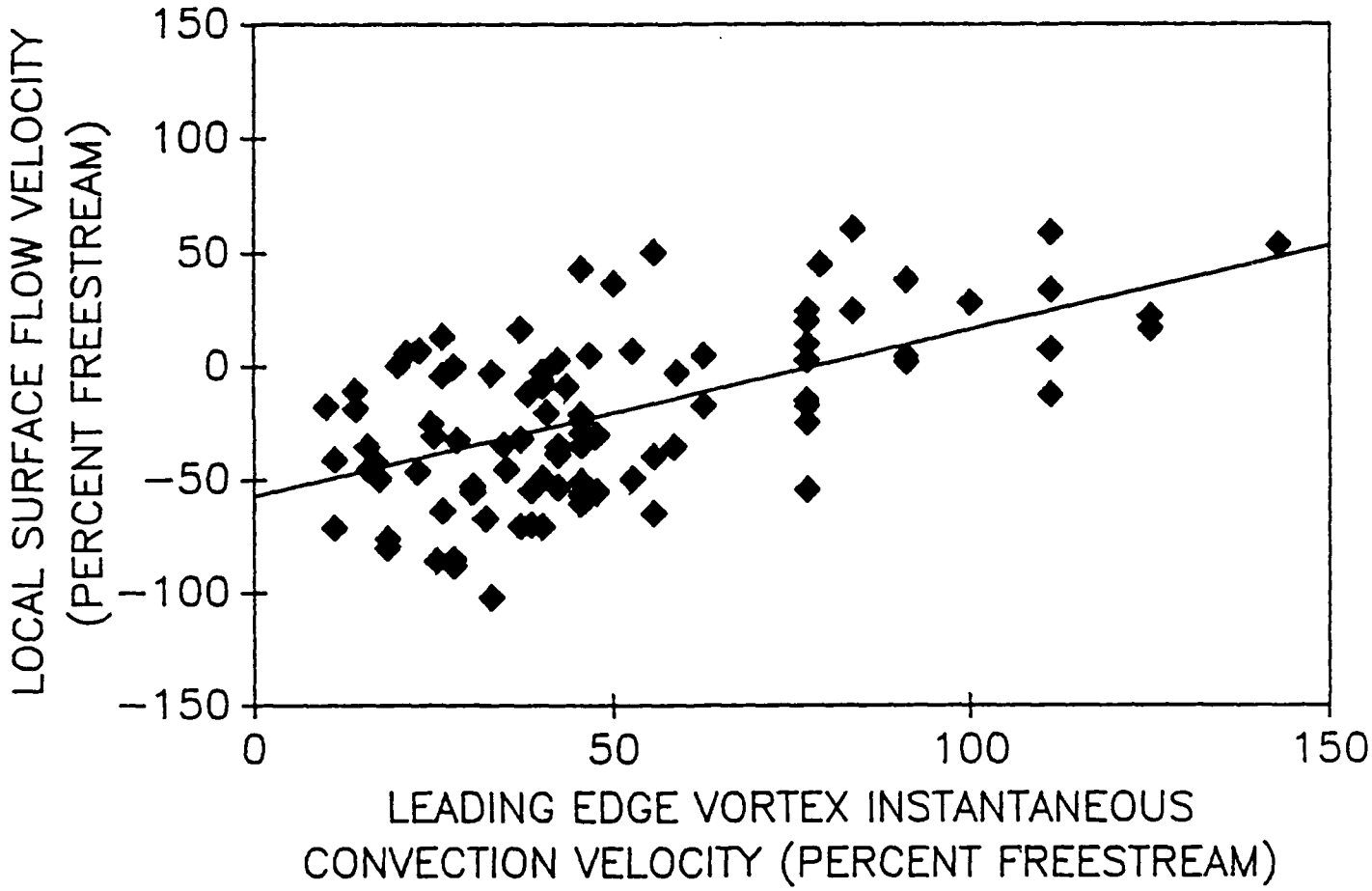

Figure 5-6. Correlation of local surface flow velocity and leading edge vortex instantaneous convection velocity for all experimental conditions. Linear least-squares fit applied to data is shown.

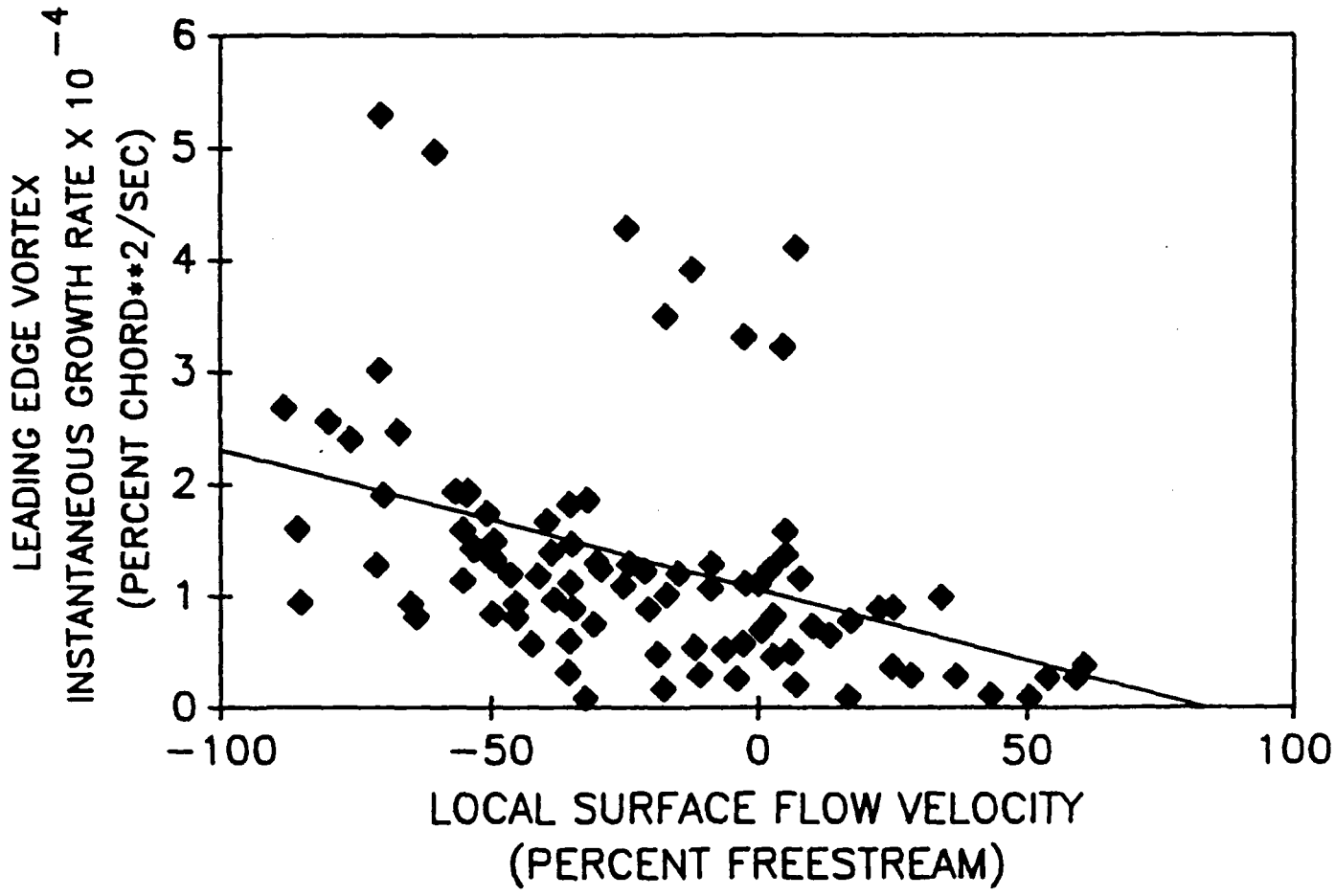

Figure 5-7. Correlation of local surface flow velocity and leading edge vortex instantaneous growth rate for all experimental conditions. Linear least-squares fit applied to data is shown.

inclined plate.

Figures 5-8 and 5-9 present correlations of leading edge vortex instantaneous growth and convection rates, projected frontal plate area and local surface flow average velocity with leading edge vortex cross-sectional area. Each of the four parameters plotted against leading edge vortex cross-sectional area has been normalized with respect to the largest magnitude attained by that parameter for that combination of reduced frequency and mean pitch angle. Correlations are not shown for all reduced frequencies and mean pitch angle combinations examined in this investigation. However, the cases included here are representative of the remaining correlations completed during this investigation but not displayed here.

Figure 5-8 shows correlations for reduced frequencies of 0.5 and 2.0, both at a mean pitch angle of 0 degrees. In the top graph, leading edge vortex instantaneous convection velocity first increased uniformly with leading edge vortex cross-sectional area growth. Eventually, this trend leveled off and vortex instantaneous convection velocity remained constant as the vortex continued to grow. Leading edge vortex instantaneous growth rate displayed a trend similar to vortex convection rate. However, just following vortex initiation, the increase in instantaneous growth rate was generally somewhat less than the increase in convection rate. Late in vortex development, instantaneous convection rate remained constant while instantaneous growth rate declined noticeably. Simultaneously, projected plate frontal area declined uniformly with leading edge vortex instantaneous growth. Local surface flow direction transitioned from reversed to downstream as the vortex grew. However, the magnitude of downstream surface flow decreased substantially after reaching a

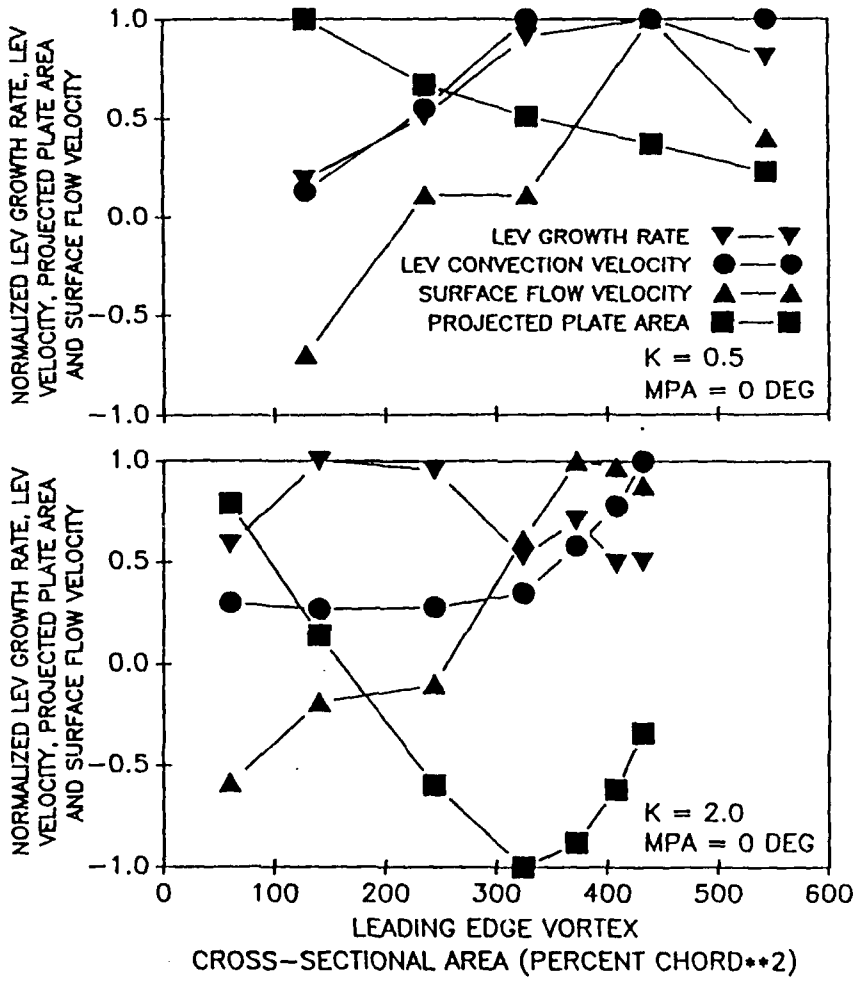

Figure 5-8. Correlation of normalized leading edge vortex instantaneous growth rate and convection velocity, plate projected frontal area and time-averaged surface flow velocity in the vicinity of the leading edge vortex, and leading edge vortex cross-sectional area. K = 0.5 and 2.0, MPA = 0 degrees.

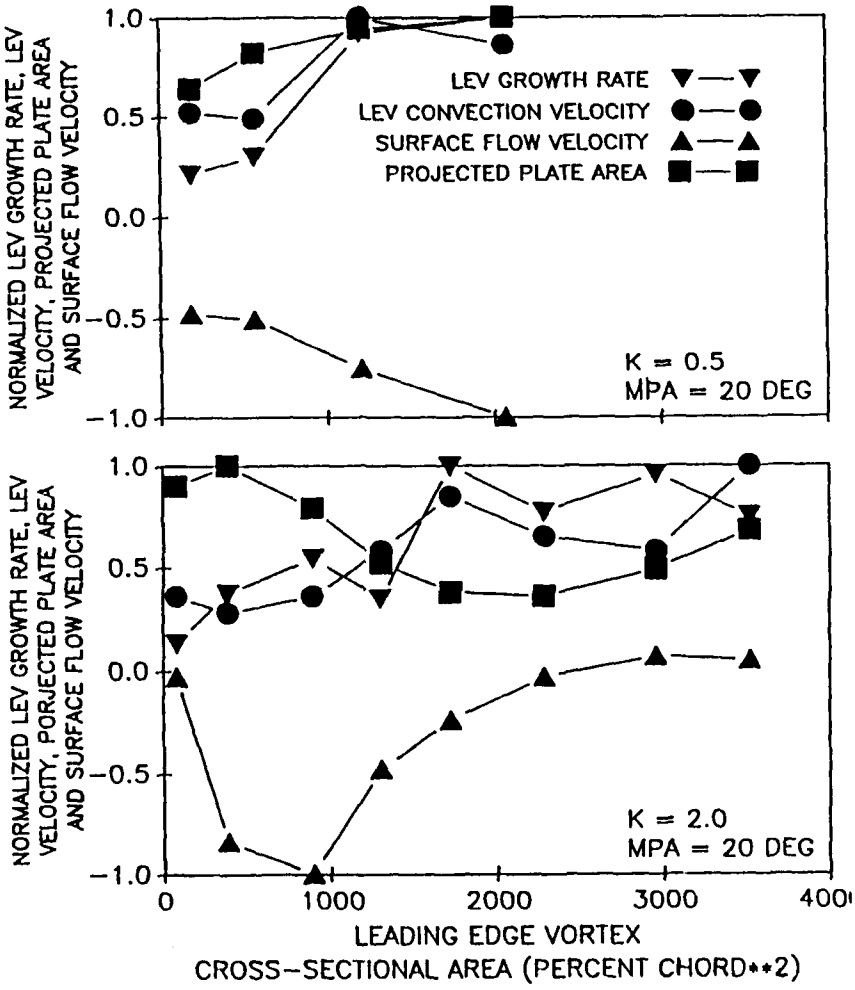

Figure 5-9. Correlation of normalized leading edge vortex instantaneous growth rate and convection velocity, plate projected frontal area and time-averaged surface flow velocity in the vicinity of the leading edge vortex, and leading edge vortex cross-sectional area. K = 0.5 and 2.0, MPA = 20 degrees.

maximum.

The bottom graph in Figure 5-8 assumed a slightly different character than the top one. In contrast to the K = 0.5 case, vortex instantaneous convection velocity and growth rate plots diverged widely. Also, in the initial stages of vortex development, instantaneous growth rate increased substantially while instantaneous convection velocity declined slightly. Thereafter, instantaneous growth rate generally decreased as instantaneous convection velocity rose. At the same time, plate frontal area first decreased with vortex instantaneous growth, and then began to increase again as the plate reached maximum downward pitch angle and started to pitch up again. Over the same time period, local surface flow direction changed from reverse to downstream flow as the leading edge vortex grew. Downstream flow speed increased nonmonotonically with leading edge vortex area, and finally showed a slight decrease in downstream flow speed.

Presented in Figure 5-9 are the correlations for reduced frequencies of 0.5 and 2.0, both at a mean pitch angle of 20 degrees. In the top graph, leading edge vortex instantaneous convection velocity initially experienced a slight decrease with vortex cross-sectional area growth while instantaneous growth rate increased. This was followed by an appreciable rise in both instantaneous convection and growth rates. Finally, instantaneous growth rate continued to rise while instantaneous convection rate declined. Concurrently, plate projected frontal area steadily increased with leading edge vortex growth. During this same time period, local surface flow remained reversed and the speed of this reverse flow generally increased.

The lower graph in Figure 5-9 is unique to the present data set because

of the strong nonmonotonic behavior it exhibits. Initially, leading edge vortex instantaneous convection velocity declined while instantaneous growth rate rose. Instantaneous growth rate then continued to rise and instantaneous convection rate began to do so as well. Subsequently, instantaneous convection rate continued rising while instantaneous growth rate declined to a local minimum and then began once again to increase. In the next stage of development, both instantaneous growth and convection rates declined at approximately the same rate. Thereafter, instantaneous convection rate continued to decrease while instantaneous growth rate increased. Finally, instantaneous convection rate grew while instantaneous growth rate decreased. Plate projected frontal area first increased with increasing leading edge vortex area, then decreased substantially and finally ascended, as the plate pitched up, down and then up again. During most of leading edge vortex development, local surface flow was reversed and relatively high speed. Later on, surface flow did transition to the downstream direction, but downstream flow speed was low.

Figure 5-10 is a refinement of Figure 5-6, with horizontal and vertical grid lines added to indicate, respectively, zero local surface flow average velocity and instantaneous leading edge vortex convection velocity equal to unperturbed freestream velocity. The linear least-squares fit applied to the data indicates that the leading edge vortex tends to convect at approximately 78 percent freestream in the presence of zero surface flow.

Figures 5-11 and 5-12 were constructed by partitioning the data from Figure 5-6 according to whether the plate was experiencing upward or downward pitching motion. A linear least-squares fit was applied to each data set that resulted from the partitioning. Slope of the line fit to the pitch up data

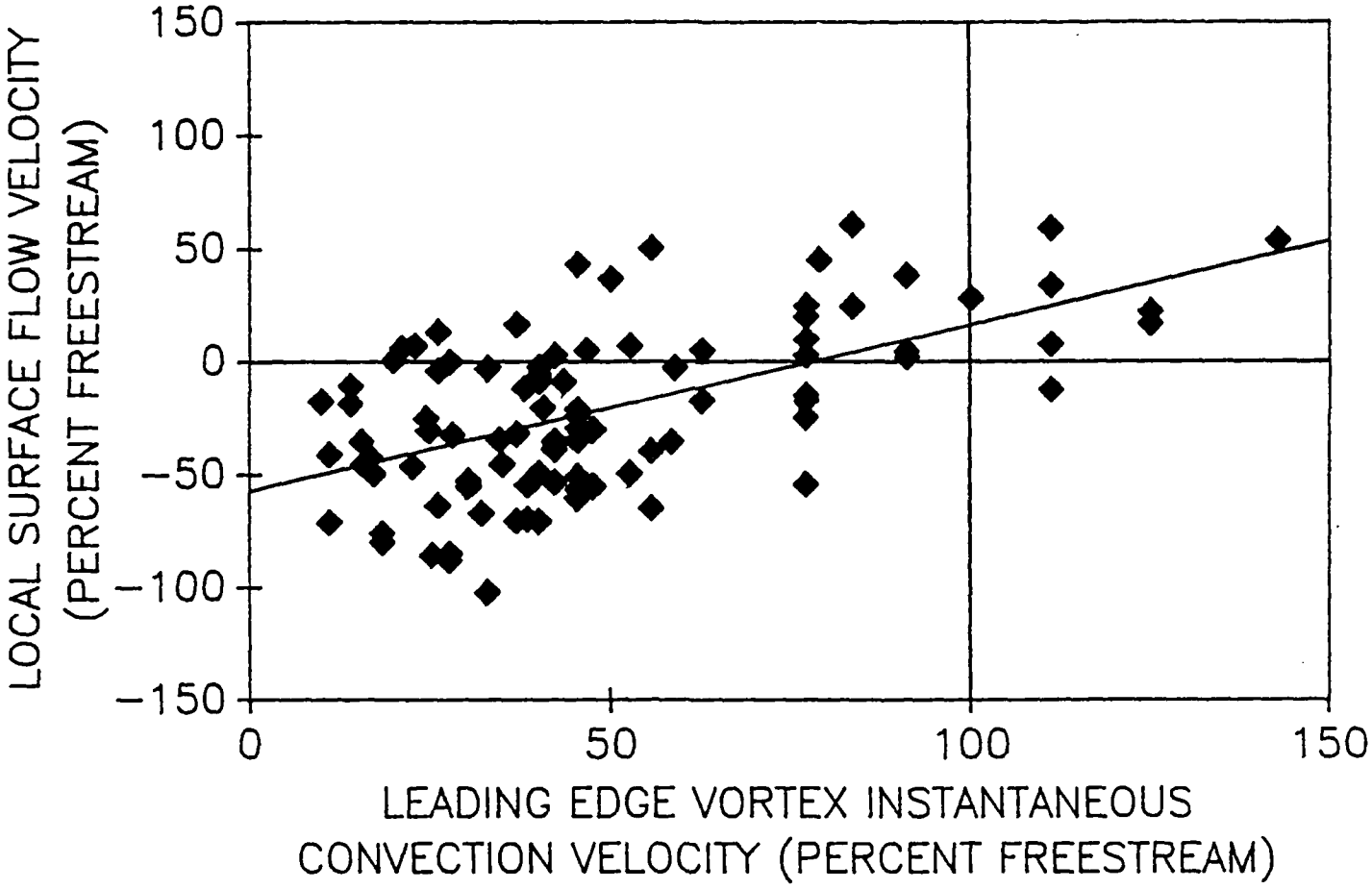

Figure 5-10. Correlation of local surface flow velocity and leading edge vortex instantaneous convection velocity for all experimental conditions. Linear least-squares fit applied to data is shown, and test section velocity is indicated on the horizontal axis.

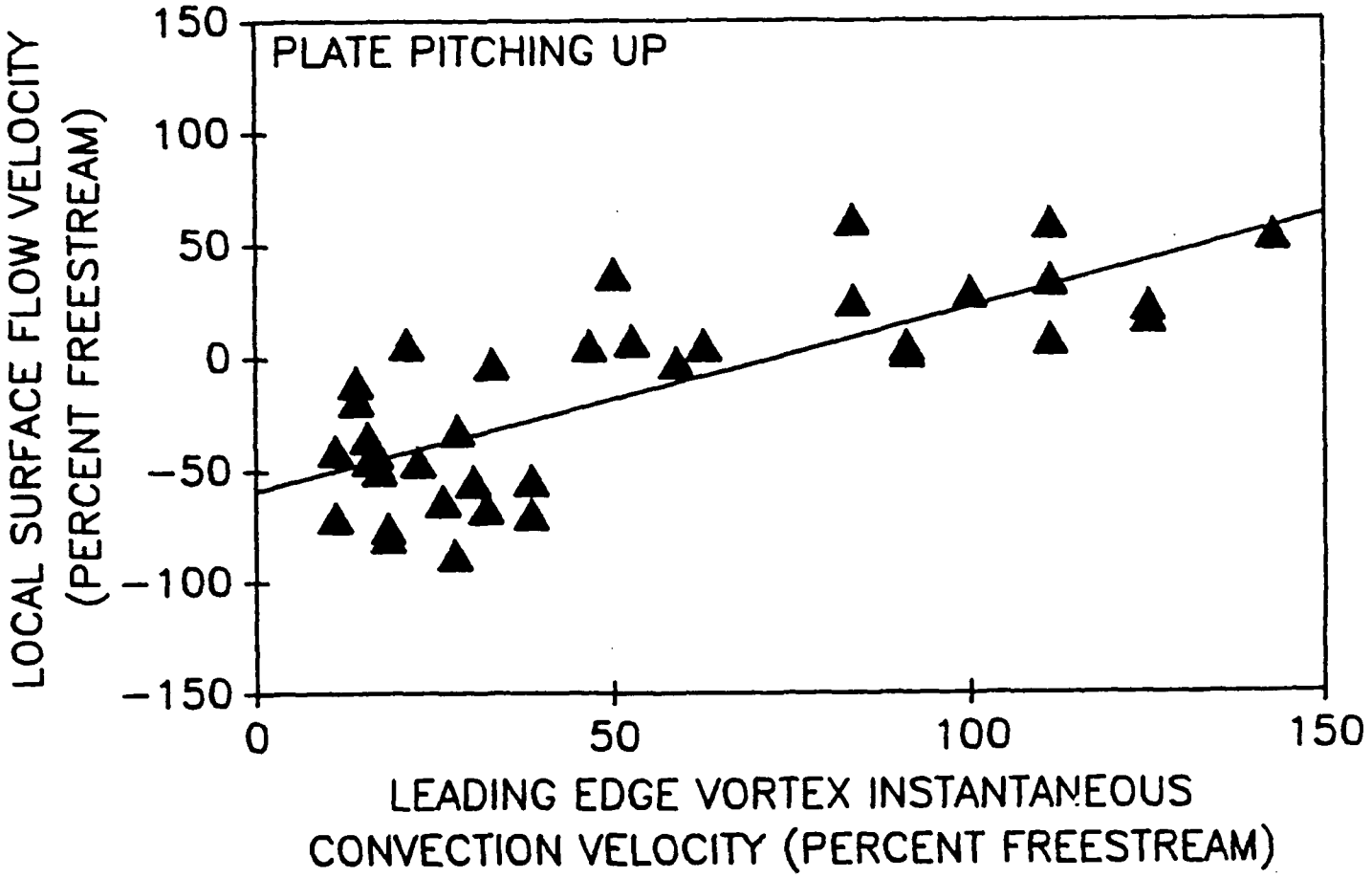

Figure 5-11. Correlation of local surface flow velocity and leading edge vortex instantaneous convection velocity for plate pitching up. Linear least-squares fit applied to data is shown.

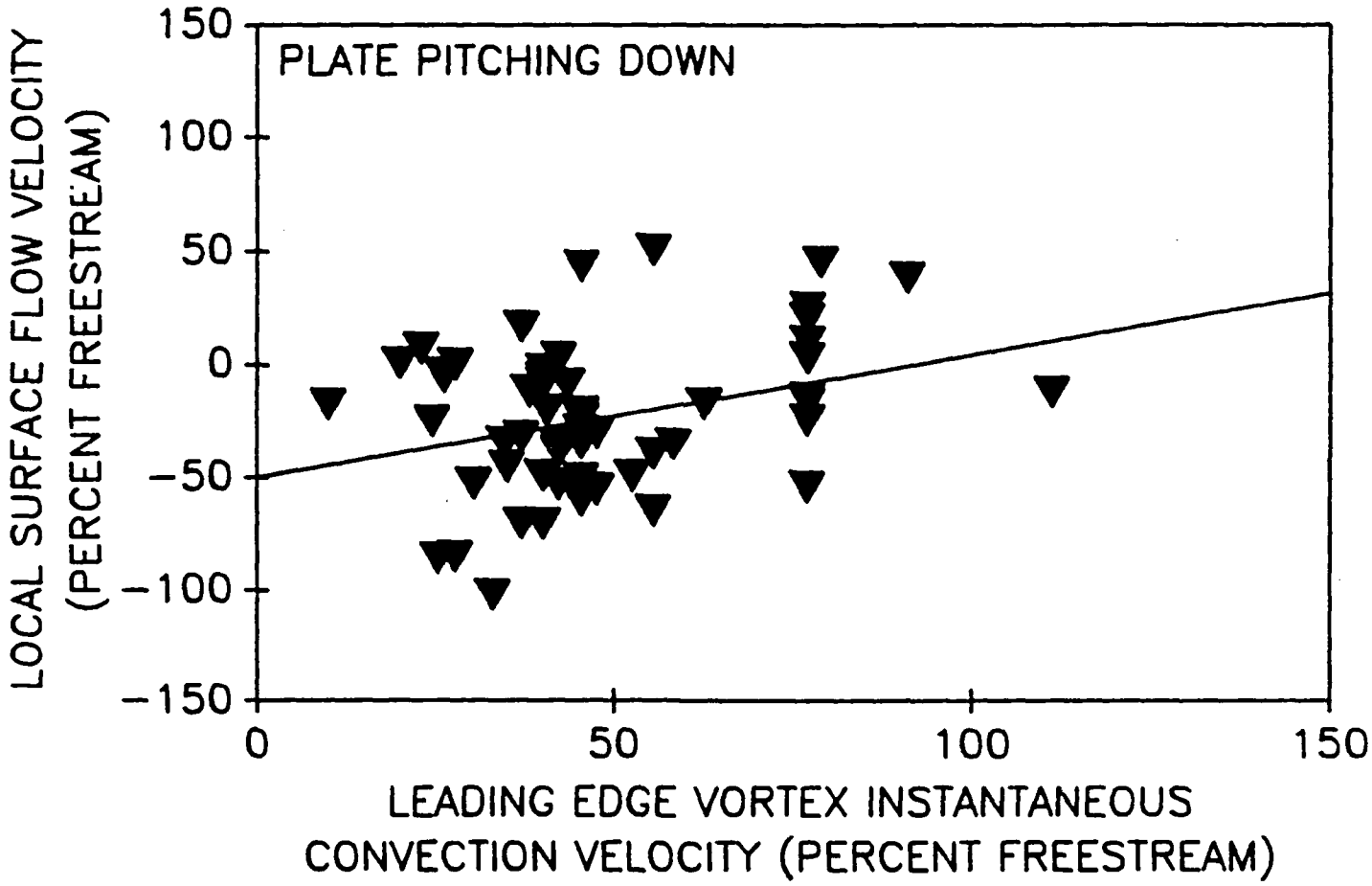

Figure 5-12. Correlation of local surface flow velocity and leading edge vortex instantaneous convection velocity for plate pitching down. Linear least-squares fit applied to data is shown.

was 50 percent steeper than the slope of that applied to the pitch down data. Also noteworthy in Figures 5-11 and 5-12 are the comparative amounts of dispersion about the line which was fit to the data. In Figure 5-11, the pitch up case, individual data points were generally distributed proximal to the linear fit. Figure 5-12, in contrast, shows that data points corresponding to pitch down were widely dispersed about the linear fit.

As with the convection data, leading edge vortex instantaneous growth rate data originally presented in Figure 5-7 were partitioned according to pitch direction to yield Figures 5-13 and 5-14. Again, a linear least-squares fit was applied to each data set that resulted from the partitioning. Slope magnitude of the line fit to the pitch up data was one half that of the slope magnitude computed for the pitch down data. Pitch up data in Figure 5-13 show a slightly greater degree of dispersion about the linear fit than do the pitch down data in Figure 5-14.

Local surface flow average velocity occurring in the vicinity of the leading edge vortex as it convected down the plate was time averaged over the vortex lifetime. This analysis was completed for all reduced frequency and mean pitch angle combinations employed in this experiment. The results, presented graphically in Figure 5-15, demonstrate clear trends. For a given reduced frequency, increasing the mean pitch angle engendered local surface flows in the leading edge vortex neighborhood characteristic of stronger reversal. Alternatively, maintaining constant mean pitch angle while increasing reduced frequency generally caused time averaged local surface flows characteristic of weaker reversal in the leading edge vortex vicinity.

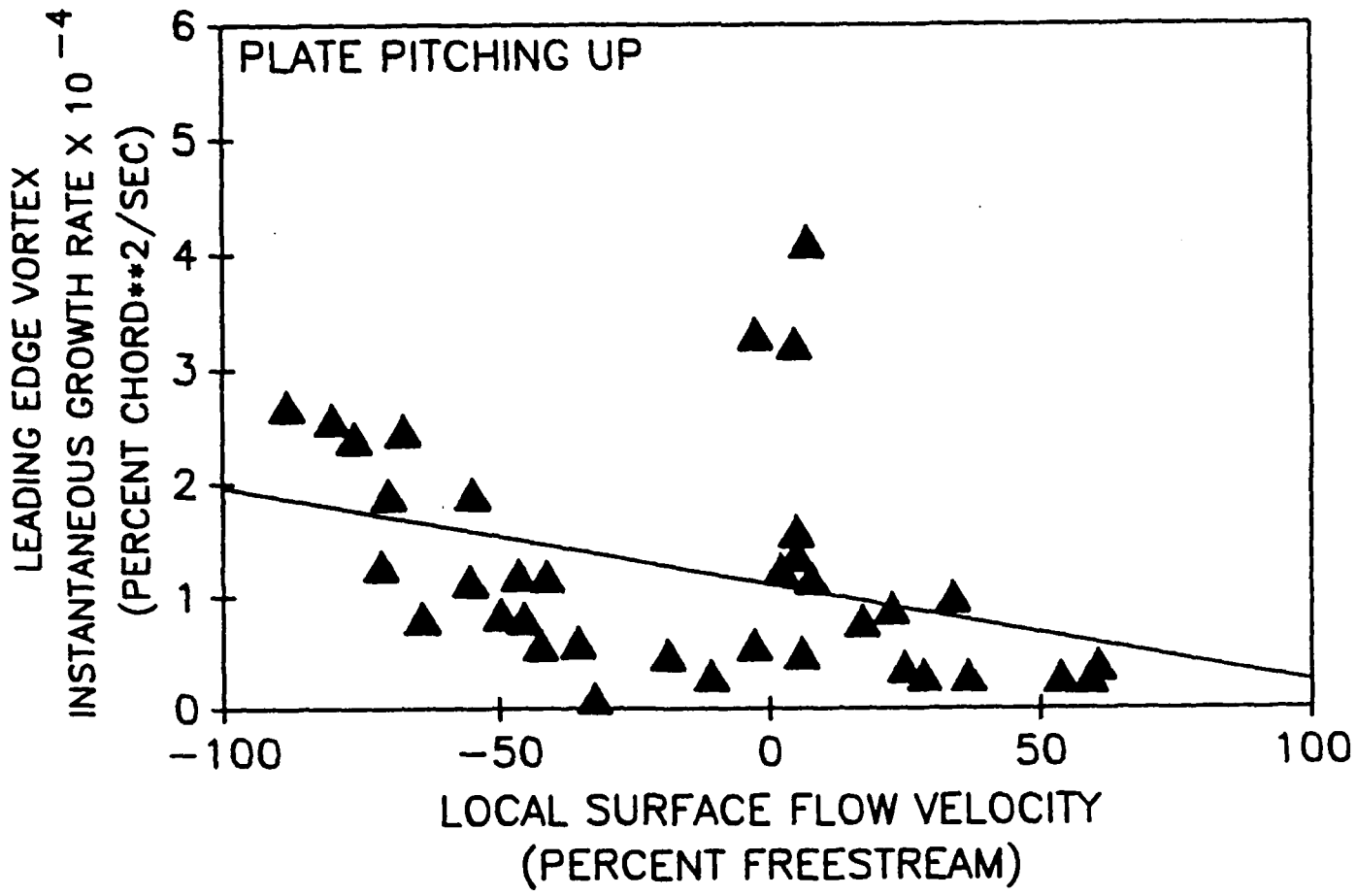

Figure 5-13. Correlation of local surface flow velocity and leading edge vortex instantaneous growth rate for plate pitching up. Linear least-squares fit applied to data is shown.

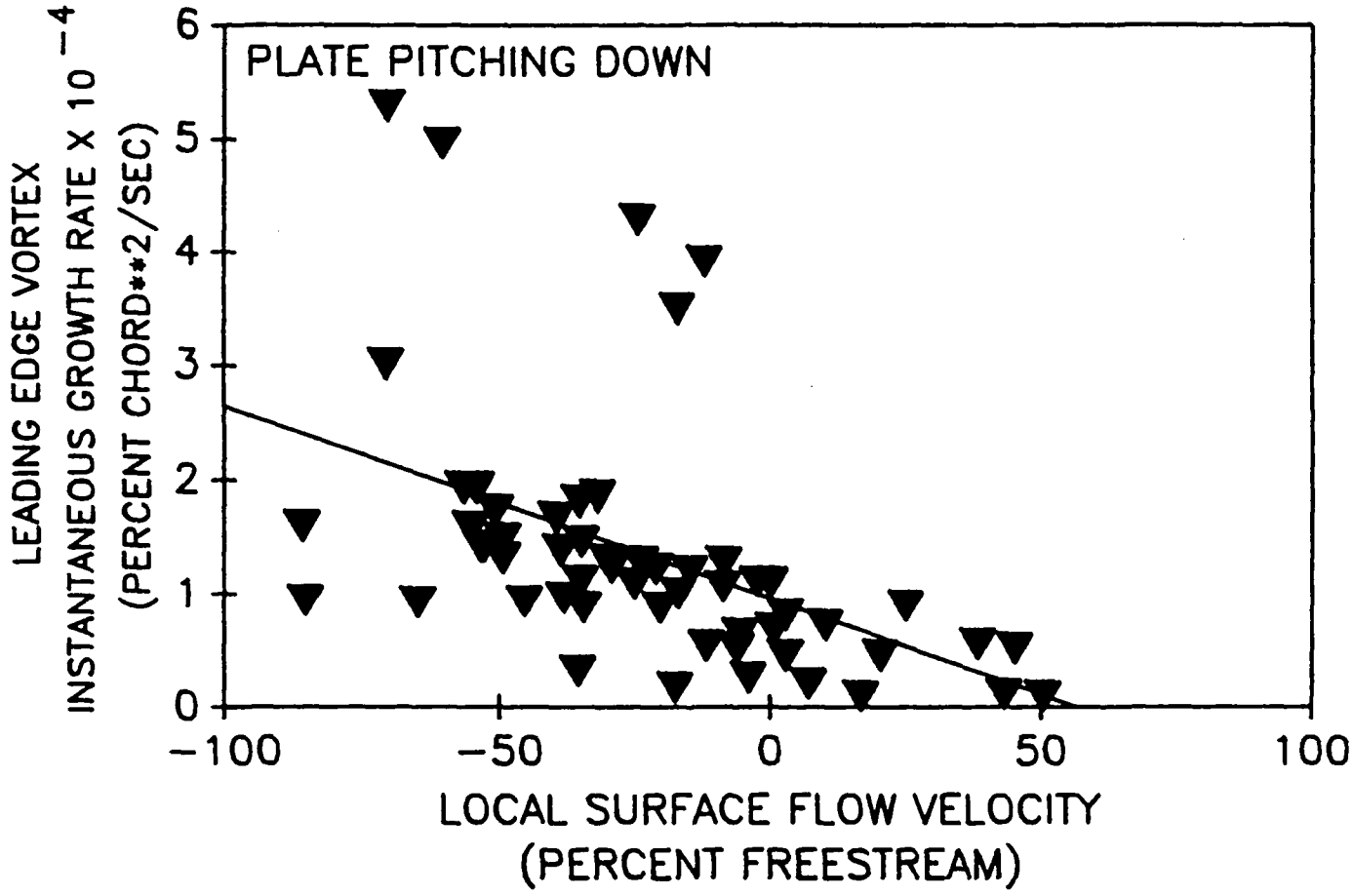

Figure 5-14. Correlation of local surface flow velocity and leading edge vortex instantaneous growth rate for plate pitching down. Linear least-squares fit applied to data is shown.

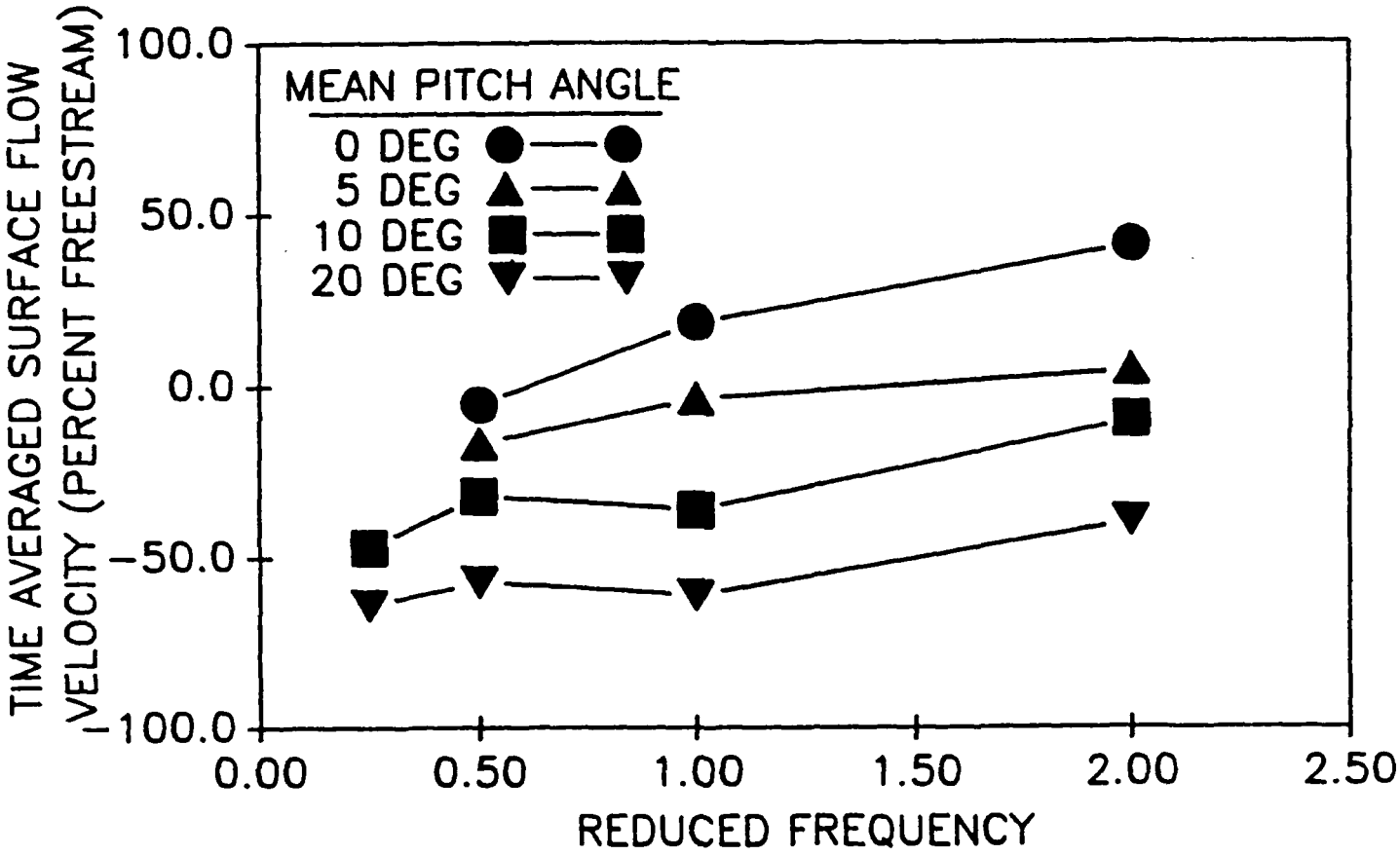

Figure 5-15. Time-averaged surface flow velocity in the leading edge vortex vicinity vs. reduced frequency.

CHAPTER VI

DISCUSSION

Vortex Structure

Spanwise visualization of the leading edge vortex revealed complex and continually evolving vortical structures, the appearance and behavior of which were responsive to variations in plate end geometry. Subsequent visualization restricted to the plane of the plate centerline yielded characterization of leading edge vortex development in this region. Analysis of these results quantified alterations in vortex convection and growth ensuing from modifications to plate end geometry. In addition, hotwire anemometry was used to validate measurements of vortex location and spatial extent performed on visualization.

Spanwise visualization of the leading edge vortex. Figures 3-1 through 3-4 documented spanwise leading edge vortex development for physically finite and infinite aspect ratio conditions, for two reduced frequencies at each condition. In each of the four cases, spanwise uniformity of vortex cross-sectional area was initially disrupted in the outboard region of the plate span soon after the vortex initiated. This disruption appeared as a tapering of vortex cross-section toward the plate ends. This tapering appeared similar to that visualized by Freymuth (1988b). A short time later in the pitching cycle, vortex cross-sectional uniformity was again disturbed farther inboard on the plate when excrescences formed on the vortex. Both the tapering in cross-

section and the excrescences migrated inboard toward the plate centerline as the vortex continued to grow and convect. Excrescence inboard migration was also accompanied by growth of this structure. The collaboration, then, of vortex tapering, excrescence growth and excrescence inboard migration tended to disrupt vortex cross-section uniformity nearer the plate centerline as the leading edge vortex convected and grew. However, even when these disruptive influences were most prevalent, vortex cross-sectional uniformity in the region of the plate centerline was not affected until the vortex had convected to approximately 80 percent chord.

Variations in reduced frequency noticeably influenced the tapering effect as well as the appearance and behavior of the excrescences. Higher reduced frequency resulted in less migration inboard of the tapering effect per pitch angle increment, thus yielding vortex cross-section uniformity across a longer length of the plate span for a greater portion of the pitching cycle. At greater reduced frequency, the excrescences initially appeared and also remained farther outboard on the plate span. In addition, elevated reduced frequency prompted formation of excrescences which were more compact and cohesive.

Transitioning from a physically three-dimensional end condition to a two-dimensional one through the addition of the splitter plate also affected leading edge vortex development. Addition of the splitter plate retarded the inboard progress of the tapering effect, resulting in a vortex which retained uniformity over a greater portion of the span for a longer duration in the pitching cycle. Splitter plate addition also elicited excrescences which were somewhat larger and migrated less toward the plate centerline than those observed in the absence of the splitter plate.

Figures 3-5 and 3-6 showed time histories of leading edge vortex chordwise position and cross-sectional area for two reduced frequencies and two plate end conditions. Introduction of the splitter plate elicited leading edge vortex initiation at earlier times in the pitching cycle and at sites nearer the plate leading edge than was observed in the absence of the splitter plate. However, following initiation, position histories for each reduced frequency appeared quite similar. These observations are consistent with those of Robinson et al. (1986a). For the case of a symmetric airfoil pitching at constant rate, Robinson and colleagues found that reducing three-dimensionality elicited leading edge vortex initiation at lower instantaneous pitch angle but altered vortex position history negligibly.

Linear least squares fits were applied to these histories to determine average vortex convection velocity. For a reduced frequency of 1.0, average vortex convection velocity with the splitter plate installed in the test section was 1.7 percent freestream less than the average convection velocity observed in the absence of the splitter plate. For a reduced frequency of 2.0, average convection velocity with the splitter plate in place was 3.7 percent freestream less than that which occurred in the unmodified test section.

Trends in leading edge vortex cross-sectional area generally replicated those observed for chordwise position. After initiation, area histories for each reduced frequency generally assumed appearances similar to each other. Linear least squares fits were applied to these histories to determine average cross-sectional area growth rate. At a reduced frequency of 1.0, average vortex growth rate without the splitter plate in place in the test section was 5.3 percent

less than the average growth rate observed with the splitter plate. For a reduced frequency of 2.0, average growth rate in the absence of the splitter plate was 16.7 percent less than that which occurred with the splitter plate installed in the test section.

Anemometric corroboration of visualization. Figures 3-7 through 3-10 contained flow visualization and velocity profiles for leading edge vortices located at chord positions of 20, 40, 60 and 80 percent chord, for two reduced frequencies. Also shown on the velocity profile were the heights of the leading edge vortex core and outermost encircling streakline. These heights were measured from the visualization using techniques consistent with those described in Chapter 4 to obtain vortex position and cross-sectional area over a much broader parameter range. In Figures 3-7 through 3-10, core height measured from visualization generally corresponded closely to a pronounced minimum in the velocity profile. Similarly, the height of the outermost encircling streakline usually coincided with a prominent maximum in the velocity profile. These observations are consistent with those reported by Robinson and Luttges (1984).

Vortex Kinematics

The flow structures and interactions observed to occur about the oscillating plate were both numerous and varied. This analysis circumstance was further compounded by the time-varying nature of the flow field. Such complexity partially obscured the intrinsic fluid-dynamic mechanisms generating the observed flow structures. When appropriately dissected, however, the experimental results furnished substantial information concerning the physical mechanisms responsible for the flow structures and interactions occurring

around the oscillating plate.

Leading edge vortex. Much attention was focused on the leading edge vortex, which seemed to play a major and pivotal role in the process under investigation. Lower reduced frequency parameter and greater mean pitch angle both yielded leading edge vortex initiation earlier in the plate oscillation cycle, as shown in Figure 4-5. Either consequence can be credibly linked to the vorticity generated around the vortex initiation site as the plate pitched up (Reynolds and Carr, 1985). Lower reduced frequency parameter allowed a greater length of fluid to pass by the plate per oscillation cycle, thus increasing the total amount of vorticity generated per pitch angle increment. As such, vorticity accumulated relatively quickly for each pitch angle increment and vortex initiation was achieved earlier in the pitching cycle, and thus at lower pitch angles.

The hastening of vortex initiation with increased mean angle can be considered by first reviewing the flow field behavior around the pitching plate and viewing Figure 4-1, as well. As pitch angle increased dynamically and the static stall angle of attack was exceeded, catastrophic flow separation was delayed by the dynamic pitch-up. As a consequence, the adverse pressure gradient experienced by the flow continued to increase in magnitude. Growth of the adverse pressure gradient, in turn, induced a vorticity-enriched localized thickening of the boundary layer near the leading edge. The thickened boundary layer, in turn, engendered a more vigorous interaction with the overrunning potential flow. Eventually, the degree of interaction between the overrunning flow and the thickening boundary layer reached the threshold level sufficient to create a vortex tongue, yielding a leading edge vortex. In light of

the previous discussion, it is clear that higher mean angle hastened vortex initiation with respect to the oscillation cycle largely by bringing about localized boundary layer thickening at an earlier time in the pitch-up portion of the cycle.

Consistent trends were noted in the average rates of leading edge vortex convection and growth, as shown in Figures 4-8 and 4-11, respectively. Greater reduced frequency parameter and lower mean angle resulted in higher average vortex convection velocities. These observations concerning vortex convection rate are consistent with those of Robinson (1985) and Lorber and Carta (1987), both of whom measured chordwise surface pressure distributions on sinusoidally oscillating airfoils. Average vortex growth rate increased monotonically with mean pitch angle, and displayed nonmonotonic behavior with respect to reduced frequency parameter, reaching a maximum at a reduced frequency of 1.0. The close relationship between average vortex convection and growth rates is a direct result of underlying physical processes, as outlined below.

As reduced frequency parameter increased beyond a value of 1.0, leading edge vortex cross-sectional area progressively decreased. A smaller frontal area of the vortex was presented to the freestream and freestream influences might be expected to decrease accordingly. However, increases in reduced frequency parameter also were accompanied by progressively longer delays into the pitching cycle for leading edge vortex initiation. As such, the vortex was initiated at decreasing instantaneous pitch angles during the downstroke, when the plate suction surface and the resident vortex experienced rapidly increasing exposure to the freestream and less plate shielding. Since average vortex convection rate generally increased with increasing reduced

frequency parameter, it seems that the freestream influence also increased with reduced frequency parameter. This could have been the case, in general, only if the reduced freestream effect due to vortex size reduction was outweighed by the increased freestream influence caused by mitigation of the shielding effect. As noted above, the phase in the pitching cycle where a vortex is produced appears to explain the paradox of a differential freestream effect. This asymmetry of effect is discussed below.

The complexity of the physical phenomenon under consideration precludes immediate and final model refinement. At least one factor contributing to the disparity between the the simple model and observed results can be identified with reasonable certainty. This factor is the simultaneous presence of multiple leading edge vortices on the same plate surface. Appreciable instantaneous convecting velocity variation not accompanied by corresponding changes in vortex size occurred predominantly in the elevated reduced frequency parameter regime. In these same tests, multiple leading edge vortices simultaneously resided on the same plate surface through portions of the plate oscillation cycle. Thus, a relationship appears to exist wherein vortex-vortex interactions influence vortex convection velocity. These influences, of course, relate closely to leading edge vortex initiation and leading edge vortex shedding time courses.

Trailing edge vortex. The trailing edge vortex also provided important physical insight into the process under investigation. The rotational sense of the trailing edge vortex indicated that it was composed of vorticity generated on the plate surface opposite that hosting the leading edge vortex most recently formed. For a considerable portion of the cycle preceding trailing edge vortex

initiation, the plate surface on which the trailing edge vortex initiated had experienced a favorable pressure gradient, thus concentrating the vorticity generated into a relatively thin boundary layer. However, pressure gradients and corresponding flow acceleration on this plate surface did not generate sufficient vorticity to reach or exceed the threshold level required for vortex initiation. Thus, the unconsolidated vorticity convected into the vicinity of the trailing edge. There, interactions not acting forward of the trailing edge precipitated coalescence of the vorticity into a vortex, at times in the cycle graphically illustrated in Figure 4-12. By presenting leading and trailing edge vortex initiation data together in Figure 4-12, trailing edge vortex initiation, in comparison to that for the leading edge vortex, is shown to be relatively independent of plate pitching. Since plate pitching undoubtedly continues to play a strong role in trailing edge vortex initiation, it is likely that other, presently undetermined interactions become equally influential in the trailing edge vicinity.

As is evident in Figure 4-13, higher reduced frequency parameter values generally resulted in the trailing edge vortex residing at the plate trailing edge for greater portions of the plate oscillation cycle. However, the trailing edge vortex was usually shed before the leading edge vortex. Trailing edge vortex residence time seems to imply an increase in leading edge vortex influence with higher reduced frequency. In contrast, the phase relationship observed between leading and trailing edge vortex shedding appears to indicate that leading edge vortex influence decreases at greater reduced frequency.

While appearing contradictory, such a circumstance merely reveals that the trailing edge vortex, although actively influenced by the leading edge

vortex, retains a certain measure of autonomy. Relative independence of the two vortices indicates that both continue to be influenced by events occurring on the surface where each originated, even after having arrived in the vicinity of the trailing edge. At elevated values of reduced frequency parameter, trailing edge vortex development may also be significantly influenced by previously-shed leading edge vortices located downstream of the plate trailing edge region. Dissimilar responses to plate pitching parameters by leading and trailing edge vortices and the resulting vortex-vortex interactions were discussed by Robinson et al. (1986b) in terms of a phase dependent, tandem vortex wake.

Figure 4-14 shows that trailing edge vortex average growth rate increases monotonically with declining mean pitch angle. Trailing edge vortex growth rate is principally governed by the rate at which vorticity of the correct sign convects into the trailing edge region. This rate, in turn, is collectively determined by the rate at which vorticity is generated on the lower plate surface and the rate at which this vorticity convects into the trailing edge vicinity. Thus, lower surface generation and convection rates are both regulated by the rate at which fluid passes over the lower surface of the plate. At higher mean pitch angle, the inclined plate presents more projected frontal surface area to the oncoming freestream. As such, the flow is likely to experience greater deceleration, which inhibits the generation and convection of vorticity into the trailing edge region.

Figure 4-14 also shows that trailing edge vortex average growth rate varies nonmonotonically with reduced frequency, reaching a minimum at a value of 0.5 and increasing at both higher and lower reduced frequencies. In Figure 4-12, it can be seen that, for a reduced frequency of 0.5, trailing edge

vortex initiation tends to occur during the first quarter of the pitching cycle. During this portion of the cycle, with zero radians corresponding to maximum upward pitch angle, the plate is pitching downward or is beginning to pitch downward for mean pitch angles of 20, 30 and 40 degrees. At other reduced frequencies for these mean pitch angles, initiation occurs when the plate is pitching up (K = 1.0, 2.0), or, if the plate is pitching down, the rate of pitching is not as high as that at initiation for a reduced frequency of 0.5 (K = 0.25).

As before, trailing edge vortex growth rate depends upon the rate at which vorticity is generated on the plate lower surface as well as the rate at which it convects into the trailing edge region. Both the vorticity generation and convection rates are governed by the rate at which fluid passes over the lower surface. When the plate is pitching up, 75 percent of the lower surface chord is generally moving upstream against the freestream, thus increasing the rate of fluid passage with respect to the plate lower surface. Alternatively, when the plate is pitching down, 75 percent of the lower surface is retreating from the approaching freestream, and the rate of fluid passage with respect to the plate lower surface decreases. Thus, less vorticity of the correct sign arrives at the trailing edge vicinity for a reduced frequency of 0.5 than for any other reduced frequency investigated.

Ancillary structures. As with structures and processes occurring over major parts of the plate surface, the ancillary structures observed in the near wake region also seemed closely linked to leading edge vortex dynamics. Both average leading edge vortex growth rate and ancillary structure wavelength behaved nonmonotonically with respect to reduced frequency parameter, and both exhibited maxima, for the set of test cases considered, at a reduced

frequency parameter value of 1.0. This was demonstrated graphically in Figures 4-11 and 4-15, respectively. Further, for a given reduced frequency parameter value, growth rate and wavelength both showed an increase with higher mean angle.

To assess these trends in terms of a vorticity balance, ancillary structure wavelength can be adopted as an index of the rate at which vorticity not incorporated into other structures is shed from the plate. Ancillary structures may assume the form of a von Karman vortex street, Freymuth's (1985) "ornamentation" or other structures. Alternatively, average vortex growth rate (and total vortex numbers) can be considered an indicator of the rate at which vorticity is incorporated into the convecting leading edge vortices. The trailing edge vortex can be considered a focal structure for vorticity accumulations near the trailing edge. At a reduced frequency parameter value of 1.0 and mean pitch angle of 10 degrees, vorticity presumably was simultaneously being shed downstream in the form of ancillary structures and being incorporated upstream into the leading edge vortex at rates greater than those observed for any other test case.

Maximum rates of vorticity shedding and incorporation are limited by the rate at which vorticity is made available by the passing fluid. That both shedding and incorporation rates attain maxima at a reduced frequency of 1.0 and a mean angle of 10 degrees suggests the amount of vorticity produced per length of passing fluid also reaches a maximum at these conditions. If leading edge vortex residence time on the plate and ancillary structure shedding durations are taken into account, the total amount of supporting vorticity assumed to be generated per cycle apparently increased with decreasing reduced

frequency parameter.

The sense of the shedding ancillary structures attests to the asymmetric accumulation of the vorticity on upper and lower plate surfaces. In addition, the fact that structures were shed from both plate surfaces in the 0 and 5 degree mean angle cases, and from only one surface in the 10 degree case, indicates the influence of pressure distribution and hysteresis upon vorticity dynamics. In the lower mean angle tests, residual vorticity supported greater amounts of symmetric shedding structures. In the 10 degree case, more vorticity was incorporated into the leading edge vortices yet the residual vorticity still supported asymmetric same-sense ancillary shedding.

Data set partitioning. Leading edge vortex average convection and growth data were partitioned according to the direction of plate pitching. These results were presented in Figures 4-16 and 4-17. Partitioning showed the occurrence of a significant increase in leading edge vortex average convection and growth rates as the plate reached maximum pitch angle and just began to pitch down. This result is typical of a significant hysteresis effect, and can be understood in terms of the potential flow field in the vicinity of the plate. As the plate attained maximum pitch angle and began the downward motion, the local freestream in the neighborhood of the vortex initiation site underwent rapid acceleration due to the sudden increase in effective angle of attack. In response to the growth in freestream influence, the nascent leading edge vortex displayed a rise in both average convection and average growth rates.

Surface Flows

Flow speed and direction fluctuations which occurred in the two-

dimensional boundary layer about the oscillating plate were diverse and abundant. Data collected using the tandem element hotwire anemometer were both voluminous and detailed. These factors tended to obscure the underlying fluid-dynamic mechanisms responsible for unsteady separation. However, leading edge vortex kinematics data derived from flow visualization were available and were used to highlight reproducible characteristics of the unsteady flow field. Hotwire anemometer data and leading edge vortex kinematics information were correlated to yield clarification of leading edge vortex initiation, convection and growth dependencies. The dependencies on reverse flow were shown to be significant.

Velocity and reversal histories. Two distinct modes of flow reversal were observed. The first mode was distinguished by the tendency of flow speed adjacent to the plate to pass through zero as velocity shifted from positive to negative values. This circumstance was generally observed as the mature leading edge vortex passed the probe location. Characteristic of the second mode was the absence of any pronounced tendency for flow speed to decrease to zero preceding the onset of reversal. This mode was observed near the plate leading edge in conjunction with initiation of the leading edge vortex, and at downstream chord stations, independent of any visualization evidence for a well defined vortical structure.

The apparent failure of flow speed to decline toward zero is a physical inconsistency inherent in the second reversal mode. It is explained by the flow visualization presented in Figure 5-2. Here, the lower photograph captured the moment of flow reversal. At this moment, the outermost streakline encircling the nascent leading edge vortex can be seen stagnating and splitting at the probe

element location. Under these conditions, the local flow velocity vector is nearly perpendicular to the probe element plane and neither element is in the wake of the other. Reversal is subsequently recorded as the stagnation point passes the probe element volume.

Chord dependent flow velocity histories presented in Figures 5-1 and 5-3 exhibited velocity variations with time that were distinctly sinusoidal in appearance. Sinusoidal velocity variations were largest near the plate leading and trailing edges, and declined for chord stations located closer to plate midchord. At chord stations near midchord on the upper surface, sinusoidal fluctuations were sometimes masked by the velocities associated with the convecting leading edge vortex. A phase shift of approximately one-half cycle was apparent between leading and trailing edge sinusoidal velocity fluctuations.

It seems plausible that plate solid body rotation contributed to the sinusoidal velocity variation in local flow histories. Consistent with experimental observations, tangential velocity on a rotating solid body increases with distance from the rotation axis. Thus, flow velocities induced on the solid body would also increase at longer distances from the axis of rotation.

Local flow velocity components induced by solid body rotation may also contribute to flow reversal on the plate lower surface at mean pitch angles greater than zero. Examples of this were presented in Figure 5-5. In this experiment, higher reduced frequency entailed faster oscillation rates. Faster oscillation rates, in turn, bring greater solid body tangential velocities, thereby engendering induced velocities of higher magnitude. Throughout the experimental parameter range, higher reduced frequency was generally accompanied by lower surface flow reversals persisting through more of the

oscillation cycle and having greater chord distributions.

Although leading edge vortex initiation was not rigorously characterized, reversal histories typified by those in Figure 5-4 facilitate two observations with regard to initiation. First, at the time of leading edge vortex initiation, flow reversal was never observed extending uninterrupted from the plate trailing edge to the vortex initiation site. Second, the spatial extent of localized reverse flow supporting initiation was usually limited, and sometimes nonexistent.

Correlations between vortex kinematics and surface anemometry. Correlations were completed for (1) leading edge vortex instantaneous growth rate, (2) leading edge vortex instantaneous convection velocity, (3) projected plate frontal area and (4) local surface flow average velocity. These were compared with leading edge vortex cross-sectional area. Each combination of reduced frequency and mean pitch angle were examined. Representative correlations, displayed in Figures 5-8 and 5-9, provide crucial insight into the physics responsible for leading edge vortex convection characteristics.

Instantaneous leading edge vortex convection velocity responded to changes in local surface flow average velocity only when leading edge vortex cross-sectional area was small and projected plate frontal area was large. Otherwise, leading edge vortex instantaneous convection velocity was most strongly influenced by variations in projected plate frontal area. Leading edge vortex instantaneous growth rate increased immediately following initiation while instantaneous convection rate generally declined. In this early period of development, vortex cross-sectional area was small and projected plate frontal area was large. During the intermediate stages of vortex development, changes

in leading edge vortex instantaneous growth and convection rates generally behaved similarly, rising and falling synchronously. In the final phase of vortex development, leading edge vortex instantaneous convection and growth rates once again displayed an inverse relationship to each other, with instantaneous growth rate generally decreasing while instantaneous convection rate tended to increase.

A correlation of local surface flow average velocity with leading edge vortex instantaneous convection velocity was performed that incorporated data from across the full range of reduced frequencies and mean pitch angles (Figure 5-10). The same was done with leading edge vortex instantaneous growth rate data and local surface flow average velocity data for the experimental range of reduced frequencies and mean pitch angles (Figure 5-7). Application of a linear least-squares fit to the data in Figures 5-10 and 5-7 demonstrated leading edge vortex responses to the simultaneous influences of both freestream and local surface flows.

The correlation data in Figure 5-10 were partitioned according to whether the data corresponded to pitch up or pitch down plate kinematics. These two resulting data sets were presented in Figures 5-11 and 5-12, and accompanied by linear least-squares fits. Slope of the linear fit was steeper for pitch up than for pitch down, indicating generally greater leading edge vortex instantaneous convection velocity responsiveness to local surface flow during pitch down. Dispersion of the individual data points about the linear fit was generally wider for the pitch down case. This observation suggested that influences other than local surface flow velocity can play prominent roles in leading edge vortex convection during pitch down.

The correlation data first presented in Figure 5-7 were also partitioned with regard to whether the plate was experiencing pitch up or pitch down. The two resulting data sets were presented in Figures 5-13 and 5-14, with linear least-squares fits. Slope magnitude of the linear fit was steeper for downward pitching than for upward pitching, which indicated that, like leading edge vortex instantaneous convection velocity, leading edge vortex instantaneous growth rate was generally more responsive to local surface flow during pitch down. Unlike the corresponding correlations for instantaneous convection rate, data point dispersion about the linear fit was generally broader for upward pitching. Once again, these observations indicated that other interactions besides local surface flow velocity can vigorously influence leading edge vortex growth during pitch up.

Figure 5-15 showed clear trends in surface flows encountered by the leading edge vortex as a function of reduced frequency and mean pitch angle. For a given reduced frequency, increasing the mean pitch angle caused the leading edge vortex to encounter local surface flows characteristic of stronger reversal. Alternatively at higher mean pitch angles, higher reduced frequency generally caused the leading edge vortex to encounter local surface flows associated with weaker reversal.

CHAPTER VII

CONCLUSIONS

Unsteady separation remains a topic of significant interest in aerodynamics due to the performance enhancements this phenomenon may eventually confer upon air vehicles. However, unsteady separated flow fields are spatially complex and temporally dependent. Thus, realization of application potential is contingent upon the thoroughness with which unsteady separation is understood. The energetic, large-scale vortical structures characteristic of unsteady separation play a central role in flow field development. As such, this investigation has examined in detail the initiation, convection and growth of these vortical structures in a simplified circumstance to clarify the physics responsible for the presence and behavior of them.

In the present study, unsteady separated flow structures generated by a flat plate undergoing sinusoidal pitching about the quarterchord were examined throughout a wide range of reduced frequency parameters and mean pitch angles. Preliminary visualization validated the assumption of two-dimensional flow along the plate centerline. In addition, hotwire anemometry corroborated vortex position and spatial extent as indicated by flow visualization. Subsequent analysis of smoke flow visualization data provided detailed characterizations of vortex kinematics for a broad parameter range. These results formed the basis for a rudimentary understanding of the intrinsic physical mechanisms

responsible for the observed vortex kinematics.

Tandem element hotwire anemometry documented flow reversals and speed fluctuations which occurred in the predominantly two-dimensional boundary layer adjacent to the oscillating plate surface. Leading edge vortex kinematics data derived from smokewire flow visualization were then analyzed in conjunction with surface flow data obtained using hotwire anemometry. The resulting analysis clarified certain aspects of the physics underlying unsteady separation, and facilitated refinement of a rudimentary physical model of leading edge vortex dynamics.

Vortex Structure

Leading edge vortex tapering as well as excrescence growth and migration collaborated to render the vortex three-dimensional progressively farther inboard as it convected along the plate. However, even when three-dimensionality was most prevalent, the leading edge vortex remained two-dimensional in the central region of the plate. Furthermore, two and three-dimensional plate end conditions did not elicit substantial variations in leading edge vortex average convection and growth rates along the plate centerline. Finally, anemometric velocity profiles confirmed the accuracy with which smoke flow visualization indicated vortex position and spatial extent.

Initiation

Leading edge vortex initiation occurred when some presumed threshold level of vorticity had been reached in the locale of the initiation site. The time that this threshold was attained, relative to plate oscillation cycle, was governed by the vorticity generation rate and by vorticity distribution area. Vorticity

generation rate, in turn, was seen to be a function of the rate at which fluid was passing over the plate in the neighborhood of the initiation site, which was closely linked to both reduced frequency parameter value and mean pitch angle. The area was dictated by the magnitude of leading edge pressure gradients. High mean angles, for example, meant that stagnation pressures and velocity-induced low pressures were quite close to each other relative to chord distribution.

Reverse flow was shown to play an incidental role in leading edge vortex initiation. Uninterrupted flow reversal extending from the plate trailing edge to the leading edge vortex initiation site was never observed at the time of initiation. Localized flow reversal was sometimes observed in the vicinity of the initiation site as a vortex initiated, but such reversal was limited to chord locations associated with the vortex initiation.

Convection

Variations in average leading edge vortex convection rate with reduced frequency parameter and mean pitch angle were satisfactorily accounted for using a simple freestream influence model. This model assumed that the sole influence driving the vortex over the plate surface was exposure to the freestream, and admitted such mitigating factors as shielding and exposure time. However, the freestream influence model was judged too simplistic, and other mechanisms were sought to reconcile the model with experimental observations. One such mechanism, vortex-vortex interactions, was immediately isolated with some certainty. In addition, leading edge vortex instantaneous convection velocity and surface flow average velocity in the locale of the leading edge

vortex were well correlated.

In the presence of minimal freestream influence, variations in local surface flow average velocity were closely associated with changes in leading edge vortex instantaneous convection velocity. In addition, the speed and direction of time averaged surface flows encountered in the vicinity of the leading edge vortex were very sensitive to changes in both reduced frequency and mean pitch angle. Flows characteristic of stronger reversal were observed at lower reduced frequencies and higher mean pitch angles. These trends are consistent with those observed in average leading edge vortex convection velocity.

Data set partitioning showed a broad disparity between the average leading edge vortex convection rates occurring before and after the plate reached maximum pitch angle. The appreciable increase in convection rate that began with pitch-down was attributed to a sharp rise in potential flow velocity in the neighborhood of the nascent leading edge vortex. This sudden increase in local potential flow velocity was engendered by a rapid shift in the potential flow field surrounding the plate. This shift, in turn, was a consequence of the abrupt angle of attack change caused by the reversal of plate motion at the top of the cycle. Leading edge vortex instantaneous convection velocity displays a heightened responsiveness to surface flows during pitch down. The same influences responsible for the rise in vortex average velocity probably contribute to the heightened vortex susceptibility to local surface flows.

Growth

Average leading edge vortex growth rate is jointly governed by the rate

at which vorticity is generated and the effectiveness with which this vorticity is collected and organized. The initial rise in average growth rate with reduced frequency is attributable to greater efficiency of the vorticity consolidating mechanism. As reduced frequency continues to increase, the consolidating mechanism continues to grow more efficient. However, with less fluid passing over the airfoil per cycle, less vorticity is generated per cycle and lower levels are available for consolidation. Thus, a decline in average vortex growth rate subsequently occurs.

A coherent view of instantaneous growth rate emerges when interpreted in conjunction with instantaneous convection rate and local surface flow average velocity. In the early stages of leading edge vortex development, the vortex is small, well shielded by the inclined plate and experiences slight freestream influence. During this time, reverse flow influence predominates, causing instantaneous convection velocity to decline and supplying angular momentum of the correct sign to the nascent leading edge to promote growth. Instantaneous convection and growth rates thus behave inversely with respect to each other. Later, as the vortex grows and undergoes a more vigorous interaction with the freestream, surface flow influence is overshadowed. The freestream appears to become the principal source of angular momentum for the growing vortex. Since the freestream influence also appears to drive the vortex downstream, instantaneous convection and growth rates display a direct relationship with respect to each other. Trailing edge interactions were, of course, not considered here due to possible three-dimensional contamination of downstream observations.

Kinematics of Other Structures

Although the leading edge vortex is easily the most prominent entity in the unsteady separated flow field, other vortical structures are present, as well. The trailing edge vortex can grow to large size and accumulate significant energy. As such, it plays a crucial role in defining flow field character. Alternatively, ancillary structures are not typically large or energetic. These smaller vortices do not exercise vigorous control over flow field development. However, presence of these structures indicates regions in the flow field where vorticity exists which has not been consolidated into other, larger vortices.

Some of the trailing edge vortex dynamics indicated that initiation, growth and shedding of this structure were all actively influenced by the leading edge vortex residing on the opposite plate surface. However, other behavior implied that the trailing edge vortex was not dominated by the leading edge vortex, but was also affected by conditions prevailing on the plate surface where it resided. Thus, influences originating from both plate surfaces interacted at the trailing edge region, giving rise to the observed trailing edge vortex behavior.

Ancillary structure behavior was incorporated into an informal vorticity balance also involving average leading edge vortex growth rate and trailing edge vortex initiation. This methodology revealed that both reduced frequency parameter value and mean pitch angle influenced vorticity generation rate, total amount of vorticity generated per cycle and vorticity accumulation site. Further, reduced frequency and mean pitch angle governed the quantity of vorticity accumulated on the plate versus the amount shed at any time during the pitching cycle. Finally, ancillary structure behavior also pointed out the

relationship between pressure distribution and hysteresis effects, and vorticity dynamics. This view tends to minimize the potential influences of vorticity annihilation.

Many of the underlying mechanisms responsible for unsteady separation continue to be elusive, and may remain so for quite some time. Unsteady separated flows that occur on lifting surfaces undergoing sinusoidal pitch oscillation continue to be an especially promising area of research. Within this subset, the present study has examined an extended range of reduced frequency parameters and mean pitch angles. The data obtained were exploited in a manner designed to disclose the intrinsic fluid dynamics. These analyses have served to establish the basis for a rudimentary model of the processes under consideration. Although not comprehensive, this model accounts for certain flow field phenomena not reconcilable with some previous, more elementary models.

Further work is required to comprehend unsteady separation in sufficient detail to facilitate prediction and control in practical circumstances. Other interactions besides those described in this effort undoubtedly contribute to vortex dynamics, and should be identified. Parameter ranges and lifting surface kinematics representative of the appropriate air vehicle flight regime should be examined. Finally, investigations should be extended into the three-dimensional regime to accommodate future application to flight vehicles.

BIBLIOGRAPHY

Adler, J.N., and Luttges, M.W., "Three-Dimensionality in Unsteady Flow About a Wing, " AIAA Paper No. 85-0132, Reno, NV, Jan. 1985.

Ashworth, J., and Luttges, M.W., "Comparisons in Three-Dimensionality in the Unsteady Flows Elicited by Straight and Swept Wings," AIAA Paper No. 86-2280, Williamsburg, VA, Proceedings AIAA CP88, Aug. 1986, pp. 446-455.

Birnbaum, W. "Die tragende Wirbelflache als Hilfsmittel zur Behandlung des ebenen Problems der Tragflugeltheorie," Zeitschrift fur angewandte Mathematik und Mechanik (ZAMM) 3, 1923, pp. 290-297.

Bublitz, P. History of Aeroelasticity in Germany from the Beginning to 1945, European Space Agency, ESA-TT-1082, July 1988, pp. 38-43, 97-101, 238-241.

Carr, L.W., McAlister, K.W. and McCroskey, W.J., "Analysis of the Development of Dynamic Stall Based Upon Oscillating Airfoil Experiments," NASA TN-8382, Jan. 1977.

Carta, F.O., "Experimental Investigation of the Unsteady Aerodynamic Characteristics of a NACA 0012 Airfoil," Research Report M-1283-1, United Aircraft Corporation, July 1960.

Eaton, J., Jeans, A., Ashjaee, J., and Johnston, J., "A Wall-Flow-Direction Probe for Use in Separating and Reattaching Flows," Transactions of the ASME, Vol. 101, Sept. 1979, pp. 364-366.

Francis, M.S., Keesee, J.E., and Retelle, J.P., "An Investigation of Airfoil Dynamic Stall with Large Amplitude Motions," FJSRL-TR-83-0010, Oct. 1983.

Freymuth, P., "The Vortex Patterns of Dynamic Separation: A Parametric and Comparative Study," Prog. Aerospace Sci., Vol. 22, pp. 161-208, 1985.

Freymuth, P., Finaish, F., and Bank, W., "Visualization of Wing Tip Vortices in Unsteady and Steady Wind," AIAA Paper No. 86-1096, Atlanta, GA, May 1986.

Freymuth, P., "Propulsive Vortical Signatures of Plunging and Pitching Airfoils," AIAA Paper No. 88-0323, Reno, NV, Jan. 1988.

Freymuth, P., "Visualizing the Connectivity of Vortex Systems for Pitching Wings," AIAA Paper No. 88-3549-CP, Cincinnati, OH, July 1988.

Freymuth, P., "Three-Dimensional Vortex Systems of Finite Wings," Journal of Aircraft, Vol. 25, No. 10, Oct. 1988, pp. 971-972.

Freymuth, P., Jackson, S., and Bank, W., "Toward Dynamic Separation Without Dynamic Stall," Experiments in Fluids, 7, 1989, pp. 187-196.

Graham, G.M., and Strickland, J.H., "The Effect of Moderate to High Pitching Rates on the Aerodynamic Performance of a NACA 0015 Airfoil at a Reynolds Number of 1 x 10^5," Report for Southeastern Center for Electrical Engineering Education, Contract No. F49620-82-C-0035, 1985.

Graham, G.M., and Strickland, J.H., "An Experimental Investigation of an Airfoil Pitching at Moderate to High Rates to Large Angles of Attack," AIAA Paper No. 86-0008, Reno, NV, Jan. 1986, pp. 1-6.

Ham, N.D., and Garelick, M.S., "Dynamic Stall Considerations in Helicopter Rotors," Journal of the American Helicopter Society, Vol. 13, No. 2, April 1968, pp. 49-55.

Ham, N.D., "Some Recent MIT Research on Dynamic Stall," J. Aircraft, Vol. 9, No. 5, May 1972, pp. 378-379.

Harper, P.W., and Flanigan, R.E., "Investigation of the Variation of Maximum Lift for a Pitching Airplane Model and Comparison with Flight Results," NACA TN-1734, Oct. 1948, pp. 1-22.

Helin, H.E., Robinson, M.C., and Luttges, M.W., "Visualization of Dynamic Stall Controlled by Large Amplitude Interrupted Pitching Motions," AIAA Paper No. 86-2281, Williamsburg, VA, Proceedings AIAA CP868, Aug. 1986, pp. 456-471.

Helmholtz, H., von, "Uber diskontinuierliche Flussigkeitsbewegunen," Mber K. Akad. Wiss. Berlin, 1868, pp. 337-346.

Kramer, M. "Die Zunahme des Maximalauftriebes von Tragflugeln bei plotzlicher Anstellwinkelvergroberung (Boeneffekt)," Zeitschrift fur Flugtechnik und Motorluftschiffahrt (ZFM) 23, 1932, pp. 185-189.

Herbst, W.B., "Supermaneuverability," Joint Automatic Control Conference, Univ. of VA, 17-19 June 1981.

Jumper, E.J., Dardis, W.J., and Stephen, E.J., "Toward an Unsteady Flow Airplane," AIAA Paper No. 88-0752, Reno, NV, 1988.

Jumper, E.J., Schreck, S.J., and Dimmick, R.L., "Lift-Curve Characteristics for an Airfoil Pitching at Constant Rate," AIAA Paper No. 86-0117, Reno, NV, 1986.

Kelvin, Lord (Thomson, W.), "On Vortex Motion," Edinburg Transactions XXV,

1869.

Lighthill, M.J., Mathematical Biofluidynamics, Society for Industrial and Applied Mathematics, Philadelphia, 1975, pp. 11-190.

Liiva, J., and Davenport, F.J., "Dynamic Stall of Airfoil Sections for High-Speed Rotors," Journal of the American Helicopter Society, Vol. 14, No. 2, April 1969, pp. 26-33.

Lippisch, A., "Versuche zur Sichtbarmachung von Stromlinien," Jahrbuch 1935 der Vereinigung fur Luftfahrtforschung (VLF), pp. 118-127.

Lorber, P., and Carta, F., "Unsteady Stall Penetration Experiments at High Reynolds Number," AFOSR TR-87-1202 (UTRC Report R87-956939-3), April 1987.

Luttges, M.W., and Kennedy, D.A., "Initiation and Use of Three-Dimensional Unsteady Separated Flows," Proceedings of Workshop II on Unsteady Separated Flow, USAF Academy, CO, 1988, pp. 211-222.

Luttges, M.W., Robinson, M.C., And Kennedy, D.A., "Control of Unsteady Separated Flow Structures on Airfoils," AIAA Paper No. 85-0531, Boulder, CO, March 1985.

Mahler, D. "Bidirectional Hot-Wire Anemometer," Review of Scientific Instruments, Vol. 53, No. 9, Sept. 1982, pp. 1465-1466.

McAlister, K.W., and Carr, L.W., "Dynamic Stall Experiments on the NACA 0012 Airfoil," NASA TP-1100, Jan. 1978, pp. 1-161.

McCroskey, W.J., and Fisher, R.K., "Detailed Aerodynamic Measurements on a Model Rotor in the Blade Stall Regime," Journal of the American Helicopter Society, Vol. 17, No. 1, Jan. 1972, pp. 20-30.

McCroskey, W.J., "Some Current Research in Unsteady Fluid Dynamics--The 1976 Freeman Scholar Lecture," ASME Journal of Fluids Engineering, Vol. 99, March 1977, pp. 8-38.

McCroskey, W.J., "Unsteady Airfoils," Annual Review of Fluid Mechanics, 1982, pp. 285-311.

McCullough, G., and Gault, D., "Examples of Three Representative Types of Airfoil-Section Stall at Low Speed," NACA TN-2502, 1951.

Navier, C.L.M.H., "Memoire sur les lois du mouvement des fluides," Mem. Acad. R. Sci., Paris, France, 1823, pp. 389-416.

Poisson, S.D., "Memoire sur les equations gereales de l'equilibre et du mouvement du corps solides elastiques et des fluides," Journal Ec. Polyt., Paris,

France, 1831, pp. 139-166.

Prandtl, L., "Uber Flussigkeitsbewegung bei sehr kleiner Reibung. Verhandlungen des III," Internationalen Mathematiker Kongresses, Heidelberg, 1904, (Leipzig, R.G. Teubner, 1905).

Prandtl, L., and Tietjens, O.G., Fundamentals of Hydro- and Aeromechanics, Dover Publications, Inc., New York, 1934, pp. 69-77, 191-194.

Reynolds, W.C., and Carr, L.W., "Review of Unsteady, Driven, Separated Flows," AIAA Paper No. 85-0527, Boulder, CO, March 1985.

Robinson, M.C., and Luttges, M.W., "Unsteady Separated Flow: Forced and Common Vorticity About Oscillating Airfoils," Workshop on Unsteady Separated Flow, United States Air Force Academy, Francis, M., and Luttges, M. (eds.), University of Colorado: 1984, pp. 117-126.

Robinson, M.C., "Development of Vorticity and Vortices from Forced Unsteady Flow Separation," Doctoral Thesis, Graduate School, University of Colorado, Boulder, Boulder, CO, 1985.

Robinson, M.C., and Luttges, M.W., "Vortices Produced by Air Pulse Injection from the Surface of an Oscillating Airfoil," AIAA Paper No. 86-0118, Reno, NV, Jan. 1986.

Robinson, M., Helin, H.,Gilliam, F., Russell, J., and Walker, J., "Visualization of Three-Dimensional Forced Unsteady Separated Flow," AIAA Paper No. 86-1066, Atlanta, GA, May 1986.

Robinson, M.C., Helin, H.E., and Luttges, M.W., "Control of Wake Structure Behind an Oscillating Airfoil," AIAA Paper No. 86-2282, Williamsburg, VA, Proceedings AIAA CP868, Aug. 1986, pp. 472-485.

Rosenhead, L., Laminar Boundary Layers, Oxford University Press, 1963, Chps. 1-3.

Saint-Venant, B., "Memoire sur la dynamique des fluides," C.R. Acad. Sci., Paris, France, 1843, pp. 1240-1242.

Schlicting, H., Boundary-Layer Theory, translated by Kestin, J., 7th ed., McGraw-Hill, New York, 1979.

Schreck, S., and Luttges, M.W., "Unsteady Separated Flow Structure: Extended K Range and Oscillation through Zero Pitch Angle," AIAA Paper No. 88-0325, Reno, NV, 1988.

Shivaprasad, B., and Simpson, R., "Evaluation of a Wall-Flow-Direction Probe for Measurements in Separated Flows," Transactions of the ASME, Vol. 104, June 1982, pp. 162-166.

Silverstein, A., Katzoff, S., and Hootman, J.A., "Comparative Flight and Full-Scale Wind-Tunnel Measurements of the Maximum Lift of an Airplane," NACA Report 618, 1938.

Stokes, G.G., "On the Theories of the Internal Friction of Fluids in Motion and of the Equilibrium and Motion of Elastic Solids," Trans. Camb. Phil. Soc., Cambridge, 1845, pp. 287-305.

Strickland, J.H., and Graham, G.M., "Dynamic Stall Inception Correlation for Airfoils Undergoing Constant Pitch Rate Motions," AIAA Journal, Vol. 24, No. 4, April 1986, pp. 678-680.

Telionis, D.P., "Calculations of Time-Dependent Boundary Layers," Unsteady Aerodynamics, Vol. 1, 1975, pp. 155-190, ed., Kinney, R.B., Symposium Proceedings at the Univ. of Ariz., March 18-20.

Walker, J.M., Helin, H.E., and Strickland, J.H., "An Experimental Investigation of an Airfoil Undergoing Large Amplitude Pitching Motions," AIAA Paper No. 85-0039, Reno, NV, Jan. 1985.

Walker, J.M., Helin, H.E., and Chou, D., "Unsteady Surface Pressure Measurements on a Pitching Airfoil," AIAA Paper No. 85-0532, Boulder, CO, March 1985.